Faculdade de Engenharia da Universidade do Porto

Automatic Measurement of Atherosclerotic Plaque Burden in Ultrasound Images of the Carotid Artery

Miguel Matos Fernandes de Oliveira Duarte

Dissertação submetida para satisfação parcial dos requisitos do grau de mestre em Bioengenharia – Engenharia Biomédica

Dissertação realizada sob a supervisão do Professor Doutor Aurélio Campilho, do Departamento de Engenharia Eletrotécnica e de Computadores da Faculdade de Engenharia da Universidade do Porto, e do Doutor José Rouco Maseda, Investigador Pós-doutoramento do Instituto de Engenharia Biomédica (INEB)

Porto, Junho de 2014

Miguel Duarte, 2014

“If I have seen further than others, it is by standing upon the shoulders of giants.”

Sir Isaac Newton

“No matter. Try again. Fail again. Fail better.”

Samuel Beckett

Resumo

Com este trabalho pretende-se desenvolver um sistema de diagnóstico assistido por computador para a medição automática de carga de placa em imagens de ultrassonografia da artéria carótida.

A aterosclerose é uma doença vascular que constitui uma das principais causas de morte e incapacidade permanente nos países desenvolvidos. Na maioria dos casos, é uma doença assintomática que apenas é diagnosticada quando leva a um evento cardiovascular, como ataque cardíaco, ou acidente vascular-cerebral. É de grande interesse encontrar marcadores com elevado valor preditivo que permitam uma deteção e diagnóstico precoce da doença. Marcadores baseados em imagem médica têm ganho especial interesse com os recentes avanços tecnológicos.

Um destes marcadores é a carga de placa, que mede a quantidade de placas ateroscleróticas presente nas artérias, e como tal é um marcador útil para o diagnóstico da doença na sua fase mais avançada, permitindo uma monitorização da evolução da aterosclerose e a sua resposta a diferentes terapias e tratamentos. A medição da carga de placa é frequentemente realizada em imagens de ultrassonografia da artéria carótida, e requer uma segmentação prévia das placas de aterosclerose.

Neste trabalho, a carga de placa é expressa como a soma das áreas de todas as placas de aterosclerose. Estas placas são segmentadas a partir de uma imagem bi-dimensional modo B de ultrassonografia da artéria carótida comum. Para esta segmentação, é proposto um método inovador que se divide em duas fases: segmentação da camada íntima-média da parede arterial; delimitação de placas a partir de contornos segmentados desta região.

Para a segmentação da parede arterial é utilizado como referência um algoritmo previamente desenvolvido, modificado de forma a melhorar a segmentação dos contornos da íntima-média em imagens altamente afetadas por ruído. As seguintes modificações são feitas ao método original: uso de um algoritmo alternativo para a deteção do lúmen que utiliza padrões locais de simetria de fase a uma escala de análise apropriada; relaxamento das restrições impostas ao contorno; uma nova função para a classificação difusa de bordos que utiliza mais informação da imagem, como a força de bordo; uma estimativa

local da força de bordos falsos causados por ruído no lúmen, calculada através de estatíticas robustas, para definir os termos de penalização e ganho desta função.

Para a segmentação de placa, o método proposto utiliza critérios objetivos para definir placa de aterosclerose propostos num consenso médico. Os contornos segmentados da região da íntima-média são utilizados para calcular medidas de espessura local da parede arterial. Estas medidas são comparadas com valores de referência específicos de cada um dos critérios para avaliar a presença de placa ao longo da parede da carótida.

O método proposto para segmentação de placa foi testado numa base de dados de imagens bi-dimendionais modo B de ultrassonografia da artéria carótida comum, contendo segmentações manuais das placas e dos contornos da íntima-média. O método mostra um bom desempenho quando os contornos desta camada são bem segmentados, apresentando segmentações comparáveis às realizadas manualmente.

Foi desenvolvida uma aplicação baseada numa interface gráfica para o cálculo da carga de placa. Esta interface permite selecionar uma imagem, segmentar as placas de aterosclerose de forma automática e quantificar o comprimento e área de cada placa. A carga de placa é expressa como a soma das áreas de todas as placas segmentadas. O valor médio e máximo da espessura da íntima-média também são apresentados.

Abstract

The aim of the present work is the development of a computer-assisted diagnosis system for the automatic measurement of plaque burden in ultrasound images of the carotid artery.

Atherosclerosis is a vascular disease that constitutes one of the main causes of death and permanent disability in developed countries. In most cases, it is asymptomatic and can only be diagnosed when it leads to a cardiovascular or cerebrovascular event, such as heart attack or stroke, respectively. It is of great interest to find markers with high predictive value that allow an early detection and diagnosis of atherosclerosis. One of these markers is plaque burden, which measures the amount of plaque present in diseased arteries, and therefore is a useful marker for the diagnosis of atherosclerosis in its later stages, allowing the monitoring of the progression of the disease and its response to different therapies and treatments. Plaque burden is usually measured in ultrasound images of the carotid artery. For this, a prior segmentation of the atherosclerotic plaques is required.

In the present work, plaque burden is expressed as the sum of the areas of the atherosclerotic plaques segmented in a two-dimensional B-mode ultrasound image of the common carotid artery. For this segmentation, a novel method is proposed which is divided in two main steps: 1) segmentation of the intima-media layer of the carotid wall and 2) plaque delimitation using the segmented contours of this region.

For the segmentation of the carotid wall a previously developed algorithm is used as reference and modified to improve the segmentation of the intima-media contours in images affected by speckle noise. The following optimizations are introduced: use of an alternative method for lumen detection based on local phase symmetry patterns at appropriate scale of analysis; relaxation of the constraints imposed to the contour; use of a new membership function for the fuzzy classification of edges that uses more image information, such as the edge strength; local estimation of the strength of false edges caused by noise in the lumen, calculated through robust statistics, to help defining the penalty and gain terms of this function.

For plaque segmentation, the proposed method uses objective criteria to define atherosclerotic plaque proposed in a medical consensus. The segmented intima-media contours are used to calculate measures of the local thickness of the arterial wall. These measures are compared with reference thresholds specific of each criteria to evaluate the presence of atherosclerotic plaques along the carotid wall.

The proposed method for plaque segmentation was tested using a dataset of 2D B-mode ultrasound images of the common carotid artery, in comparison with manual segmentations of atherosclerotic plaques and the contours of the intima-media region. The method demonstrates a good performance when the intima- media layer is correctly segmented, showing plaque segmentations comparable to those obtained manually.

A graphical user interface was developed for the calculation of the image plaque burden. It allows to select the image, automatically segment the atherosclerotic plaques and quantitatively characterize the length and area of each plaque. Plaque burden is expressed as the sum of the areas of all the plaques in the image. The average and maximum value of the local intima-media thickness are also presented.

Agradecimentos

Gostaria de agradecer ao meu orientador, o Professor Aurélio Campilho, pela disponibilidade, interesse e orientação prestada.

Gostaria de agradecer ao meu co-orientador, José Rouco Maseda, pela orientação, deponibilidade e apoio constantes, e ainda pela enorme preserverança que demonstrou durante todo o meu trabalho de investigação e escrita da dissertação. Gostaria de agradecer ao departamento de Neurossonologia do Centro Hospitalar São João por disponibilizar as imagens de ultrassonografia utilizadas, assim como segmentações manuais para algumas delas.

Por fim, gostaria de agradecer aos meus pais, que foram, são e serão a minha eterna fonte de inspiração, modelos de valores e atitudes pelos quais me guio na minha vida de todos os dias, e cujo apoio e amor incondicionais foram o motor propulsor durante todo o meu percurso académico.

Table of contents

Resumo vii
Abstract ix
Agradecimentos xi
Table of contents xiii
List of figures xvii
List of tables xxiii
List of abbreviations xxv
1 Introduction 1
1.1 Motivation 1
1.2 Objectives 2
1.3 Contributions 2
1.4 Thesis overview 3
2 Methods for measuring plaque burden 5
2.1 Anatomy of the carotid artery 5
2.2 Atherosclerosis 6
2.3 Diagnosis of atherosclerosis 7
2.4 Ultrasound imaging of the carotid 9
2.5 Plaque burden measurement 12
2.6 Plaque segmentation 14
2.7 Concluding remarks 16
3 Methodology 19
3.1 Basic concepts 19

3.1.1 Instantaneous coefficient of variation 19
3.1.2 Fuzzy classification 20
3.1.3 Grading of the detected edges using fuzzy classification 21
3.1.4 Robust statistics 21
3.1.5 Dynamic programming 22
3.1.6 Convolution of one-dimensional signals 23
3.2 Segmentation of atherosclerotic plaques 23
3.3 Segmentation of the intima-media region 24
3.3.1 Original method 25
3.3.2 Original method parameters 28
3.3.3 Proposed improvements 29
3.3.3.1 Improved lumen axis detection 30
3.3.3.2 Relaxing the constraints 31
3.3.3.3 Fuzzy membership function 32
3.3.3.4 Image dependent parameters 34
3.3.3.5 Considerations about improvements in the segmentation of the media-adventitia interface 34
3.3.3.6 Method limitations 34
3.3.4 Proposed method parameters 35
3.4 Plaque delimitation from intima-media contours 36
3.4.1 Criteria to define atherosclerotic plaque 37
3.4.2 Criteria implementation 37
3.4.2.1 Criterion 1 38
3.4.2.2 Criterion 2 38
3.4.2.3 Criterion 3 40
3.4.2.4 Criteria combination 41
3.4.3 Surrounding intima-media thickness 41
3.4.3.1 Median 41
3.4.3.2 Gaussian average 42
3.4.4 Normal intima-media thickness for the patient 43

3.4.5 Plaque shape restriction 44
3.5 Plaque burden measurement 44
3.6 Methodology summary 45
4 Experimental evaluation 47
4.1 Image database 47
4.2 Acquisition of a ground truth 48
4.3 Quantitative evaluation metrics 49
4.3.1 Segmentation of the intima-media region 49
4.3.2 Plaque segmentation 50
4.3.2.1 Length measures 50
4.3.2.2 Area measures 50
4.3.3 Statistical significance 51
4.4 Segmentation of the carotid wall 51
4.4.1 Lumen axis detection 52
4.4.1.1 Parameter optimization 52
4.4.1.2 Method selection 52
4.4.2 Intima-media segmentation 53
4.4.2.1 Parameter optimization 53
4.4.2.2 Method selection 55
4.5 Plaque segmentation 59
4.5.1 Surrounding intima-media thickness 60
4.5.1.1 Parameter optimization 60
4.5.1.2 Method selection 63
4.5.2 Normal intima-media thickness 64
4.5.3 Plaque delimitation using different criteria to define plaque 67
4.6 Overall performance of the proposed method for plaque segmentation 68
5 CAD system for measuring plaque burden 73
6 Conclusions and future work 77
References 81

Appendix A - Reference values for the normal intima-media thickness of the common carotid artery.....87

List of figures

Figure 2.1 (a) Arterial tree of the right carotid (terrykingmd.com). (b) Anatomy of the arterial wall with its different layers (Wikstrand, 2007). 5

Figure 2.2 Schematic diagram representing the carotid arterial tree and the three definitions of plaque proposed in the medical consensus (Touboul et al., 2012). A – Intima-media thickness > 1.5 mm. B – Lumen encroachment > 50% of surrounding intima-media thickness value. C – Lumen encroachment > 0.5 mm (Aznaouridis, Dhawan and Quyyumi, 2010). 6

Figure 2.3 (a) Myocardial infarction caused by coronary heart disease (medimoon.com). B – Ischemic stroke, caused by a blood clot that interrupts the blood flow of a cerebral artery (jellygamatt.com). 7

Figure 2.4 Bifurcation of the carotid artery, showing atherosclerotic plaques, and a cross-section of the carotid artery. The IMT is the combined thickness of the intima and media layers (Yang *et al.*, 2012). 7

Figure 2.5 Calculation of the degree of stenosis (Berletti *et al*., 2014). 8

Figure 2.6 Hyperechoic (bone), hypoechoic (grey tissue) and anechoic (black fluid) structures in US image (fetal.com). 9

Figure 2.7 Duplex US image of the carotid. The white arrow highlights a plaque (supersonicimagine.com).....10

Figure 2.8 3D US image of a diseased carotid artery obtained through the mechanical linear scanning process. The white arrow highlights a plaque (Fenster, Downey and Cardinal, 2001). 10

Figure 2.9 (a) Schematic representation of the carotid tree (Touboul *et al*., 2012). (b) Longitudinal slice including the bifurcation and portions of the CCA, ICA and ECA (cardiologydoc.wordpress.com). (c) Transverse slice acquired upstream of the bifurcation (aeronline.org). (d) Transverse slice acquired downstream of the bifurcation

(annalsofian.org). (e) Atherosclerotic plaque in the CCA (theskepticalcardiologist.com). 11

Figure 2.10 Maximum plaque thickness is highlighted by the yellow crosshairs (Callahan *et al.*, 2012). 12

Figure 2.11 Measuring plaque area as performed by Spence *et al.* (2002). This particular plaque is in the right CCA and measures 0.55 cm^2. 13

Figure 2.12 (a) A segment of the carotid artery containing a plaque (orange) is scanned with a linear array transducer as a series of transverse slices. (b) CCA with no plaque. The blue and red borders represent the lumen-intima and media-adventitia boundaries, respectively. (c) CCA with plaque. The orange border represents the boundary of the plaque (Sillesen *et al.*, 2012). 14

Figure 2.13 Plaque segmentation results on a longitudinal US B-mode image of the carotid artery. (a) Manual segmentation performed by expert. (b) Active contour segmentation (Loizou *et al.*, 2007b). 15

Figure 2.14 Carotid wall segmentation performed by the method proposed by Delsanto *et al*. (2005, 2006 and 2007). IL$_{CULEX}$ and MA$_{CULEX}$ represent the segmented contours of the lumen-intima and media-adventitia interfaces of the FW, respectively. SCM and JV stand for sternocleidomastoid muscle and jugular vein, respectively (Delsanto *et al.*, 2007). 16

Figure 2.15 Segmentation of the carotid wall in US images of the carotid artery performed by the method proposed by Rocha, Silva and Campilho (2012). The yellow lines represent the automatically segmented contours, and the green lines represent the manual tracings performed by a clinical expert. 16

Figure 3.1 Edge detection using the ICOV in a US image of the carotid artery. 20

Figure 3.2 Fuzzy classification of edges detected using the ICOV. 21

Figure 3.3 Segmented contour as a longitudinal path $P(j)$ connecting image pixels of consecutive columns across the entire image length. 22

Figure 3.4 Main steps of the proposed method for plaque segmentation. The yellow lines represent the segmented contours of the IM region of the carotid wall. The segmented plaque is represented as a red overlay. 24

Figure 3.5 Segmentation of the IM region of the carotid wall. The segmented contours of the lumen-intima and media-adventitia interfaces are the longitudinal paths $LI(j)$ and $MA(j)$ represented by the yellow and red lines, respectively, and defined for the N image columns. 24

Figure 3.6 Block diagram of the algorithm proposed by Rocha, Silva and Campilho (2012) for the segmentation of the IM region of the carotid wall. 25

Figure 3.7 Lumen axis detection (blue line) and corresponding ROI (red lines). 26

Figure 3.8 Typical edges found in the carotid wall. The intensity profile on the right belongs to the image column which is highlighted by a vertical blue line in the image on the left. 26

Figure 3.9 Fuzzy edge maps. (a) $f_{FM}(i, j)$. (b) $f_{FVM}(i, j)$. (c) $f_{FAM}(i, j)$. 27

Figure 3.10 Examples of the segmentation of the IM region performed by the original method. The red and yellow lines represent the MA and LI contours, respectively. 28

Figure 3.11 The original method's worst segmentations are due to (a) misdetection of L and (b) wrong segmentation of LI. The red and yellow lines represent the LI and MA contours, respectively. 30

Figure 3.12 Comparison between different algorithms used for lumen detection. (a) The algorithm used by Rocha, Silva and Campilho (2012) fails to segment L due to the presence of background noise. (b) L is correctly segmented by the algorithm proposed by Rouco and Campilho (2013). The blue line represents the detected lumen axis and the red lines delimit the selected ROI. 30

Figure 3.13 Gradient (blue arrows) assumes opposite directions along the LI contour (green line). 31

Figure 3.14 Comparison between different forms of penalizing pixels which show opposite gradient orientation. (a) $-\infty$. (b) 0. The yellow line represents the FW LI contour. 31

Figure 3.15 Gaussian normal distribution used as membership function for the fuzzy classification of edges ($\sigma FM = 0.5$). 32

Figure 3.16 Proposed membership function for the fuzzy classification of edges ($\alpha = 0.4$; $\beta = 0.6$). 33

Figure 3.17 Comparison between different membership functions for fuzzy classification of edges. (a) Gaussian function. (b) Proposed function. The yellow line represents the FW LI contour. 33

Figure 3.18 The proposed method fails to segment an echolucent LI interface in the NW. The yellow and red lines represent the LI and MA contours, respectively. The white arrow points to the true LI interface. 34

Figure 3.19 Plaque limits in the longitudinal direction. The yellow lines represent the segmented contours of the IM region of the carotid wall. jL and jR are the image columns which correspond to the plaque's left and right limits, respectively. 37

Figure 3.20 Atherosclerotic plaque according to criterion 1 of the medical consensus. The red stripes highlight the plaque's area. The blue and green vertical lines mark the plaque's left and right limits, respectively. The brown dashed line marks the 1.5 mm threshold. 38

Figure 3.21 Atherosclerotic plaque according to criterion 2 of the medical consensus. The blue and green stripes mark the detected left and right plaque flanks, respectively, and the red stripes highlight the plaque's area. 39

Figure 3.22 The left flank of a plaque is detected (blue stripes), but the right one is not. The plaque's right limit (green vertical line) is set to be the last column of the segmented IM region in the opposite direction of the detected flank. The red stripes highlight the plaque's area. 39

Figure 3.23 Depression inside a plaque causes the illusion of a plaque-free region. By comparing the local values of the intima-media thickness inside this region with a reference value we conclude that it is a depression inside a plaque. The blue and green stripes mark the detected left and right plaque flanks, respectively. The red stripes highlight the plaque's area.....40

Figure 3.24 Atherosclerotic plaque according to criterion 3 of the medical consensus. The red stripes highlight the plaque's area. The blue and green vertical lines mark the plaque's left and right limits, respectively. The brown dashed line marks the $IMT_p + 0.5$ mm threshold.....41

Figure 3.25 Estimation of the left surrounding intima-media thickness as the median of the local intima-media thickness of a neighbour region.....42

Figure 3.26 Estimation of the left surrounding intima-media thickness as the Gaussian average of the local intima-media thickness of a neighbour region. 43

Figure 3.27 Block diagram illustrating the proposed methodology for measurement of plaque burden in ultrasound images of the carotid artery. 46

Figure 4.1 GUI for manual segmentation of the IM region of the carotid wall and atherosclerotic plaques in US images of the carotid artery. 49

Figure 4.2 Cumulative distributions of RMSE(GTi; Ai) for the four segmented contours of the IM region using the original (red line) and proposed (blue line) methods. The black vertical line represents an RMSE(GTi; Ai) error of 1 mm. 56

Figure 4.3 Segmentation of the NW improves by increasing the value of k and expanding Ω for the estimation of parameter α. (a) Original method. (b) Proposed method with $k = 1$. (c) Proposed method with $k = 8$. The red and yellow lines represent the automatic MA and LI contours, respectively. The magenta and green lines represent the manual MA and LI contours, respectively. 57

Figure 4.4 Comparison between the two methods used for the segmentation of the IM region. In the top image row the original method is used. In the bottom image row the proposed method is used. The yellow and red lines represent the LI and MA contours, respectively. 58

Figure 4.5 Best and worst results for the segmentation of the IM region of the carotid wall in US images as performed by the proposed method. A, B and C – FW best. D, E and F – NW best. G – FW worst. H – NW worst. The red and yellow lines represent the MA and LI automatically segmented contours, respectively. The magenta and green lines represent the MA and LI manually segmented contours, respectively. 59

Figure 4.6 (a) – εL plotted as a function of h and σ for Gaussian estimation of the surrounding intima-media thickness. (b) – εA plotted as a function of h and σ for Gaussian estimation of the surrounding intima-media thickness. 61

Figure 4.7 (a) – εL plotted as a function of h and l for median estimation of the surrounding intima-media thickness. (b) –εA plotted as a function of h and l for median estimation of the surrounding intima-media thickness. 62

Figure 4.8 Cumulative distributions of (a) $\varepsilon\, Li$ and (b) $\varepsilon\, Ai$ for plaque segmentation using the Gaussian (red line) and median (blue line) estimations of the surrounding intima-media thickness. 63

Figure 4.9 Comparison between the different methods of estimating the surrounding intima-media thickness. (a) Ground truth plaque segmentation. (b) Automatic plaque segmentation using the Gaussian estimation. (c) Automatic plaque segmentation using the median estimation. The green and yellow lines represent the manual and automatic contours of the IM region, respectively, and the segmented plaques are highlighted with a red overlay. 64

Figure 4.10 Cumulative distributions of $\varepsilon\, Li$ and $\varepsilon\, Ai$ for plaque segmentation using different methods of obtaining $IMTP$. (a) $\varepsilon\, Li$ using the GT IM contours. (b) $\varepsilon\, Ai$ using the GT IM contours. (c) $\varepsilon\, Li$ using the automatic IM contours. (d) $\varepsilon\, Ai$ using the automatic IM contours. 66

Figure 4.12 Cumulative distributions of (a) $\varepsilon\, Li$ and (b) $\varepsilon\, Ai$ for the plaque segmentation using the proposed method. 69

Figure 4.13 Examples of the best plaque segmentations performed by the proposed method for the FW (bottom two image rows) and NW (top two image rows) of the carotid artery. (a) GT plaque segmentation. (b) Automatic plaque segmentation. The green and yellow lines represent the manual and automatic contours of the IM region, respectively, and the segmented plaques are highlighted with a red overlay. 71

Figure 4.14 Examples of the worst plaque segmentations performed by the proposed method. In the top image row noisy IM contours lead to the segmentation of an inexistent plaque in the FW. In the bottom image row the segmentation of the LI interface fails and a NW plaque is not segmented. (a) GT plaque segmentation. (b) Automatic plaque segmentation. The green and yellow lines represent the manual and automatic contours of the IM region, respectively, and the segmented plaques are highlighted with a red overlay. 72

Figure 5.1 Proposed CAD system for automatic measurement of PB in US images of the carotid artery.....73

Figure 5.2 CAD system for automatic measurement of PB in US images of the carotid artery. (a) By clicking on the "Segment Contours" button the segmented contours of the carotid wall become visible in the image, represented by yellow lines. (b) By clicking on the "Segment Plaque" button the segmented atherosclerotic plaques are superimposed in the image as a red overlay. A textbox containing the quantitative characterization of each segmented plaque becomes visible, including its length and area, the image plaque burden and also the average and maximum values of the intima-media thickness. (c) By clicking on the "Show Maximum IMT" button the region of the carotid wall which shows the maximum intima-media thickness is highlighted by a green vertical line. 75

List of tables

Table I Parameters of the original method for the segmentation of the IM region. 29

Table II Parameters of the proposed method for the segmentation of the intima-media region. 35

Table III Optimum parameter values for the two methods used for lumen axis detection. 52

Table IV Quantitative comparison between the two methods used for lumen axis detection. 53

Table V Values set for λe (Rocha, Silva and Campilho (2012)). 54

Table VI Optimum parameter values for the two methods used for segmenting the LI contour. 54

Table VII Optimum parameter values for the two methods used for segmenting the MA contour. 55

Table VIII Quantitative comparison between the two methods for segmenting the IM region. 55

Table IX p-value of KW comparing the two methods for segmenting the IM region. ..56

Table X Optimum parameter values for Gaussian estimation of the surrounding intima-media thickness. 61

Table XI Optimum parameter values for median estimation of the surrounding intima-media thickness. 62

Table XII Quantitative comparison of the two methods for the estimation of the surrounding intima-media thickness. 63

Table XIII p-value of KW comparing the two methods for the estimation of the surrounding intima-media thickness. 63

Table XIV Quantitative comparison of different methods to obtain the normal intima-media thickness for the patient. 65

Table XV Quantitative comparison of different criteria to define plaque and their combination. 67

Table XVI p-value of KW comparing different criteria to define plaque and their combination. 67

Table AI Reference values for the normal intima-media thickness of the common carotid artery provided by large European cohort studies (Stein *et al. 2008*). 87

List of abbreviations

Carotid Atherosclerosis Progression Study	CAPS
Centro Hospitalar São João	CHSJ
Common carotid artery	CCA
Computer-assisted diagnosis	CAD
Degree of stenosis	%ST
Dynamic programming	DP
Edinburgh Artery Study	EAS
External carotid artery	ECA
Far-end wall	FW
Graphical user interface	GUI
Ground truth	GT
Instantaneous coefficient of variation	ICOV
Internal carotid artery	ICA
Intima-media	IM
Intima-media thickness	IMT
Kruskal-Wallis statistical test	KW
Lumen-intima	LI
Maximum plaque thickness	MPT
Media-adventitia	MA
Median	med
Median absolute deviation	MAD
Near-end wall	NW
One-dimensional	1D
Plaque burden	PB
Power Doppler imaging	PDI
Region of interest	ROI
Step edge	SE

Three-dimensional	3D
Total plaque area	TPA
Two-dimensional	2D
Ultrasound	US
Valley shaped edge	VE

1 Introduction

1.1 Motivation

Atherosclerosis is a vascular disease that constitutes one of the main causes of death and permanent disability in developed countries, being the leading underlying cause for myocardial infarction (heart attack) and stroke. In most cases, it is asymptomatic and can only be diagnosed when it leads to a cardiovascular or cerebrovascular event. It is of great interest to find markers with high predictive value that allow an early detection and diagnosis of atherosclerosis to reduce its morbidity and disability rates.

Markers based on medical imaging have a significant edge over classical clinical markers as they take advantage of the recent technological advances in electronics, visualization technologies and computer science. These markers constitute objective and reproducible measures which can be used to perform an early and reliable diagnosis of atherosclerosis, evaluate its progression in order to direct the course of treatment and make decisions about surgical procedures such as endarterectomy (Fenster *et al.*, 2008).

One of these imaging-based markers is plaque burden (PB), which quantifies the amount of atherosclerotic plaque present in diseased arteries. It has proven to be useful in the diagnosis and grading of atherosclerosis, monitoring and following the efficacy of anti-atherosclerosis therapies, and predicting cardiac and cerebrovascular events. As the formation of plaques occurs late in the pathology's course of progression, PB is especially useful and important for diagnosing atherosclerosis when the disease is in its later stages (Sillesen *et al.*, 2012).

Ultrasound (US) is the most used imaging modality to visualize the carotid artery and diagnose atherosclerosis due to several advantages: requires relatively inexpensive and portable equipment, provides high resolution and real-time images without exposing the patient to harmful radiation and it is used as a non-invasive imaging modality. For measuring PB in US images of the carotid artery, a prior detection and segmentation of atherosclerotic plaques is needed. This segmentation is still performed manually by clinical experts. It has the disadvantage of being time-consuming, which limits the amount

of exams and patients that can be subjected to diagnosis. It is also subjective, as different clinical experts will have different opinions and criteria on the same exam, depending on their experience, knowledge and physical capacities, such as visual acuity (Nikolaides *et al.*, 2012). A computer-assisted diagnosis (CAD) system that helps clinicians and clinical experts to detect, segment and quantify atherosclerotic plaques would increase accuracy and reproducibility, reducing subjectivity and the time of analysis.

The present work was conducted within the Biomedical Imaging Laboratory of INESC TEC, based on the past experience of the team in the development of algorithms for the automatic detection and segmentation of the carotid artery in US images. A new algorithm was proposed for the automatic detection of the carotid lumen based on local phase symmetry patterns (Rouco and Campilho, 2013), and several methods for the automatic segmentation of the anatomical layers of the carotid wall have been reported by the group (Rocha, 2007; Rocha *et al.*, 2010, 2011; Rocha, Silva and Campilho, 2012). This research has been conducted with the department of Neurosonology of Centro Hospitalar São João (CHSJ), led by Doctor Elsa Azevedo, who has provided the US images of the carotid artery and the clinical expertise required for the validation of the proposed methods. However, no algorithms or methods have been developed by the group for the segmentation of atherosclerotic plaques or measurement of plaque burden.

1.2 Objectives

The main objective of the present work is to develop a robust and accurate fully automatic CAD system for measuring PB in two-dimensional (2D) US B-mode images of the common carotid artery (CCA). This purpose requires computer algorithms that:

- Segment the contours of the different anatomical layers of the carotid wall.
- Segment atherosclerotic plaques, based on objective criteria to define plaque proposed in a European medical consensus (Touboul *et al*., 2012).
- Integrate the segmentation of atherosclerotic plaques in a graphical user interface (GUI) for the automatic measurement of PB.

1.3 Contributions

A fully automatic CAD system for measuring PB in 2D B-mode US images of the CCA was developed.

A novel method for the segmentation of atherosclerotic plaques is proposed. This method uses objective criteria to define atherosclerotic plaque proposed in a European medical consensus (Touboul *et al*., 2012), together with the segmentation of the different

anatomical layers of the carotid wall. This segmentation is required to obtain local measures of the thickness of these layers, which are the basis for the definition of plaque according to these criteria.

For the automatic segmentation of the carotid wall, the algorithm proposed by Rocha, Silva and Campilho (2012) is used as reference and modified to improve the segmentation in images affected by speckle noise. The following optimizations are introduced: use of an alternative method for lumen detection based on local phase symmetry patterns at appropriate scale of analysis (Rouco and Campilho, 2013); relaxation of the constraints imposed to the contour; use of a new membership function for the fuzzy classification of edges that uses more image information, such as the edge strength; local estimation of the strength of false edges caused by noise in the lumen, calculated through robust statistics, to help defining the penalty and gain terms of this function.

A GUI was developed for the calculation of PB. It allows to select the image, automatically segment the atherosclerotic plaques and quantitatively characterize the length and area of each plaque. The image PB is expressed as the sum of all the plaque areas in the image. The average and maximum value of the local intima-media thickness are also presented.

1.4 Thesis overview

The thesis is divided in six chapters. The motivation and the objectives have already been described in this chapter.

Chapter 2 describes the anatomy of the carotid artery, the pathologic mechanism for the development of atherosclerosis and the diagnosis of the disease using different markers based on medical imaging. The current techniques used to measure PB and segment atherosclerotic plaques and the arterial wall in US images of the carotid are briefly described.

Chapter 3 describes a novel method proposed for plaque segmentation that uses objective criteria to define atherosclerotic plaque proposed in a medical consensus (Touboul *et al*., 2012). These criteria are based on measures of the carotid wall thickness and so its anatomical layers are segmented in order to calculate these measures.

Chapter 4 describes the experimental evaluation of the proposed method for plaque segmentation, including a description of the image database, acquisition of manual segmentations to be used as ground truth, metrics and statistics for the quantitative assessment of the method's performance, parameter optimization and selection among alternative methods to be used in the different stages. In the end of the chapter, a global evaluation of the proposed method is provided, along with segmentation examples.

Chapter 5 describes the proposed CAD system for measuring PB in US images of the carotid artery, based on the results of the experimental evaluation described in the previous chapter.

Chapter 6 summarizes the conclusions of the research reported in this dissertation and discusses future work.

2 Methods for measuring plaque burden

This chapter describes the basic anatomy of the carotid artery, the pathological mechanisms that lead to the development of atherosclerosis and the diagnosis of the disease using markers based on medical imaging, with emphasis on plaque burden (PB) and intima-media thickness (IMT). The current techniques used to measure PB, segment atherosclerotic plaques and the carotid wall in ultrasound (US) images of the carotid artery are described.

2.1 Anatomy of the carotid artery

The carotid artery is responsible for supplying with arterial blood the head, neck and all its organs, tissues and structures. It is a paired artery, meaning that there is a left and right carotid. It is divided in different segments: common carotid (CCA), carotid sinus or bifurcation, internal (ICA) and external (ECA) carotid artery, as shown in figure 2.1 (a). Like in every artery, the carotid wall is composed of three anatomical layers, the intima, the media and the adventitia, shown in figure 2.1 (b) (O'Rahilly, and Müller, 1983).

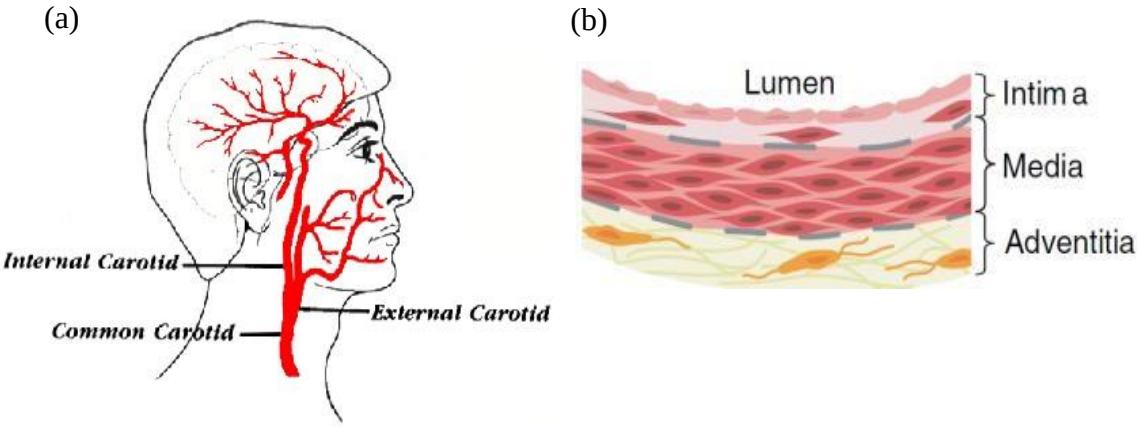

Figure 2.1 (a) Arterial tree of the right carotid (terrykingmd.com). (b) Anatomy of the arterial wall with its different layers (Wikstrand, 2007).

2.2 Atherosclerosis

Atherosclerosis is a complex and profound modification of the arterial wall physiognomy characterized by the formation of complex lesions called atherosclerotic plaques. The disease has several stages of development. In the early stages, a thickening of the arterial wall occurs due to the accumulation of cholesterol and triglycerides. This progressive enlargement eventually leads to the formation of plaques. According to the current medical consensus (Touboul *et al*., 2012), an atherosclerotic plaque can be defined as a focal structure that encroaches into the arterial lumen of at least 0.5 mm or 50% of the surrounding intima-media thickness value or demonstrates a thickness greater than 1.5 mm (see figure 2.2). These criteria help clinicians to differentiate a plaque lesion from a global thickening of the arterial wall which may be due to non-atherosclerotic mechanisms.

With the progressive accumulation of lipids and dead cells inside the plaque, its protrusion into the vessel's lumen increases. This leads to a thinning and weakening of the fibrous cap that encapsulates the growing necrotic core. These plaques become vulnerable and prone to rupture. Eventually, the fibrous cap breaks and the plaque's content is exposed to the blood flow, followed by a clotting process. The clot may be enough to completely obstruct the blood flow. The obstruction can also be caused by clot or plaque fragments that are released into the blood stream, reaching narrower arteries. The lack of blood supply is the cause of myocardial infarction, if it happens in the coronary arteries, as shown in figure 2.3 (a), or stroke, if it happens in the cerebral arteries, as shown in figure 2.3 (b) (Davis, 2005).

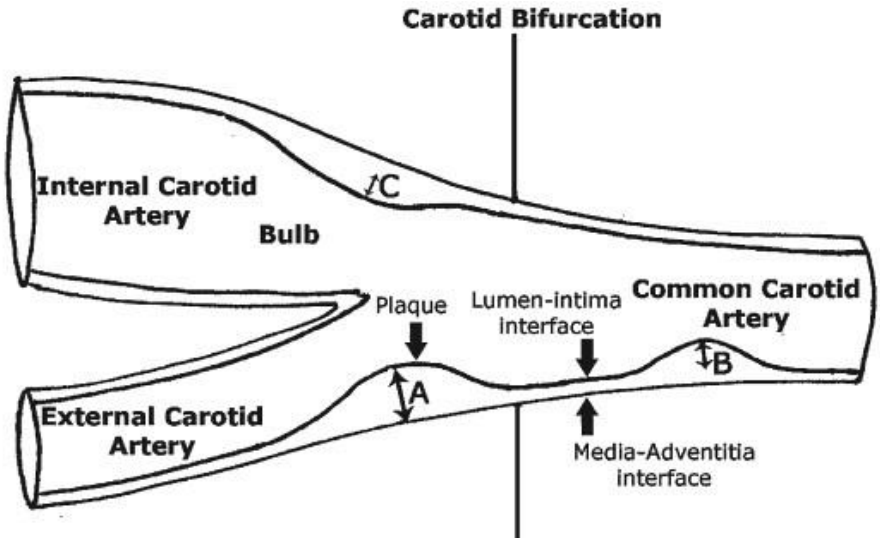

Figure 2.2 Schematic diagram representing the carotid arterial tree and the three definitions of plaque proposed in the medical consensus (Touboul et al., 2012). A – Intima-media thickness > 1.5 mm. B – Lumen encroachment > 50% of surrounding intima-media thickness value. C – Lumen encroachment > 0.5 mm (Aznaouridis, Dhawan and Quyyumi, 2010).

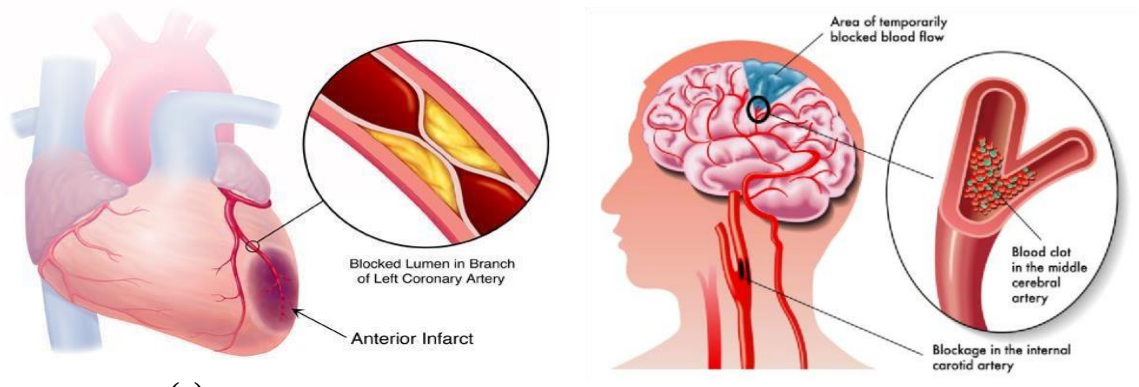

(a) (b)

Figure 2.3 (a) Myocardial infarction caused by coronary heart disease (medimoon.com). B – Ischemic stroke, caused by a blood clot that interrupts the blood flow of a cerebral artery (jellygamatt.com).

2.3 Diagnosis of atherosclerosis

Atherosclerosis can progress through its different stages without causing any clinical symptoms and may go completely unnoticed until the blood supply to an area of the heart or brain is severely narrowed or blocked, causing a heart attack or stroke. Ideally, the diagnosis should be performed while atherosclerosis is still in its early stages, thus preventing cardio and cerebrovascular events (Simon, Chironi and Levenson, 2006). It is important to find markers with high predictive value for the different stages of the disease, in order to provide a reliable early diagnosis and to enable the evaluation of its severity, the monitoring of its development and the validation of the treatment effects.

While fully developed atherosclerosis is evidenced by plaque formation, early stages of the disease are characterized by a thickening of the arterial wall, and also by hardening of the tissues and loss of some of its elasticity. Based on the disease's physiology, several image markers have been proposed to diagnose atherosclerosis in its different stages.

Intima-media thickness is the combined thickness of the intima and media layers of the carotid wall, as shown in figure 2.4.

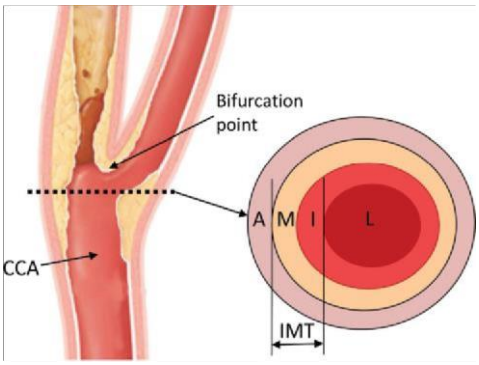

Figure 2.4 Bifurcation of the carotid artery, showing atherosclerotic plaques, and a cross-section of the carotid artery. The IMT is the combined thickness of the intima and media layers (Yang *et al.*, 2012).

IMT has been validated as a measure of risk of cardiovascular events and atherosclerosis disease burden (Amato *et al.*, 2007; Lorenz *et al.*, 2007). It can predict possible future enlargement of vessel walls and help in the prevention of plaque formation in the early stages of the disease when no plaque is present. However, in some situations the enlargement of the arterial wall occurs due to natural compensatory mechanisms of the body (Costanzo *et al.*, 2010; Vukusich *et al.*, 2010).

Markers that assess the elasticity and stiffness of the arterial tissue are also suitable for early diagnosis of atherosclerosis. Examples of these markers are: ankle-brachial pressure index, which represents the ratio between the systolic blood pressure in the lower legs and the systolic blood pressure in the arms; pulse pressure, which is the difference between the systolic and diastolic pressure readings; pulse wave velocity, which characterizes the movement of pressure waves down the vessel (Nichols *et al*., 2008).

In more advanced stages of atherosclerosis, other imaging-based markers are used, such as: degree of stenosis, blood velocity, plaque morphology and lipid content of the necrotic core. These markers evaluate the risk of plaque rupture and occurrence of thromboembolic events (Schaub *et al*., 2012).

The degree of stenosis (%ST) is the most frequently used marker to predict future strokes. It establishes a comparison between a narrowed and a healthy and plaque-free lumen section and is calculated as shown in figure 2.5. %ST determines if a surgical intervention (endarterectomy) should be performed in asymptomatic patients.

Measures that quantify the amount of atherosclerotic plaque in a diseased artery are regarded as plaque burden. Different studies have shown that PB is useful for detection and diagnosis of atherosclerosis (Pollex *et al.*, 2005), monitoring the efficacy of antiatherosclerosis therapies (Ainsworth *et al.*, 2005; Wannarong *et al.*, 2013), and has a good predictive value when it comes to cardiac and vascular events (Spence *et al.*, 2002; Störk *et al.* 2004; Sillesen *et al.*, 2012). The present work is centred on the use of this marker because few studies focus on its potential for diagnosing atherosclerosis, and it has been reported that it has a higher predictive value for cardiovascular events when compared to other markers for the disease (Johnsen *et al*., 2007; Finn, Kolodgie and Virmani, 2009; Sillesen *et al*., 2012).

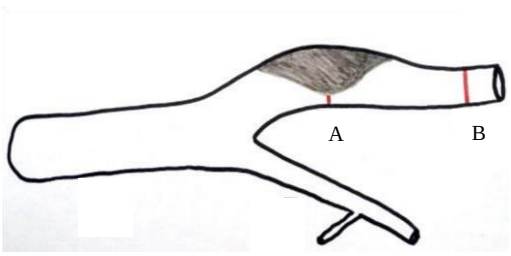

$$\%ST = (1 - \frac{A}{B}) \times 100$$

Figure 2.5 Calculation of the degree of stenosis (Berletti *et al*., 2014).

IMT, PB and %ST can be evaluated through invasive and non-invasive techniques, but external ultrasound is the imaging modality which is most frequently used.

2.4 Ultrasound imaging of the carotid

US is the most used imaging modality for the diagnosis of atherosclerosis in the carotid artery due to several advantages: it requires relatively inexpensive and portable equipment; provides high resolution and real-time images without exposing the patient to harmful radiation; in most of its diagnostic applications US is used as a non-invasive imaging modality. It relies on the sound propagating properties of different human tissues. When a US wave travels through a particular tissue and reaches the anatomical barrier that separates a tissue with different composition and structure, part of the wave is reflected on this interface, and the other part is transmitted (assuming that the sound wave reaches the interface in a perpendicular fashion). If the new tissue has high acoustic impedance, the majority of the US wave is reflected back to the source (the transducer/probe held by the operator) as an echo, producing a high-contrast image. There are different types of US that essentially differ on how the echo information is extracted and presented (Hofer, 2005).

Two-dimensional (2D) B-mode US is frequently used for studying the carotid's anatomy and to diagnose atherosclerosis. In B-mode images, the brightness depends on the echo's intensity. The tissue areas in the B-mode image can be characterized as hyperechoic (great amount of energy from returning echoes results in white pixels), hypoechoic (low amount of energy from returning echoes results in grey pixels) or anechoic (no returning echoes, originates black pixels), as shown in figure 2.6. The acoustic impedance of a tissue is directly proportional to the energy of the returning echoes. The greatest reflection of echoes back to the probe comes from interfaces between tissues with the greatest differences in acoustic impedance.

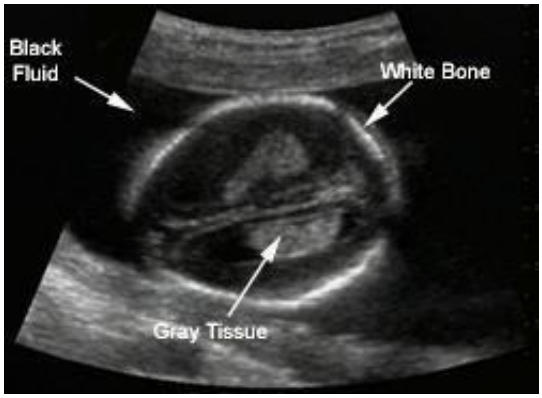

Figure 2.6 Hyperechoic (bone), hypoechoic (grey tissue) and anechoic (black fluid) structures in US image (fetal.com).

B-mode images can be complemented with information from Doppler ultrasound. Doppler US is based on the Doppler Effect, in which a shift in the frequency of the reflected US wave occurs due to the relative movement between the echo source (transducer) and the target physical interface. There are two modes of Doppler US: colour Doppler and power Doppler imaging (PDI). In colour Doppler, the venous and arterial blood flows are filled with different colours, allowing the determination of their direction and the distinction between types of blood (Eagle, 2006). In PDI, a special processing is used to display the amplitude or strength of the Doppler signal, instead of the velocity and directional information represented in colour Doppler (Hudson-Dixon, Long and Cox, 1999). Duplex images result from the overlap of a 2D B-mode and a Doppler image acquired simultaneously with a single scan. This is especially useful in the segmentation of echolucent plaques, which are very difficult to discriminate in a B-mode image, as shown in figure 2.7.

Three-dimensional (3D) imaging, which is also possible with US, allows a multi-angle visualization, measurement and characterization of plaques, and therefore has a greater informative value when compared to 2D projections (Fenster, Parraga and Bax, 2011). An example of a 3D US B-mode image is shown in figure 2.8.

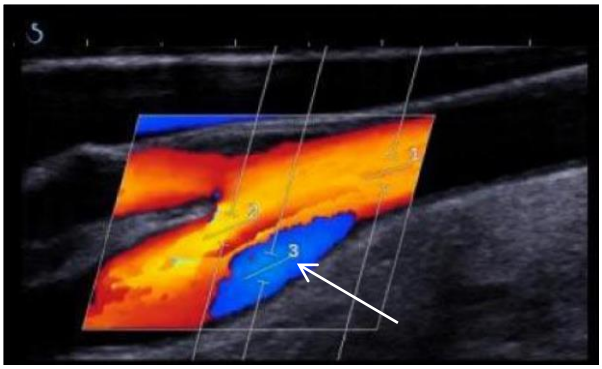

Figure 2.7 Duplex US image of the carotid. The white arrow highlights a plaque (supersonicimagine.com).

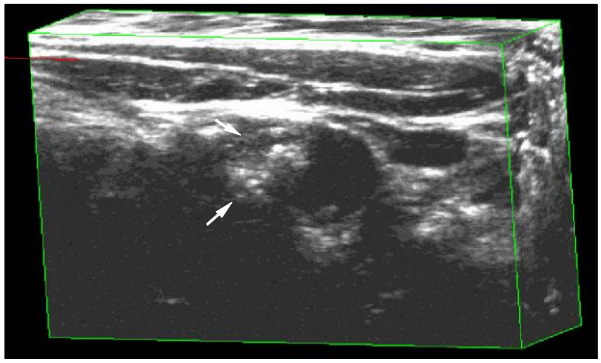

Figure 2.8 3D US image of a diseased carotid artery obtained through the mechanical linear scanning process. The white arrow highlights a plaque (Fenster, Downey and Cardinal, 2001).

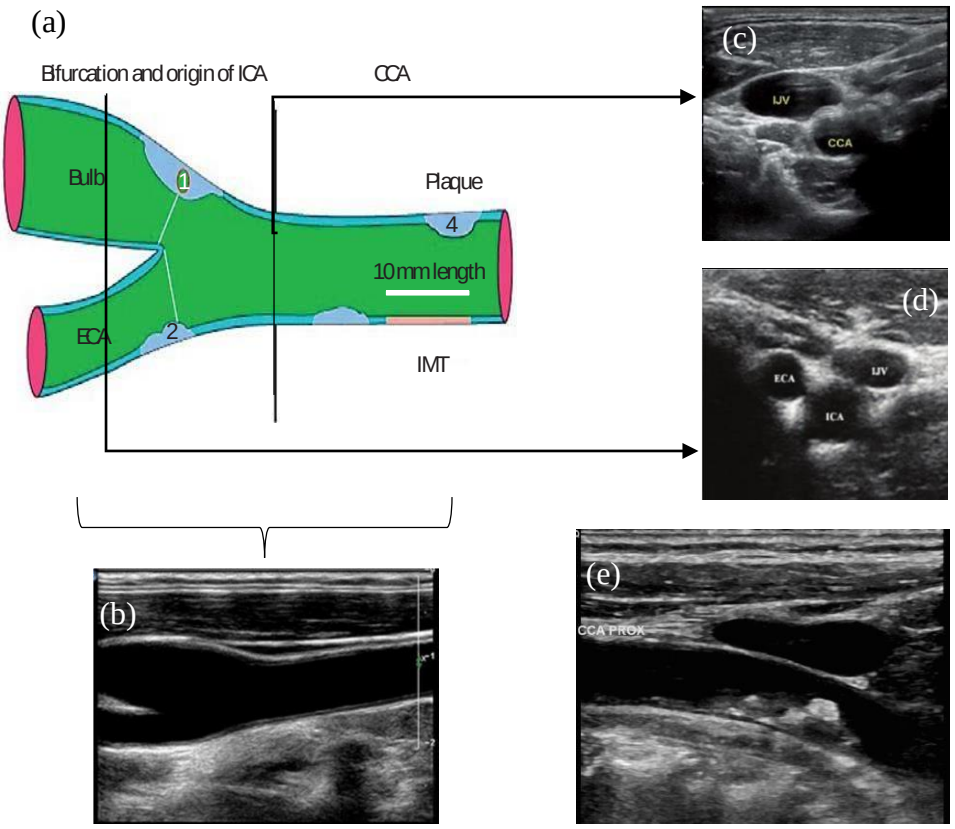

Figure 2.9 (a) Schematic representation of the carotid tree (Touboul *et al.*, 2012). (b) Longitudinal slice including the bifurcation and portions of the CCA, ICA and ECA (cardiologydoc.wordpress.com). (c) Transverse slice acquired upstream of the bifurcation (aeronline.org). (d) Transverse slice acquired downstream of the bifurcation (annalsofian.org). (e) Atherosclerotic plaque in the CCA (theskepticalcardiologist.com).

US images of the carotid can be longitudinal or transverse. Figure 2.9 shows transverse and longitudinal slices targeted on the artery's different segments.

Longitudinal slices can be targeted on the CCA, bifurcation, ICA and ECA, as shown in figure 2.9 (b). The bifurcation has turbulent hemodynamics of the blood flow and plaque formation usually occurs at this spot. Longitudinal US images are better suited for the detection and segmentation of plaques in this site, and also for measuring the intima-media thickness. In longitudinal views, the carotid wall is seen as a regular stripe pattern that correlates with its anatomical layers**.** In plaque-free regions, the stripe pattern is constituted by two almost parallel echogenic lines appearing with bright intensity, the tunica intima and adventitia, separated by a darker, hypoechogenic region which corresponds to the tunica media. When a plaque is present, a thickening of the intima-media layer occurs, increasing the area of the hypoechogenic region and the spacing between the two bright lines, as shown in figure 2.9 (e). Plaques can have different echogenicity and texture.

Transverse slices are required for 3D US image reconstruction and for a more complete documentation of the carotid artery. They can be targeted on any segment of the carotid artery, as shown in figure 2.9 (c) and (d).

There are some difficulties associated to the US image acquisition as it is highly operator-dependent and images may have low quality due to noise, speckle, shadowing, contrast variations and movement artifacts.

2.5 Plaque burden measurement

Plaque burden measures can range from the simple accounting for the number of plaques to measures with one (1D), two or three dimensions such as plaque thickness, length, area or volume, respectively.

The number of atherosclerotic plaques can be accounted along a pre-determined extension of the artery. However, the number of plaques does not show the extent of atherosclerosis of a certain patient, because a large number of small plaques may be less dangerous for the patient's health than one large plaque that is causing serious lumen stenosis and compromising the blood flow (Falk, Prediman and Fuster, 1995). This is why some studies rank the plaques in classes according to their degree of protrusion into the vessel's lumen (Störk *et al.*, 2004; van der Meer *et al.*, 2004).

1D measures, such as maximum plaque thickness (MPT), are another way of expressing PB. MPT is defined as the greatest prominence found in any of the three carotid segments. Its measurement can be performed in longitudinal and transverse US views (see figure 2.10). It is a useful measure, as it enables the calculation of %ST if the luminal diameter in a plaque-free region is known (Elkind *et al.*, 2010).

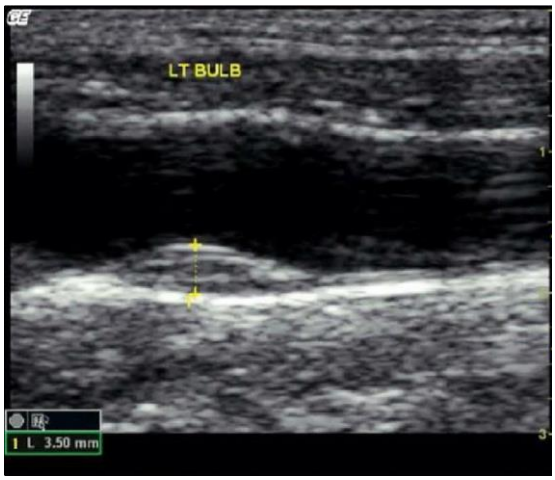

Figure 2.10 Maximum plaque thickness is highlighted by the yellow crosshairs (Callahan *et al.*, 2012).

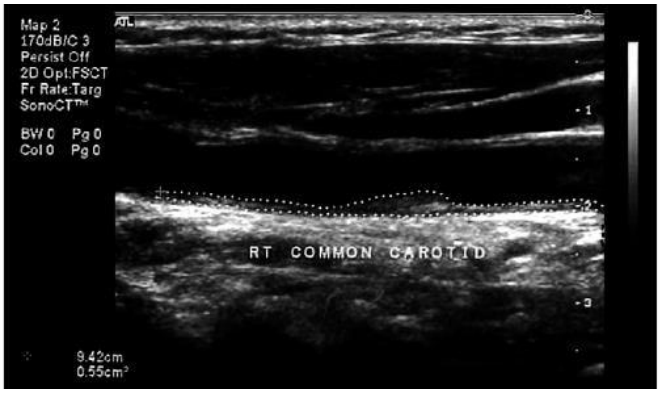

Figure 2.11 Measuring plaque area as performed by Spence *et al.* (2002). This particular plaque is in the right CCA and measures 0.55 cm^2.

Other studies have expressed PB as total plaque area (TPA), which is the sum of the areas from all the plaques found in the different carotid segments. This requires a prior segmentation of the plaques boundaries, which is usually performed manually. Figure 2.11 shows the area measurement of a plaque which was manually segmented in a longitudinal plane, as performed by Spence *et al.* (Spence *et al.*, 2002; Spence, Matthew and Hegele, 2003; Al-Shali *et al.*, 2005; Mallett *et al.*, 2009).

Volume measurements provide the most complete information about the degree and progression of atherosclerosis, as they take into consideration the plaque's 3D structure. They allow a real-time following of the plaque growth rates, enabling an accurate evaluation of the effects of anti-atherosclerosis therapies. However, these methods require expensive equipment for the US image acquisition and complex computer software to perform image reconstruction from 2D projections (Fenster *et al.*, 2008). Sillesen *et al.* (2012) measured plaque volume in 2D B-mode US transverse slices of the carotid artery arranged in a digital video. Semi-automatic software was used to assess the presence of plaque and quantification of the plaque's area in each video frame. The calculated areas were summed and multiplied by the inter-slice distance, defining the patient's total plaque volume. This procedure is shown in figure 2.12.

In the present work, PB is expressed as TPA, and it is calculated as the sum of the areas of the plaques present in a longitudinal 2D B-mode US image of the CCA. TPA comprises information regarding each plaque in a 2D plane, and therefore is more useful and complete when compared to 1D measures. Additionally, this measure can be extracted from 2D US projections of the carotid artery, which is the most common and easily available image type, and does not require the complex and expensive equipment that is needed for 3D measures. For measuring TPA, a prior segmentation of the atherosclerotic plaques in the US image is required. Current techniques for plaque segmentation are discussed in the next section.

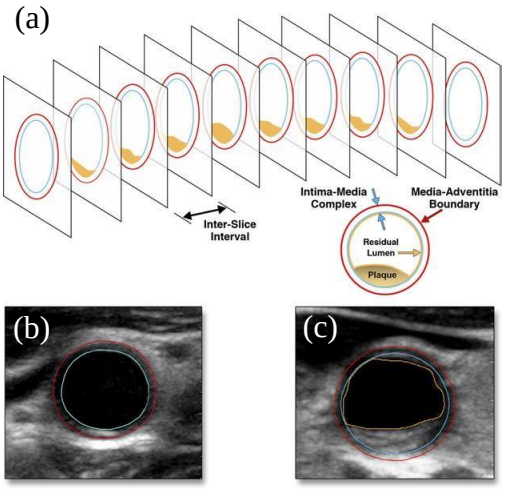

Figure 2.12 (a) A segment of the carotid artery containing a plaque (orange) is scanned with a linear array transducer as a series of transverse slices. (b) CCA with no plaque. The blue and red borders represent the lumen-intima and media-adventitia boundaries, respectively. (c) CCA with plaque. The orange border represents the boundary of the plaque (Sillesen *et al.*, 2012).

2.6 Plaque segmentation

There are currently no fully automatic methods for the segmentation of atherosclerotic plaques in US images of the carotid artery. This segmentation is still performed manually by clinical experts. Plaque segmentation usually needs complementary information from

Doppler US for a more reliable and correct demarcation of the plaque's boundaries (Schminke *et al.*, 2000; Afonso *et al.*, 2012). M'Ath® is a commercially available software tool dedicated to the measurement of the intima-media thickness, %ST and atherosclerotic plaques. The plaque segmentation in US images is done with an edge detection-based algorithm, and studies that used this software for plaque boundary demarcation report high reproducibility (Touboul *et al*., 2005; Kuo *et al*., 2012).

A review of the current techniques for plaque segmentation in carotid US images and video is provided in (Loizou *et al.*, 2014). The reviewed methods are based on Canny edge detection, morphological-based approaches, Kalman filtering, Bayesian model, Hough transform and deformable models, such as active contours (snakes).

Loizou *et al.* have developed several algorithms for plaque segmentation in US images and video of the carotid artery based on snakes (Loizou *et al*. 2007a, 2007b, 2012, 2014). Figure 2.13 shows an example of a successful plaque segmentation achieved by active contours. However, this type of segmentation always needs some kind of manual initialization of the snake so it is placed as close as possible to the real contour, otherwise it may be trapped in local minima or false edges in an iterative process, converging to the wrong location (Molinari *et al*., 2012) This reduces the potential of active contours of being used as a fully automatic method for plaque segmentation.

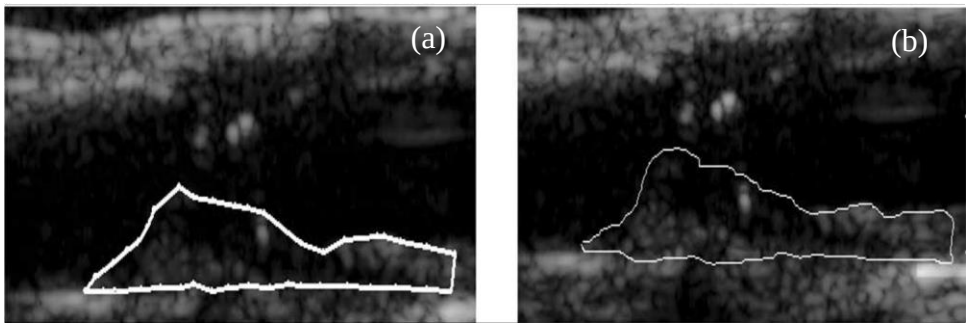

Figure 2.13 Plaque segmentation results on a longitudinal US B-mode image of the carotid artery. (a) Manual segmentation performed by expert. (b) Active contour segmentation (Loizou *et al.*, 2007b).

Plaques can be segmented using a prior extraction of the anatomical layers of the carotid wall. Once the contours of these layers are segmented across the entire image length, local measures of their thickness can be calculated. These measures can then be evaluated along the carotid wall according to objective criteria to define atherosclerotic plaque proposed in a European medical consensus (Touboul *et al*., 2012).

Several computer-assisted techniques have been proposed for the segmentation of the carotid wall in US images. These methods can be divided in two categories: 1) the ones that extract the different anatomical layers along the entire US image and 2) the ones that are specifically designed to measure the intima-media thickness, and therefore perform this segmentation in a narrow region of interest of the carotid wall, where the double-line pattern is clearly visible. Examples of the latter are the commercially available systems AutoIMT™ (Samsung Medison) and QuickIMT (Ultrasonix). For the segmentation of atherosclerotic plaques according to the aforementioned criteria to define plaque a complete segmentation of the carotid wall across the entire image length is required.

Delsanto *et al*. (2005, 2006 and 2007) proposed a completely automatic method for the segmentation of the carotid wall, called Completely User-independent Layers Extraction. It uses a fuzzy K-means algorithm for the estimation of local statistics calculated on pixel intensity values for contour initialization and gradient-based snake segmentation for contour refinement. This method requires no user intervention. It has shown to perform an effective segmentation of both echogenic and echolucent plaques present in the nearend wall (NW) and far-end wall (FW), as shown in figure 2.14. The contours traced by this method are statically comparable to the ones of a human trained operator. However, the algorithm showed limitations in the segmentation of calcified plaques. Also, it cannot provide real-time segmentation, taking in average 50s per plaque. This is due to the integration of different image analysis techniques, such as local statistics, gradient estimation and snake-based segmentation (Suri, Chirinjeev and Molinari, 2011).

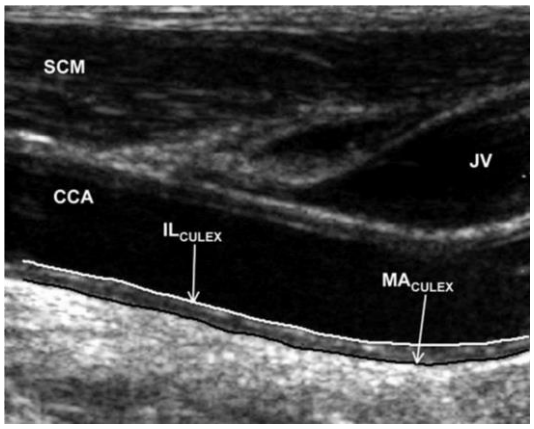

Figure 2.14 Carotid wall segmentation performed by the method proposed by Delsanto *et al*. (2005, 2006 and 2007). IL$_{CULEX}$ and MA$_{CULEX}$ represent the segmented contours of the lumen-intima and media-adventitia interfaces of the FW, respectively. SCM and JV stand for sternocleidomastoid muscle and jugular vein, respectively (Delsanto *et al*., 2007).

In this work, a complete segmentation of the carotid wall is required. The method that performs this segmentation is based on the one proposed by Rocha, Silva and Campilho (2012). Examples of the segmentation performed by this method are shown in figure 2.15.

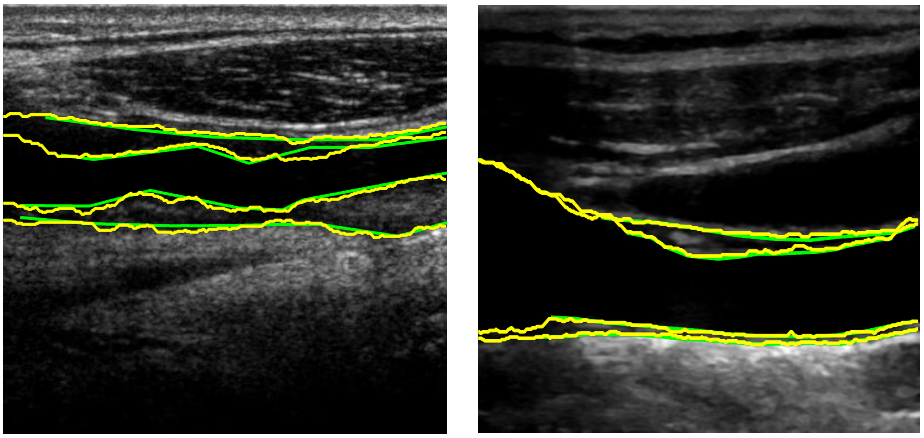

Figure 2.15 Segmentation of the carotid wall in US images of the carotid artery performed by the method proposed by Rocha, Silva and Campilho (2012). The yellow lines represent the automatically segmented contours, and the green lines represent the manual tracings performed by a clinical expert.

2.7 Concluding remarks

Atherosclerosis is a vascular disease that causes thousands of deaths and disabilities every year. In most cases, the disease is asymptomatic. Imaging-based markers for diagnosing atherosclerosis have shown a growing potential with the recent technological advances in medical imaging.

Plaque burden is an imaging-based marker which quantifies the amount of plaque that is present in diseased arteries and is useful for the diagnosis of atherosclerosis in its later stages, monitoring the progression of the disease and its response to different therapies.

2D measures for expressing PB, such as total plaque area, have a greater informative value when compared to 1D measures and do not require expensive and complex equipment. For measuring PB, a segmentation of atherosclerotic plaques is required.

Currently, there are no automatic methods for segmenting atherosclerotic plaques in US images. This segmentation can be performed using local measures of the thickness of the carotid wall and standard criteria to define plaque based on these measures. For this, a prior segmentation of the different interfaces of the carotid wall is required, for which there are many automatic and semi-automatic methods.

3 Methodology

In order to measure plaque burden (PB), a segmentation of the atherosclerotic plaques in the ultrasound image (US) is needed. In this chapter, a novel method to perform this segmentation is proposed. This method uses a prior segmentation of the carotid wall to extract its anatomical layers. Local measures of the thickness of these layers are computed and used to segment plaques according to objective criteria provided by a European medical consensus (Touboul *et al*., 2012).

Section 3.1 presents the different techniques of signal processing and image analysis that are used. Section 3.2 provides an overview of the two main steps of the proposed method for plaque segmentation. Section 3.3 describes the method used for the segmentation of the contours of the carotid wall. Section 3.4 describes how plaque delimitation is performed using the segmented contours. Section 3.5 describes how PB is measured once the atherosclerotic plaques are segmented. Section 3.6 provides a summary of the methodology followed in this work.

3.1 Basic concepts

The signal processing and image analysis techniques used in the proposed method for plaque segmentation are: edge detection using the instantaneous coefficient of variation, fuzzy classification of edges, robust statistics, dynamic programming and convolution of one-dimensional signals.

3.1.1 Instantaneous coefficient of variation

Speckle is a multiplicative type of noise characteristic of US imaging which causes contrast and resolution reduction, texture degradation and may create gaps on continuous anatomical boundaries (Loizou, 2005). The instantaneous coefficient of variation (ICOV) is an edge detector that performs well in images affected by speckle noise, and therefore is well adapted for US images (Yu and Acton, 2004; Rocha *et al.*, 2010).

The ICOV value at an image pixel (i, j) is calculated as:

$$\mathrm{ICOV(i,j)} = \sqrt{\frac{\left|\frac{1}{2}\|\nabla I(i,j)\|^2 - \frac{1}{16}(\nabla^2 I(i,j))^2\right|}{(I(i,j)+\frac{1}{4}\nabla^2 I(i,j))^2}} \tag{3.1}$$

where $I(i, j)$ is the image, $\nabla I(i, j)$ is the image gradient, $\nabla^2 I(i, j)$ is the image Laplacian, $\|\nabla I(i, j)\|$ is the magnitude of the image gradient and $|\ |$ is the absolute value. The ICOV combines the image intensity with first (gradient) and second (Laplacian) derivative operators, which are commonly used for edge detection in image processing.

Figure 3.1 shows an example of edge detection using the ICOV in a US image of the carotid artery. It is now necessary to discriminate edges that are actual boundaries from false edges caused by speckle noise. Both types of edges are pointed-out by white arrows.

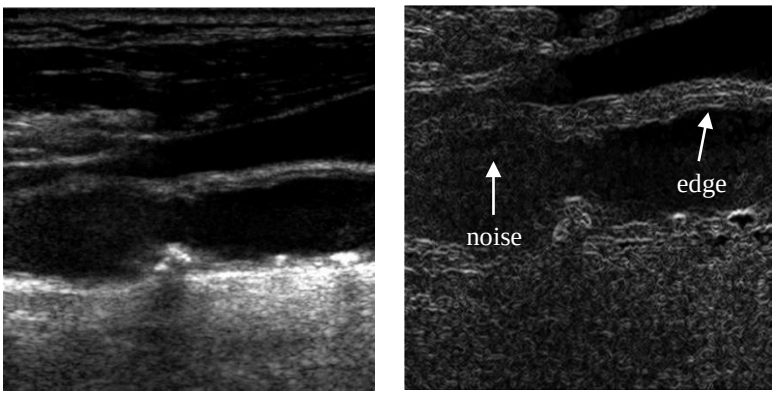

Figure 3.1 Edge detection using the ICOV in a US image of the carotid artery.

3.1.2 Fuzzy classification

In general, classification methods allow to organize a complex dataset by grouping its samples into classes. In traditional binary or crisp classification, the likelihood of a sample belonging to a given class (degree of membership) is either 1, if that class is the best fit, or 0, if it is not. In fuzzy classification, a sample can have different degrees of membership to different classes, ranging from 0 to 1, which are calculated through the class membership function. This type of classification is more appropriate to continuous datasets which samples don't fall neatly into discrete classes (Brown, 1998).

In edge detection, fuzzy classification can be used to grade the likelihood of one edge being an actual boundary and discriminate false edges caused by noise. This may avoid the use of other techniques such as low-pass filtering, which main goal is to remove noise but can cause image blurring and loss of information.

3.1.3 Grading of the detected edges using fuzzy classification

The edges that are detected in an image can be graded regarding their likelihood of being actual boundaries, in order to discriminate false edges caused by noise. This can be done using fuzzy classification. Tukey's function is used as a membership function that attributes to each pixel in an edge map $M(i,j)$ a fuzzy score given by:

$$\tau(i,j) = \begin{cases} \left[\left(\frac{M(i,j)}{\sigma_s}\right)^2\right]^2, & M(i,j) < \sigma_s \\ 1, & M(i,j) \geq \sigma_s \end{cases} \tag{3.2}$$

where σ_s is a threshold for the edge map $M(i,j)$. Edges that are actual boundaries are outliers of $M(i,j)$ and are above σ_s. The value set for this parameter should be image-specific, as it depends on the relation between the strength of false edges caused by noise and true edges. Figure 3.2 shows the result of grading the edges detected in figure 3.1 through fuzzy classification. In this example, the edge map $M(i,j)$ of equation 3.2 is the image ICOV, calculated using equation 3.1.

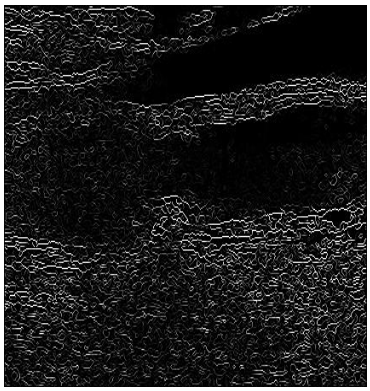

Figure 3.2 Fuzzy classification of edges detected using the ICOV.

3.1.4 Robust statistics

Robust statistics are statistical measures which show a good performance in data which is not modelled by a normal distribution. One of these measures is proposed by Tauber (2005). It is computed over a sample of data points $f(i,j)$ and is based on the median absolute deviation (MAD).

It is given by

$$\gamma = \mathrm{C}.\,\mathrm{MAD}_{\Omega}(f(i,j)) + \mathrm{med}_{\Omega}(f(i,j))$$
$$= C.\,\mathrm{med}_{\Omega}|f(i,j) - \mathrm{med}_{\Omega}(f(i,j))| + \mathrm{med}_{\Omega}(f(i,j)) \quad (3.3)$$

where med is the median, Ω is the sample domain and $C = 1.4826$ is a constant, derived from the fact that the MAD of a zero-mean normal distribution with unit variance is $1/1.4826$. This measure can be used to estimate an image-specific value of threshold σ_s for the edge map $M(i,j)$ in the fuzzy classification of edges (equation 3.2). In the specific case of $M(i,j) = \mathrm{ICOV}(i,j)$, this threshold is given by $\sigma_s = \sqrt{5} \times \sigma_e$, where σ_e is the image edge scale.

3.1.5 Dynamic programming

Dynamic programming (DP) is a technique widely used in computer science that allows to transform a complex problem into a sequence of smaller sub-problems, which solutions will contribute to quickly calculate the solution for the larger problem. The solutions for the sub-problems are saved and reused in all the complex problems that contain them, which avoids recalculation (Gonzalez and Woods, 2007).

DP can be used for contour segmentation by searching the optimum path $P(j)$ in an image according to some gain function G_P. The strategy consist on computing G_P for the paths ending on each position (i,j), on the basis of the gain obtained for the neighbouring pixel positions in the previous column $j-1$. These solutions are shared for all the paths passing by each position (i,j) in the columns ahead. This allows solving the optimization problem in linear time. Figure 3.3 shows an example of a longitudinal path $P(j)$ connecting pixels of consecutive columns across the entire image length.

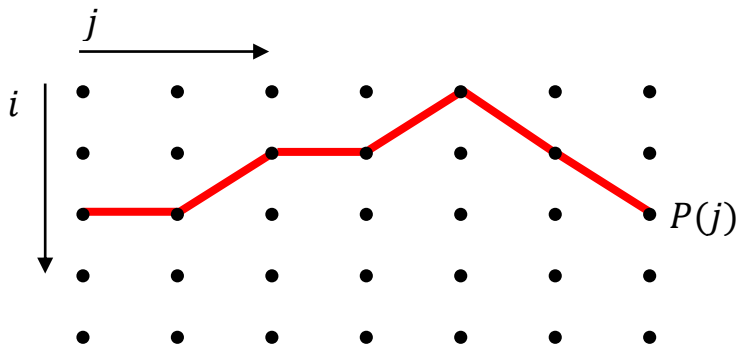

Figure 3.3 Segmented contour as a longitudinal path $P(j)$ connecting image pixels of consecutive columns across the entire image length.

G_P has the generic form:

$$G_P = \psi(x_1, y_1) + \sum_{j=2}^{N} \left[\psi\left(x_j, y_j\right) + \lambda\rho\left(x_j, y_j\right)\right] \quad (3.4)$$

where N is the number of image columns, (x_j, y_j) are the path coordinates at column j, $\psi(x_j, y_j)$ is an image feature map, $\rho(x_j, y_j)$ is a geometric smoothness term and λ is a weight term that controls the path smoothness. Different image features can be integrated in the cost function, depending on the purpose. Also, different geometric constraints can be included in $\lambda\rho(x_j, y_j)$ to produce contours which are more or less smooth.

3.1.6 Convolution of one-dimensional signals

Convolution is a common operation used in signal processing where two input signals are combined to form the output signal. The convolution between two discrete signals $f[n]$ and $g[n]$ is given by:

$$(f * g)[n] = \sum_{k=-\infty}^{+\infty} f[k].\, g[n-k] \quad (3.5)$$

Convolution is the basic operation behind signal filtering. It transforms a signal by replacing each of its data points by the result of a linear mathematical operation computed over its neighbours. The number of adjacent points used in the operation depends on the length of the sliding window which defines the neighbourhood of each data point (Oppenheim, Willsky and Hamid, 1996).

3.2 Segmentation of atherosclerotic plaques

There are different medical consensus on carotid atherosclerosis. One of them provides objective criteria to define atherosclerotic plaque based on the thickness of the intima-media (IM) layer (Touboul *et al*., 2012). These thickness measures can be calculated on the basis of the segmented contours delimiting the target layers. Thus, the application of the criteria over the intima-media thickness should allow the delimitation of plaques.

This strategy motivates the proposal of a novel method for plaque segmentation in the present work. Thus, the proposed method has two main steps:

- Segmentation of the IM region of the carotid wall.
- Plaque delimitation from IM contours.

These steps are schematized in figure 3.4.

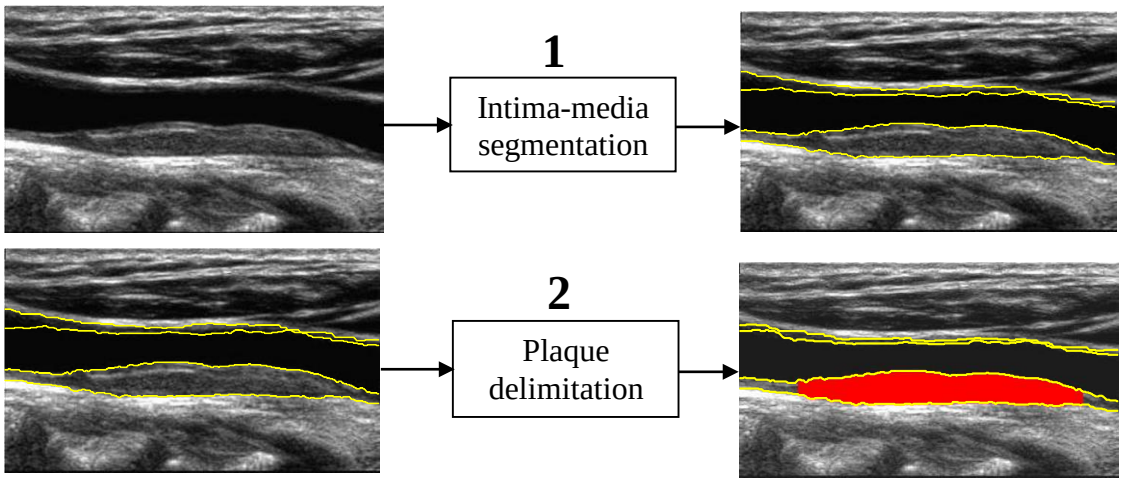

Figure 3.4 Main steps of the proposed method for plaque segmentation. The yellow lines represent the segmented contours of the IM region of the carotid wall. The segmented plaque is represented as a red overlay.

3.3 Segmentation of the intima-media region

A digital US image is a bi-dimensional matrix of $N \times M$ pixels. This block takes as input a US image of the common carotid artery (CCA) and returns four segmented contours, corresponding to the media-adventitia (MA) and lumen-intima (LI) interfaces of its near-end (NW) and far-end (FW) walls. The segmented contours are longitudinal paths defined for the N image columns, as shown in figure 3.5.

For the segmentation of the IM region we followed the method proposed by Rocha, Silva and Campilho (2012), which will be referred as original method. A brief description of this method is provided in the next section.

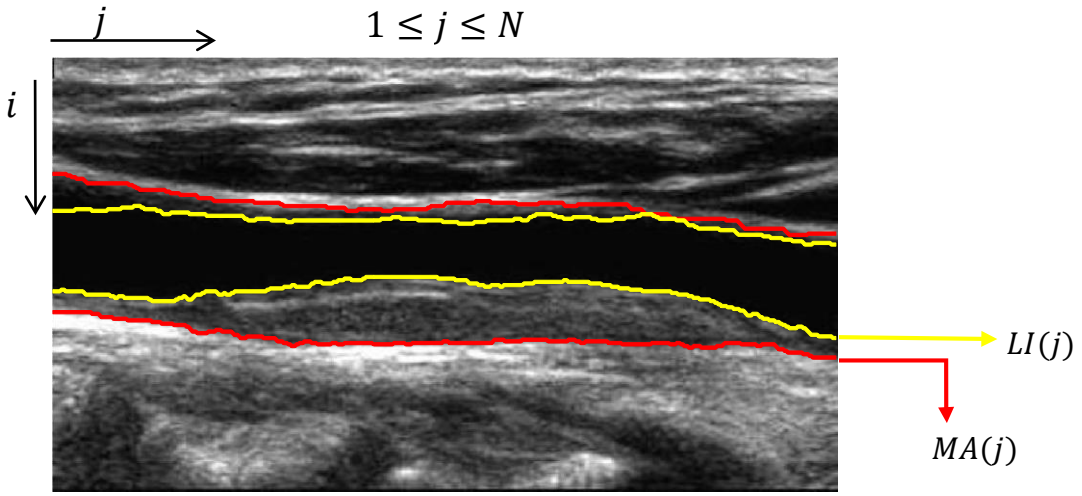

Figure 3.5 Segmentation of the IM region of the carotid wall. The segmented contours of the lumen-intima and media-adventitia interfaces are the longitudinal paths $LI(j)$ and $MA(j)$ represented by the yellow and red lines, respectively, and defined for the N image columns.

3.3.1 Original method

For the segmentation of the IM region, the method proposed by Rocha, Silva and Campilho (2012) uses edge detection with ICOV, fuzzy classification of the detected edges and dynamic programming. Figure 3.6 shows a flowchart representing the main blocks of the algorithm.

The algorithm is divided in several steps. First, a region of interest (ROI) is selected with the aim of reducing the area where the contours are searched. This helps avoiding possible anatomical structures which may lead to the misdetection of the carotid. For this step, the lumen axis (L) is detected. The lumen region is detected using a threshold-based segmentation, and a map of vertical distances to the boundaries of this region is computed. A dynamic programming search estimates L as the longitudinal contour crossing the highest number of local maxima of the vertical distance map. Then, the ROI is computed as a rectangular window enclosing all the pixels which vertical distance to L is less than$2 \times CR_{max} - d_{LB}$, where CR_{max} is the maximum expected carotid vertical radius and d_{LB} is the array of vertical distances, along the longitudinal direction, from L to the boundaries of the lumen region. An example of the detected lumen axis and the resulting ROI is shown in figure 3.7.

The next step is the detection of step edges (SE) and valley-shaped edges (VE). SE are typical of the LI interface, while both SE and VE appear in the MA interface, as shown in figure 3.8.

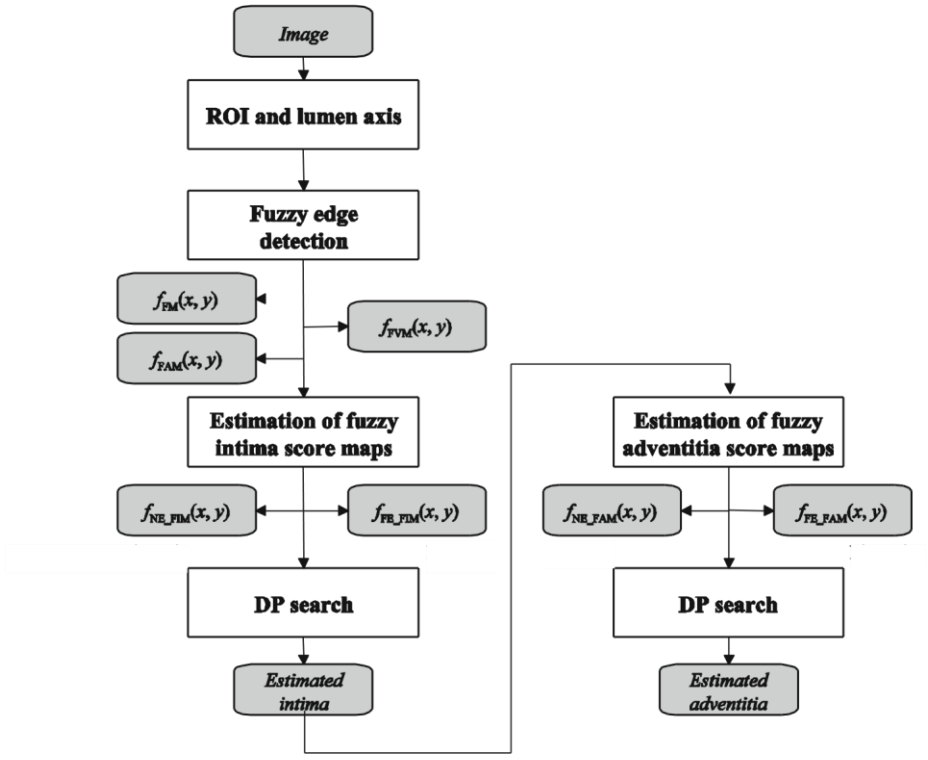

Figure 3.6 Block diagram of the algorithm proposed by Rocha, Silva and Campilho (2012) for the segmentation of the IM region of the carotid wall.

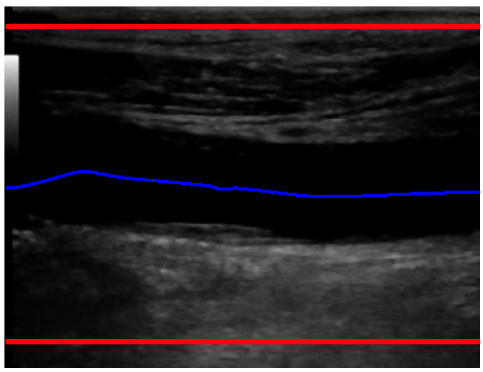

Figure 3.7 Lumen axis detection (blue line) and corresponding ROI (red lines).

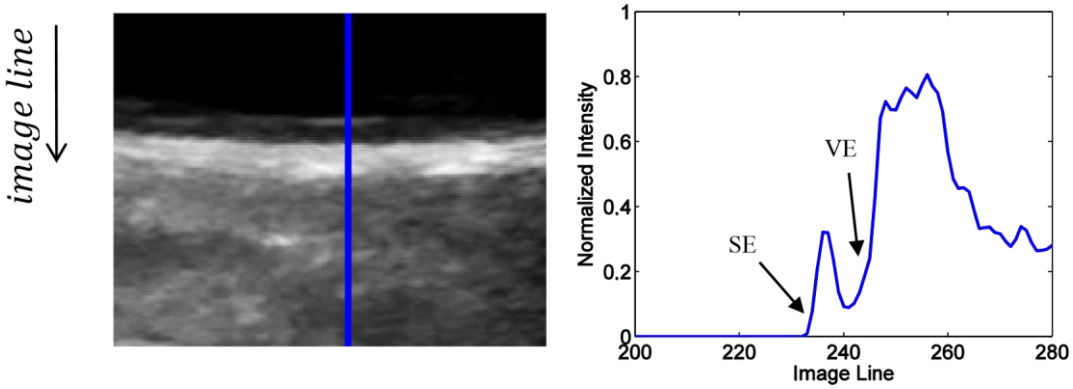

Figure 3.8 Typical edges found in the carotid wall. The intensity profile on the right belongs to the image column which is highlighted by a vertical blue line in the image on the left.

SE are detected using the image ICOV (section 3.1.1). The detected edges are graded using fuzzy classification (section 3.1.3) and the image edge scale is calculated from the set of pixels with positive ICOV through robust statistics (section 3.1.4). This results in the step edge map $f_{FM}(i,j)$, shown in figure 3.9 (a).

For VE detection, the same method is used but a measure of the valley edge strength, $\Delta I(i,j)$, is used instead of the ICOV. $\Delta I(i,j)$ is defined as:

$$\Delta I(i,j) = (I_P - I_v)/(I_v + \varepsilon) \tag{3.6}$$

where I_v and I_p are the image intensity levels at the valley between the two local maxima and at the lower maximum of a typical valley edge intensity profile, respectively, and ε is a small number to avoid divisions by 0. σ_v is used for thresholding the detected VE. It is given by $\sigma_v = \sqrt{5} \times \sigma_p$, where σ_p is a scale for the normalized amplitude of the lower maximum and is calculated from the set of pixels with positive I_P through robust statistics (section 3.1.4). This results in the valley edge map $f_{FVM}(i,j)$, shown in figure 3.9 (b).

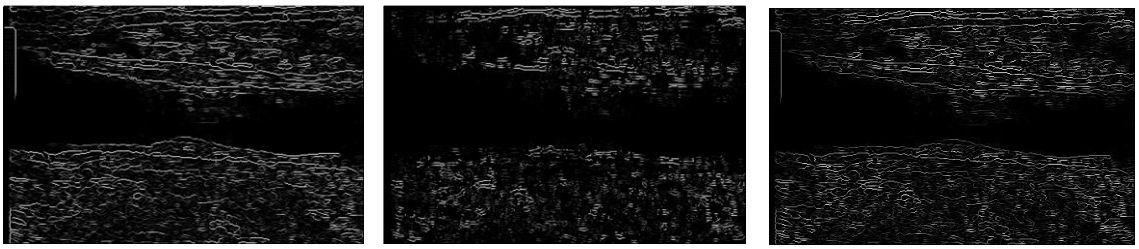

(a) (b) (c)

Figure 3.9 Fuzzy edge maps. (a) $f_{FM}(i, j)$. (b) $f_{FVM}(i, j)$. (c) $f_{FAM}(i, j)$.

The adventitia edge map ($f_{FAM}(i, j)$) is calculated as:

$$f_{FAM}(i,j) = \frac{1}{2}(f_{FM}(i,j) + f_{FVM}(i,j)) \tag{3.7}$$

to give equal importance to SE and VE. It is shown in figure 3.9 (c).

In the next step the LI interfaces are segmented. To do this, the algorithm first computes two intima score maps, one for each wall ($f_{FISM}(i, j)$), in which a fuzzy classification of the non-rejected edges is performed. A score is attributed to each pixel depending on its likelihood of belonging to the LI interface. The pixels that do not meet the following constraints are marked for rejection, with a score of $-\infty$: 1) being above or below L (for the NW or the FW, respectively); 2) at any column, the vertical distance between the pixel and L is not larger than the difference between $2 \times CR_{max}$ and the value of d_{LB} for that column; 3) gradient points upward or downward (NW or FW, respectively). For the remaining pixels the fuzzy score is computed as:

$$f_{FISM}(i,j) = e^{-\frac{z^2}{2}} \tag{3.8}$$

where $z = FM_{max}/\sigma_{FM}$, FM_{max} is the maximum f_{FM} value between the pixel (i, j) and L at the same column, and σ_{FM} is a scale parameter.

After computing these fuzzy score maps, a DP algorithm searches for the longitudinal path which maximizes the gain function expressed in equation 3.4 (section 3.1.5). Here, $\psi(x_j, y_j)$ is $f_{FISM}(i, j)$ and $\rho(x_j, y_j)$ is a geometric term which assumes the value of 1 if $y_j = y_{j-1}$ and $1/\sqrt{2}$ otherwise. The λ parameter is given by $\lambda = \lambda_e \times \sigma_e$ in order to make it proportional to the edge scale.

Once the LI interfaces are segmented, a similar method is used for the MA contours. The fuzzy adventitia score map ($f_{FASM}(i, j)$) is computed for the NW and FW. The pixels that do not meet the following constraints are marked for rejection, with a score of $-\infty$: 1) being above NW LI (for the NW MA interface) or below FW LI (for the FW MA interface); 2) the vertical distance between the pixel and the opposite LI contour is smaller

than $2 \times CR_{max}$; 3) gradient points upward or downward (NW or FW, respectively). For the remaining pixels the fuzzy score is computed as:

$$f_{FASM}(i,j) = f_{FAM}(i,j)e^{-\frac{z^2}{2}} \tag{3.9}$$

where $z = FAM_{max}/\sigma_{FAM}$, FAM_{max} is the maximum f_{FAM} value between the pixel (i,j) and the LI contour at the same column, and σ_{FAM} is a scale parameter.

Once these maps are computed, the same DP search used for the LI contours is performed, again following equation 3.4 (section 3.1.5), where $\psi(x_j, y_j)$ is $f_{FASM}(i,j)$. Figure 3.10 shows examples of the segmentation performed by this method.

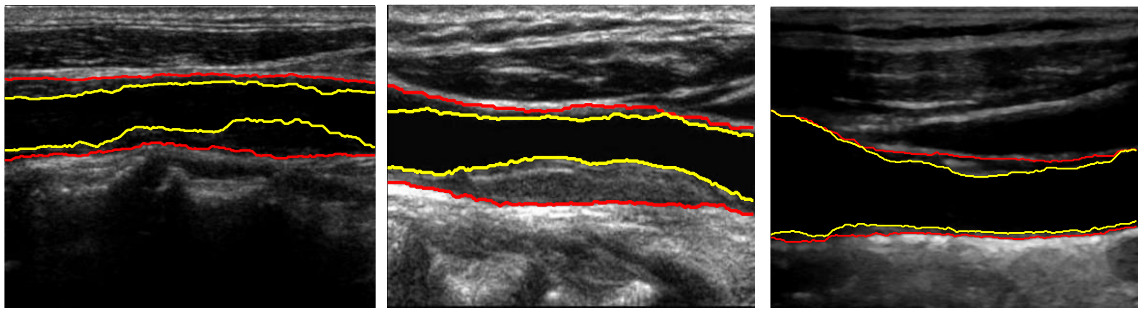

Figure 3.10 Examples of the segmentation of the IM region performed by the original method. The red and yellow lines represent the MA and LI contours, respectively.

3.3.2 Original method parameters

Table I summarizes the parameters which characterize the different stages of the original method for the segmentation of the IM region. The term "Database" means that the parameter has a global value for the image database. The term "Wall" means that each carotid wall has a specific value for the parameter, fixed for the whole database. The term "Interface" means that each carotid interface has a specific value for the parameter, fixed for the whole database. The term "Image-specific" means that the parameter assumes a different value depending on the image, which is calculated automatically.

LR_{min} is the minimum lumen vertical radius. LR_{min} and CR_{max} restrict the dimensions allowed for the carotid artery. If the interval defined by these parameters is too large misdetections can happen caused by similar structures. On the contrary, if the interval is too narrow, L may not be detected and the whole segmentation fails.

Parameters σ_e and σ_p are calculated automatically for each image through robust statistics (section 3.1.4).

σ_{FM} and σ_{FAM} are scale parameters which control the fuzziness of the membership function used for the classification of intima and adventitia edges, respectively. A tradeoff must be established between robustness to noise and sensitivity to weak echolucent edges, and reflected on the values set for σ_{FM} and σ_{FAM}. Small values of these parameters enable the segmentation of echolucent edges, but increase the sensitivity to noise.

λ_e controls the weight of the term for geometrical smoothness in the gain function which is maximized during the DP search (equation 3.4, section 3.1.5). Larger values set for this parameter result in a smoother contour and make the segmentation less sensitive to false edges caused by noise, but reduce the contour's adaptability to irregular edges.

Table I Parameters of the original method for the segmentation of the IM region.

Parameter	Stage	Value
LR_{min} (mm)	Lumen detection and ROI selection	Database
CR_{max} (mm)	Lumen detection and ROI selection; edge rejection	Database
σ_e	Step edge detection	Image-specific
σ_p	Valley-shaped edge detection	Image-specific
σ_{FM}	Intima score map	Wall
σ_{FAM}	Adventitia score map	Wall
λ_e	Dynamic programming	Interface

3.3.3 Proposed improvements

The segmentation performed by this method is comparable to manual segmentations performed by clinical experts when the image shows resolution and contrast, but in cases where it is highly affected by speckle noise the quality of the segmentation decreases. This happens for two reasons: 1) misdetection of *L*, as shown in figure 3.11 (a), and 2) wrong segmentation of the LI interface, as shown in figure 3.11 (b). This usually results in a wrong segmentation of the MA contour as well. If the segmentation of IM is incorrect, the delimitation of plaques using these contours is not reliable, which precludes an accurate quantification of the image plaque burden. The next sections describe the modifications to the original algorithm proposed in the present work to improve the IM segmentation.

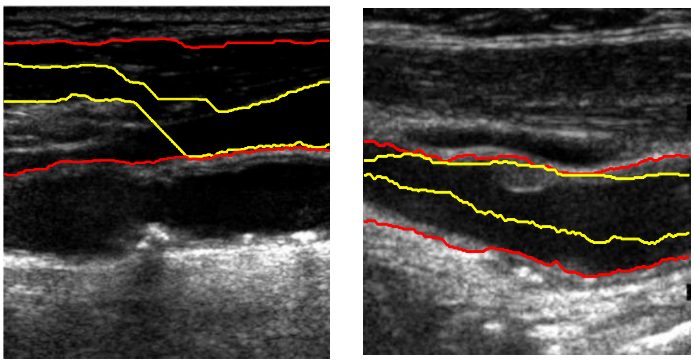

(a) (b)

Figure 3.11 The original method's worst segmentations are due to (a) misdetection of *L* and (b) wrong segmentation of LI. The red and yellow lines represent the LI and MA contours, respectively.

3.3.3.1 Improved lumen axis detection

The algorithm for lumen axis detection may misdetect noisy images where the jugular vein or the sternocleidomastoid muscle are present and show echogenicity and texture similar to the carotid artery. This leads to the selection of a ROI which may not include both carotid walls, as shown in figure 3.12 (a). The threshold-based segmentation uses information from the image intensity histogram to compute the lumen region, and therefore is very sensitive to background noise. In figure 3.12 (a), this segmentation fails to set to black part of the lumen which automatically excludes the possibility of this region containing *L*. The lumen axis is attracted to a similar structure, less affected by noise.

An alternative method used to detect *L* is proposed by Rouco and Campilho (2013). It searches the image for local phase symmetry patterns at appropriate scale of analysis. This symmetry measure is robust to high contrast artifacts and different textures of the structures present in the US image, and enables the detection of *L* in images affected by noise, as shown in figure 3.12 (b). This method may also fail if the value for the symmetry measure is greater for structures similar to the carotid artery that also present in the image.

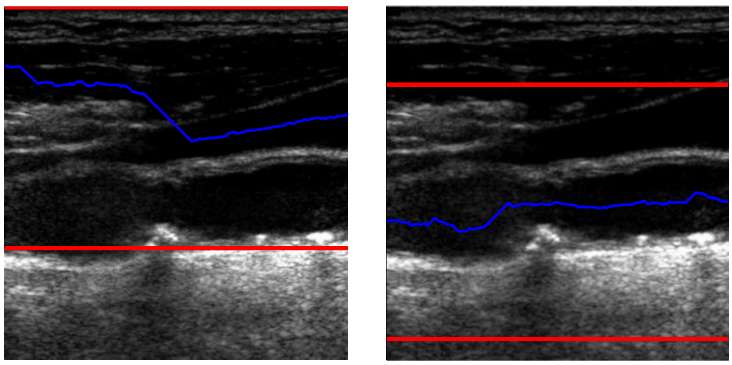

(a) (b)

Figure 3.12 Comparison between different algorithms used for lumen detection. (a) The algorithm used by Rocha, Silva and Campilho (2012) fails to segment *L* due to the presence of background noise. (b) *L* is correctly segmented by the algorithm proposed by Rouco and Campilho (2013). The blue line represents the detected lumen axis and the red lines delimit the selected ROI.

3.3.3.2 Relaxing the constraints

The first step for the computation of the fuzzy intima score maps is mark for rejection pixels that don't respect the constraints that are intrinsic to a LI interface and are referred in section 3.3.1. A score of $-\infty$ is attributed to these pixels, which automatically makes them unsuitable for incorporating the final contour. This is understandable by looking at the gain function that is maximized during the DP search (equation 3.4, section 3.1.5). If a given path crosses a pixel with a value for $\psi(x_j, y_j)$ equal to $-\infty$, the overall score for that path will also be $-\infty$, independently of the scores of the other pixels. This leads to the rejection of the path.

The $-\infty$ penalty is appropriate for pixels that do not respect the first two constraints, since the LI interface must necessarily lie between L andCR_{max}. However, the penalty must not be so heavy for pixels showing a wrong gradient orientation, since the optimum LI contour may cross regions where the local gradient assumes opposite directions, especially in noisy edges typical of US imaging, as shown in figure 3.13. By changing the penalty given to these pixels from $-\infty$ to 0, they are no longer excluded and can be part of the final contour, as shown in figure 3.14. In (a), a penalty of $-\infty$ is used, causing the LI contour to go underneath a plaque in the FW. In (b), this penalty is changed to 0, allowing the LI contour to approach the plaque's luminal surface.

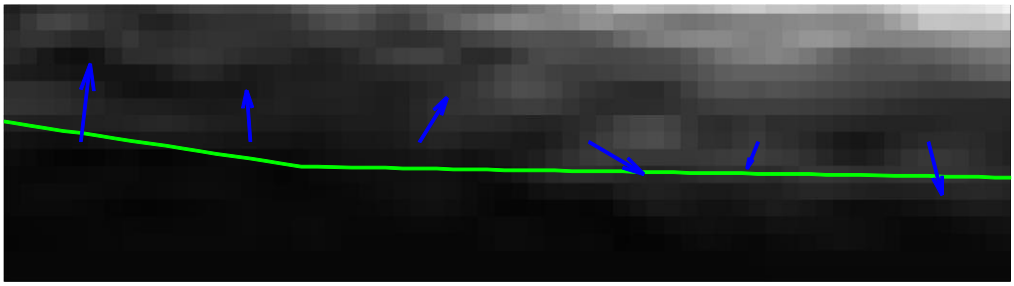

Figure 3.13 Gradient (blue arrows) assumes opposite directions along the LI contour (green line).

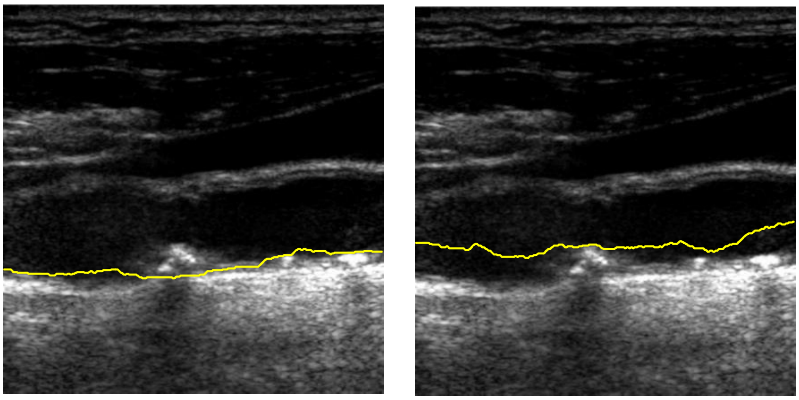

(a) (b)

Figure 3.14 Comparison between different forms of penalizing pixels which show opposite gradient orientation. (a) $-\infty$. (b) 0. The yellow line represents the FW LI contour.

3.3.3.3 Fuzzy membership function

In figure 3.14, changing the penalty from $-\infty$ to 0 allows the segmentation of the plaque's luminal surface, but the contour is above the LI interface in the surrounding plaque-free regions. The reason for this lies in the membership function used to calculate the fuzzy scores.

Figure 3.15 shows the shape of the Gaussian function used as membership function for the fuzzy classification of non-rejected step edge pixels (equation 3.8, section 3.3.1). The score attributed to a given pixel (i, j) depends exclusively on the existence of edges between i and L, and how strong they are. This function does not consider the likelihood of the pixel being an actual boundary, which is the pixel's value in the fuzzy step edge map $f_{FM}(i, j)$.

Here, a new membership function is proposed for the fuzzy classification of edges. It is based on the product of a penalty term and a gain term. The penalty term considers the luminal noise and it is a function of FM_{max}, while the gain term considers edge strength and is a function of the pixel's value in $f_{FM}(i, j)$.

$$f_{FISM}(i, j) = (1 - f(FM_{max}; \alpha; \beta)) \times f(f_{FM}(i, j); \alpha; \beta) \tag{3.10}$$

where $f(x; a, b)$ is a s-shaped function defined by:

$$f(x; \alpha, \beta) = \begin{cases} 0, & x < \alpha \\ 2\left(\frac{x-\alpha}{\beta-\alpha}\right)^2, & \alpha \le x \le \frac{\alpha+\beta}{2} \\ 1, & x \ge \beta \end{cases} \tag{3.11}$$

Figure 3.16 shows the shape of the proposed membership function.

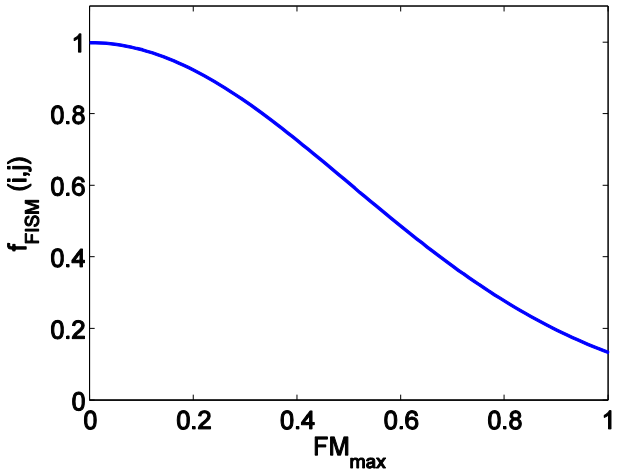

Figure 3.15 Gaussian normal distribution used as membership function for the fuzzy classification of edges (σ_{FM} = 0.5).

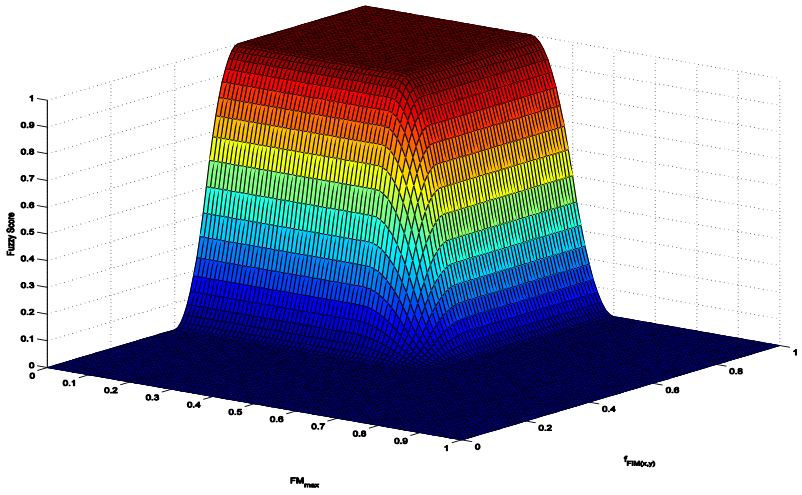

Figure 3.16 Proposed membership function for the fuzzy classification of edges ($\alpha = 0.4$; $\beta = 0.6$).

Parameters α and β are thresholds for the edge strength in $f_{FM}(i, j)$ and control the fuzziness of $f(x; \alpha, \beta)$ by defining its cut-off values. α is the lower threshold and is discussed in the next section. β is the upper threshold. An edge pixel (i, j) with edge strength greater than β is guaranteed to be part of a true anatomical boundary and its value for the gain term in equation 3.10 is 1. On the other hand, if the value of FM_{max} is greater than β, there is a true physical interface between (i, j) and L, and the value of the penalty term will be 0 for this pixel. Here β is expressed as $\beta = \alpha + s$, where s is the spread factor. Unlike the Gaussian function, the product of s-shaped functions enables reaching scores of absolute 0 for values of FM_{max} greater than β and values of $f_{FM}(i, j)$ smaller than α.

Figure 3.17 shows compares the segmentation using the Gaussian (a) and the proposed membership function (b) for the fuzzy classification of edges. The greater edge strength of the pixels belonging to the LI interface compensates the large penalty which is attributed to these pixels for having false edges caused by noise between them and L, resulting in a higher overall score and allowing the LI contour to be correctly segmented.

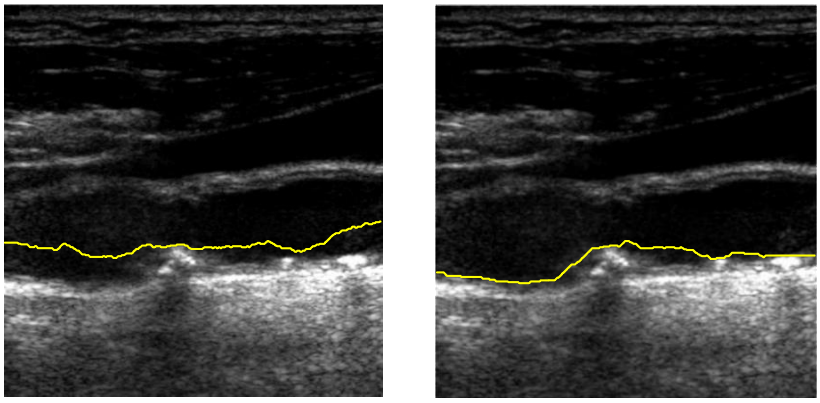

(a) (b)

Figure 3.17 Comparison between different membership functions for fuzzy classification of edges. (a) Gaussian function. (b) Proposed function. The yellow line represents the FW LI contour.

3.3.3.4 Image dependent parameters

α is the lower threshold for the edge strength in $f_{FM}(i,j)$ that discriminates true edges from false edges caused by noise, assuming that the former have greater strength than the latter. A fuzzy score of 0 is attributed to a given pixel (i,j) if its edge strength in $f_{FM}(i,j)$ is smaller than α. The value of the penalty term is 1 if FM_{max} is smaller than α. Thus, α is a measure of the strength of false edges caused by noise present in the lumen region. To calculate α the image is divided in ten equally sized windows. For each window, α is calculated using robust statistics (section 3.1.4). In equation 3.3, $f(i,j)$ is the step edge map $fFM(i,j)$ and Ω is the lumen region, defined as:

$$\Omega = [L - kLR_{min}; L + kLR_{min}] \tag{3.12}$$

where k is an integer value defined empirically from the image database. This region is assumed to exclusively contain pixels belonging to the lumen. A linear interpolation is performed for every image column using the values of α calculated for each window.

3.3.3.5 Considerations about improvements in the segmentation of the media-adventitia interface

Once the LI interface is correctly segmented, the algorithm proposed by Rocha, Silva and Campilho (2012) usually performs a correct segmentation of the MA contour, and so no modifications are performed regarding the segmentation of this interface.

3.3.3.6 Method limitations

The main assumption of the proposed method is that in the lumen region there are no edges, and if there are they are caused by noise. Interfaces showing echolucency similar to the lumen will not be segmented correctly, as shown in figure 3.18.

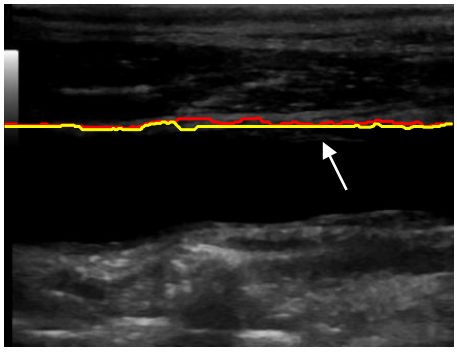

Figure 3.18 The proposed method fails to segment an echolucent LI interface in the NW. The yellow and red lines represent the LI and MA contours, respectively. The white arrow points to the true LI interface.

3.3.4 Proposed method parameters

Table II summarizes the parameters which characterize the different stages of the proposed method for the segmentation of the IM region. The term "Database" means that the parameter has a global value for the image database. The term "Wall" means that each carotid wall has a specific value for the parameter, fixed for the whole database. The term "Interface" means that each carotid interface has a specific value for the parameter, fixed for the whole database. The term "Image-specific" means that the parameter assumes a different value depending on the image, which is calculated automatically. The column "Replace" contains the parameter of the original method which is replaced by the new parameter. The term "Same" means that the parameter is preserved from the original method.

Table II Parameters of the proposed method for the segmentation of the intima-media region.

Parameter	**Stage**	**Value**	**Replace**
CR_{min} (mm)	Lumen detection and ROI selection	Database	LR_{min}
CR_{max} (mm)	Lumen detection and ROI selection; edge rejection	Database	Same
σ_e	Step edge detection	Image-specific	Same
σ_p	Valley-shaped edge detection	Image-specific	Same
α	Intima score map	Image-specific	σ_{FM}
k	Intima score map	Database	σ_{FM}
LR_{min} (mm)	Intima-score map	Database	σ_{FM}
s	Intima score map	Wall	σ_{FM}
σ_{FAM}	Adventitia score map	Wall	Same
λ_e	Dynamic programming	Interface	Same

CR_{min} is the minimum carotid vertical radius. CR_{min} and CR_{max} restrict the dimensions allowed for the carotid artery. If the interval defined by these parameters is too large, misdetections can happen caused by similar structures. On the contrary, if the interval is too narrow L may not be detected and the whole segmentation fails.

Parameters σ_e, σ_p and α are calculated automatically for each image through robust statistics (section 3.1.4).

s and σ_{FAM} are scale parameters which control the fuzziness of the membership function used for the classification of intima and adventitia edges, respectively. A tradeoff must be established between robustness to noise and sensitivity to weak echolucent edges, and reflected on the values set for s and σ_{FAM}. Small values of these parameters enable the segmentation of echolucent edges, but increase the sensitivity to noise.

λ_e controls the weight of the term for geometrical smoothness in the gain function which is maximized during the DP search (equation 3.4, section 3.1.5). Larger values set for this parameter result in a smoother contour and make the segmentation less sensitive to false edges caused by noise, but reduce the contour's adaptability to irregular edges.

k and LR_{min} control the width of Ω where parameter α is calculated for lumen noise estimation (equation 3.12, section 3.3.3.4). If Ω is too wide, it may include echo from a plaque and the LI interface may go underneath it, but if it is too narrow it may lead to the calculation of a non-representative value of α for the luminal noise, resulting in an incorrect segmentation.

3.4 Plaque delimitation from intima-media contours

The proposed method for plaque segmentation uses three objective criteria which are proposed in a European medical consensus to define atherosclerotic plaque (Touboul *et al*., 2012). This definition is based on the thickness of the IM layer. For each image column j, the local intima-media thickness is compared with a specific reference value, and if it exceeds a certain threshold specified in the consensus a plaque is present. This reference value can be fixed or vary with the specific region of the carotid wall, depending on the criterion.

This block takes as input the four segmented contours of the LI and MA interfaces of the carotid NW and FW and returns the image columns which correspond to the right (j_R) and left (j_L) limits of the segmented plaques, as shown in figure 3.19.

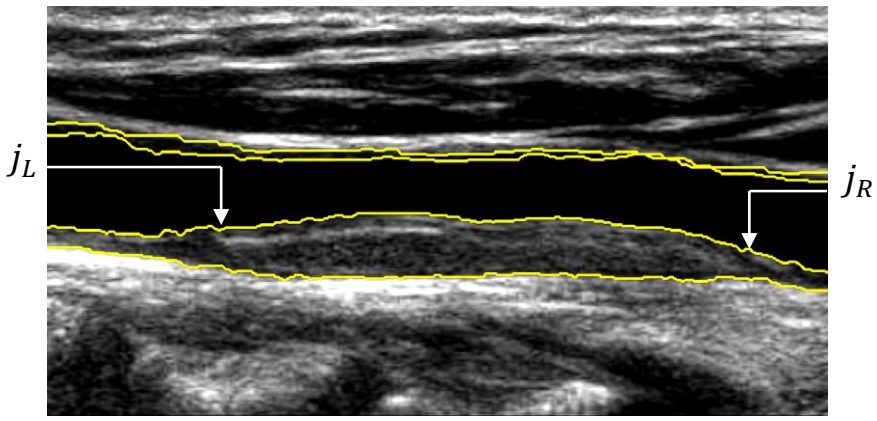

Figure 3.19 Plaque limits in the longitudinal direction. The yellow lines represent the segmented contours of the IM region of the carotid wall. j_L and j_R are the image columns which correspond to the plaque's left and right limits, respectively.

3.4.1 Criteria to define atherosclerotic plaque

In the European medical consensus for carotid atherosclerosis three criteria are proposed for the objective definition of atherosclerotic plaque (Touboul *et al.*, 2012). These criteria define plaque as a focal structure that:

- **Criterion 1 –** demonstrates an intima-media thickness greater than 1.5 mm.
- **Criterion 2 –** encroaches into the lumen of at least 50% of the surrounding intima-media thickness.
- **Criterion 3 –** encroaches into the arterial lumen of at least 0.5 mm.

The term "focal" means that it must be limited in length and helps clinical experts discriminating plaques from a generalized thickening of the IM region. The implementation of these criteria is described in the next section.

3.4.2 Criteria implementation

The local intima-media thickness for a given image column j is calculated as:

$$IMT(j) = |LI(j) - MA(j)| \times dx0, \quad 1 \leq j \leq N \tag{3.13}$$

where $LI(j)$ and $MA(j)$ are the rows of longitudinal paths corresponding to the segmented contours of the LI and MA interfaces for column j, respectively, N is the number of image columns and $dx0$ is the reference scale for pixel size in mm/pixel.

The local intima-media thickness is compared with different reference values, depending on the criterion.

3.4.2.1 Criterion 1

Criterion 1 is easy to implement, as it applies directly to $IMT(j)$:

$$IMT(j) > 1.5 \text{ mm} \tag{3.14}$$

If this condition is fulfilled for a given image column, that column is marked as plaque-positive. The leftmost and rightmost columns of continuous plaque-positive segments are the left and right plaque limits, respectively. This is shown in figure 3.20.

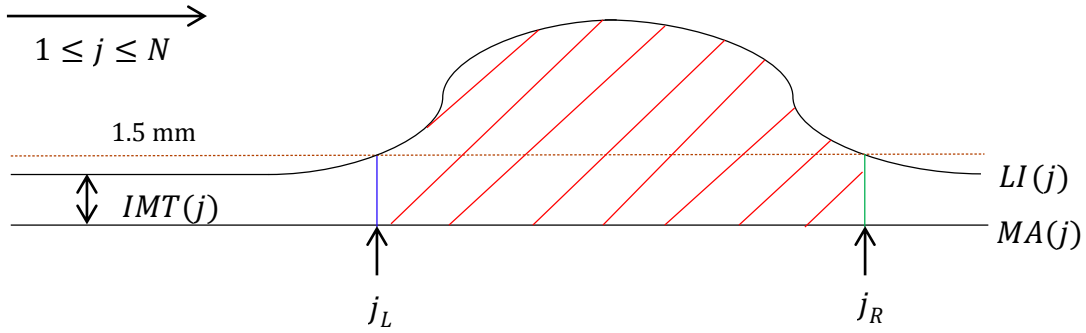

Figure 3.20 Atherosclerotic plaque according to criterion 1 of the medical consensus. The red stripes highlight the plaque's area. The blue and green vertical lines mark the plaque's left and right limits, respectively. The brown dashed line marks the 1.5 mm threshold.

3.4.2.2 Criterion 2

Implementing criterion 2 is not as straightforward, because to define the lumen encroachment the local intima-media thickness is compared with the surrounding intima-media thickness. This concept is vague as no objective definition of "surrounding" is given in the consensus. In the present work, two values of this measure are calculated for each image column j: the left ($lIMT_s(j)$) and right ($lIMT_s(j)$) surrounding intima-media thickness. A description of how these measures are calculated is provided in section 3.4.3.

This criterion enables the detection of plaque flanks, where there are larger variations of the intima-media thickness. In the central region of a plaque the wall thickness tends to stabilize and the values of the local and surrounding intima-media thickness are similar. For a given image column j, the left flank of a plaque is present if:

$$IMT(j) - lIMT_s(j) > 0.5 \times lIMT_s(j) \tag{3.15}$$

and the right flank of a plaque is present if:

$$IMT(j) - rIMT_s(j) > 0.5 \times rIMT_s(j) \tag{3.16}$$

The plaque's left limit is the leftmost column of the left flank and the right limit is the rightmost column of the right flank.

Several left flanks in a row can be detected and vice-versa, depending on the plaque's shape. The plaque left limit corresponds to the leftmost column of the first left flank, and the right limit corresponds to the rightmost column of the last right flank, as shown in figure 3.21.

Situations may occur where only the left or right plaque flank(s) is detected. This can be caused by: 1) the algorithm failed to detect the opposite flank(s) or 2) the plaque's full extension was not scanned, and the flank(s) of one side falls out of the image boundaries. When this happens the remaining extension of the IM region is segmented as plaque in the opposite direction of the detected flank(s), as shown in figure 3.22.

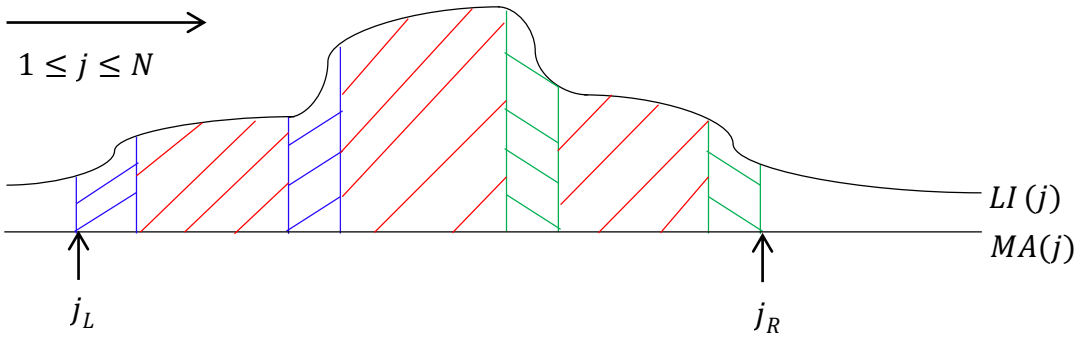

Figure 3.21 Atherosclerotic plaque according to criterion 2 of the medical consensus. The blue and green stripes mark the detected left and right plaque flanks, respectively, and the red stripes highlight the plaque's area.

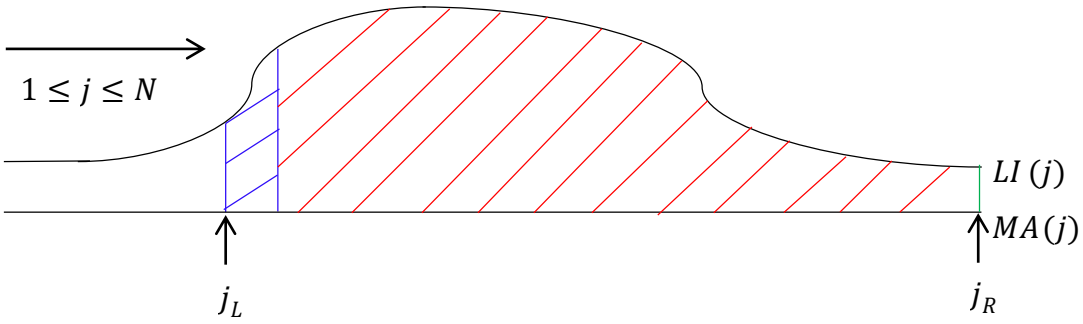

Figure 3.22 The left flank of a plaque is detected (blue stripes), but the right one is not. The plaque's right limit (green vertical line) is set to be the last column of the segmented IM region in the opposite direction of the detected flank. The red stripes highlight the plaque's area.

Some plaques may present depressions, which causes the illusion of plaque-free regions. When this happens, the local values of the intima-media thickness for this region are compared with a reference value (Ref), in order to determine if this is actually a plaque-free region or a depression inside a plaque.

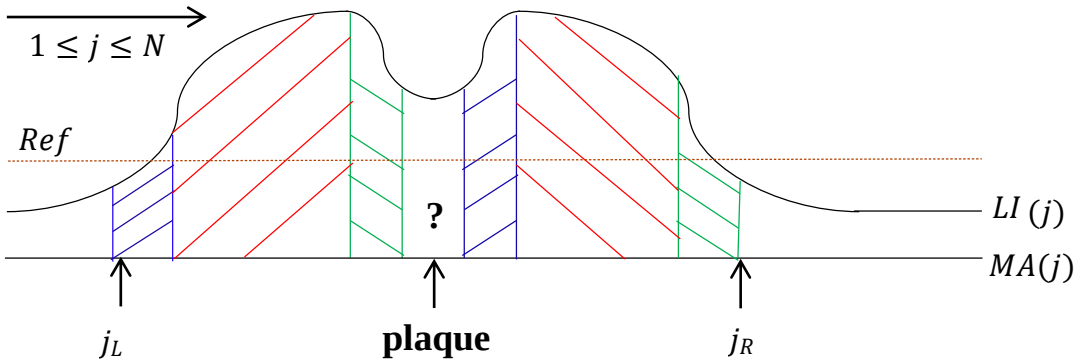

Figure 3.23 Depression inside a plaque causes the illusion of a plaque-free region. By comparing the local values of the intima-media thickness inside this region with a reference value we conclude that it is a depression inside a plaque. The blue and green stripes mark the detected left and right plaque flanks, respectively. The red stripes highlight the plaque's area.

Ref is given by:

$$Ref = \frac{lIMT_s(j_L)+rIMT_s(j_R)}{2} \tag{3.17}$$

where $lIMT_s(j_L)$ is the surrounding intima-media thickness of the column which corresponds to the left limit of the left plaque (j_L) and $rIMT_s(j_R)$ is the surrounding intima-media thickness of the column which corresponds to the right limit of the right plaque (j_R). If the values of the local intima-media thickness are above Ref, the middle region corresponds to a depression and is included in the segmented plaque. This situation is exemplified in figure 3.23.

3.4.2.3 Criterion 3

The consensus does not clarify a reference measure with which the local intima-media thickness should be compared for plaque definition according to criterion 3. There are two options for this reference measure: 1) local value, such as the surrounding intima-media thickness for criterion 2 and 2) global value for a patient, which represents the normal intima-media thickness in healthy and plaque-free regions of the arterial wall. The second option was chosen in this work. A description of how this measure is obtained is provided in section 3.4.4. Once the normal intima-media thickness for the patient (IMT_P) is defined, criterion 3 is expressed as:

$$IMT(j) > IMT_p + 0.5 \text{ mm} \tag{3.18}$$

If this condition is fulfilled for a given image column, that column is marked as plaque-positive. The leftmost and rightmost columns of continuous plaque-positive segments are the left and right plaque limits, respectively. This is shown in figure 3.24.

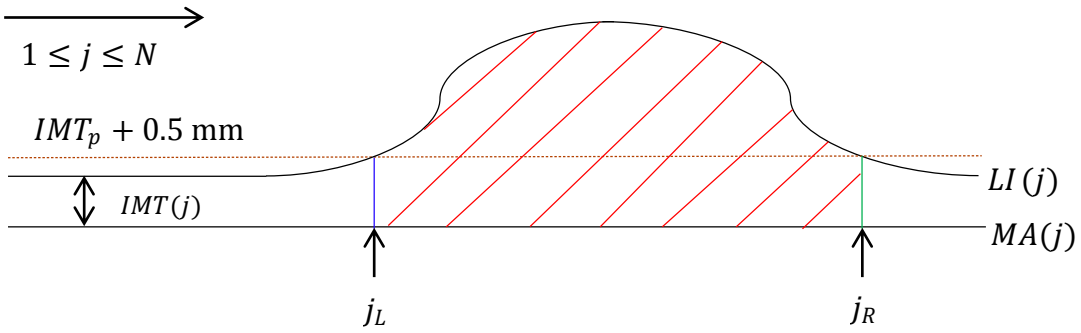

Figure 3.24 Atherosclerotic plaque according to criterion 3 of the medical consensus. The red stripes highlight the plaque's area. The blue and green vertical lines mark the plaque's left and right limits, respectively. The brown dashed line marks the $IMT_p + 0.5$ mm threshold.

3.4.2.4 Criteria combination

Each of the described criteria is implemented separately and provides an independent segmentation of atherosclerotic plaques. However, they can also be used together. For this, the plaques that were segmented by each criteria are combined. Plaques which do not overlap with others preserve their left and right limits. When two or more plaques overlap, new limits are defined to include all of them in a single plaque.

3.4.3 Surrounding intima-media thickness

In the present work, the surrounding intima-media thickness for a given image column j is estimated by two alternative methods: median ($IMT_s^{med}(j)$) or Gaussian average ($IMT_s^G(j)$) of the local intima-media thickness values of a neighbour region near j. The next sections describe, for each method, how the surrounding intima-media thickness is calculated.

3.4.3.1 Median

For the median estimation, the neighbour region of column j is a set of columns defined as:

$$A(j) = \left[(j \pm h) - \frac{l}{2}; (j \pm h) + \frac{l}{2}\right] \tag{3.19}$$

where l is the length of $A(j)$ and h is the offset which separates j from the centre column of $A(j)$. h can be positive or negative, depending if the left or right surrounding intima-media thickness is being calculated.

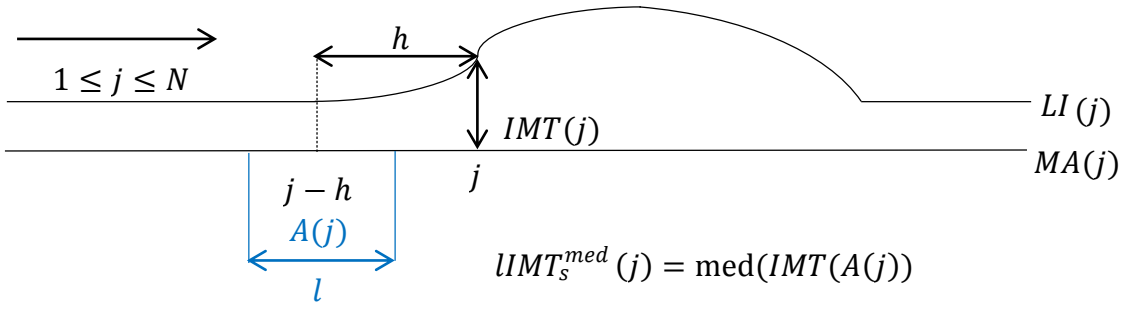

Figure 3.25 Estimation of the left surrounding intima-media thickness as the median of the local intima-media thickness of a neighbour region.

The surrounding intima-media thickness is defined as:

$$IMT_s^{med}(j) = \text{med}(IMT(A(j)) \tag{3.20}$$

where med is the median and $IMT(A(j))$ is the local intima-media thickness in the image columns of the neighbour region $A(j)$.

Figure 3.25 shows an example where the left surrounding intima-media thickness is calculated through this method. For the right side, the procedure is similar, but h is positive instead of negative.

The values set for h and l depend on the slope of the plaque flanks to be detected. Plaques showing smooth and elongated flanks require larger values for h when compared to plaques with abrupt transitions. The value set for l depends on h, as the neighbour region where the surrounding intima-media thickness is calculated should not include the plaque flank we wish to detect. These parameters require optimization over a dataset of training images.

3.4.3.2 Gaussian average

The Gaussian average of the local intima-media thickness is calculated as:

$$IMT^G(j) = IMT(j) * G_\sigma(j) \tag{3.21}$$

where $G_\sigma(j)$ is a discrete approximation of a Gaussian function centered in column j with standard deviation σ. The surrounding intima-media thickness is obtained by shifting the convolution to column $j \pm h$.

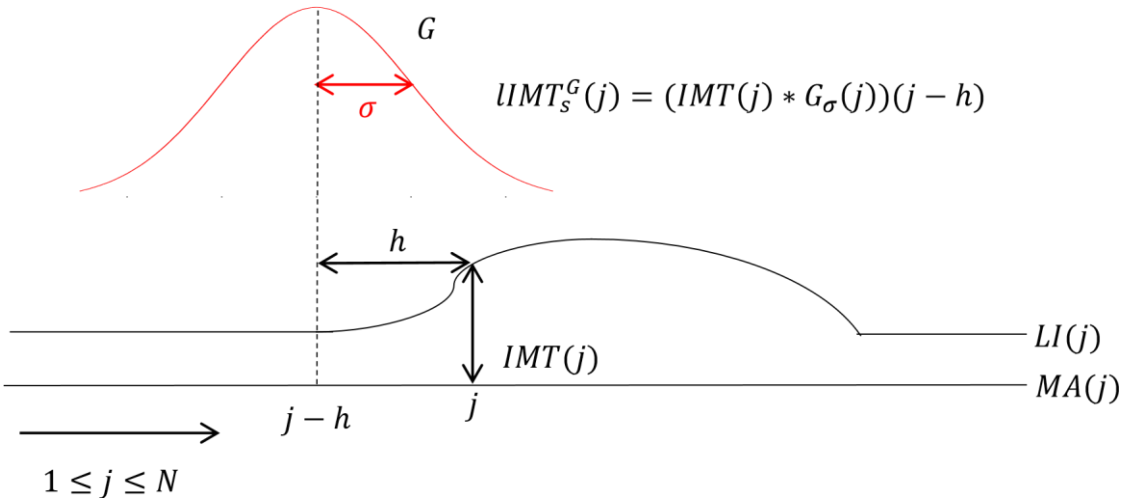

Figure 3.26 Estimation of the left surrounding intima-media thickness as the Gaussian average of the local intima-media thickness of a neighbour region.

It is given by:

$$IMT_s{}^G(j) = IMT^G(j \pm h) \tag{3.22}$$

where h is the offset which separates j from the centre column of the neighbour region. h can be positive or negative, depending if the left or right surrounding intima-media thickness is being calculated.

Figure 3.26 shows an example where the left surrounding intima-media thickness is calculated through this method. For the right side, the procedure is similar, but h is positive instead of negative.

The values set for h and σ depend on the slope of the plaque flanks to be detected. Plaques showing smooth and elongated flanks require larger values for h when compared to plaques showing abrupt transitions. The value set for σ is depends on h, as the neighbour region where the surrounding intima-media thickness is calculated should not include the plaque flank we wish to detect. These parameters require optimization over an image training dataset.

3.4.4 Normal intima-media thickness for the patient

The concept of normal intima-media thickness for a patient (IMT_p) is subjective, as it is individual-specific and depends on factors such as age, gender, race, etc. Ideally, IMT_p should be a measure performed by clinical experts in healthy and plaque-free regions of the carotid artery according to standardized protocols established in a medical consensus (Lim *et al.*, 2008). However, this is not always possible for several reasons: it requires manual intervention; US images often show poor contrast and resolution, and the double-

line pattern is not always visible; atherosclerotic plaques are present in diseased arteries, making it harder to find a suitable region for the measurement.

Clinical studies provide tables with reference values for the normal intima-media thickness of the carotid artery in healthy people according to their race, gender and age. These tables are provided by large population-based cohort studies conducted in Europe and the United States and are shown in Appendix A (Stein *et al.*, 2008). This can be used to estimate the normal intima-media thickness for a given patient on the basis of his age and gender. However, these tables are stratified by age sectors. Thus, in order to obtain a more accurate estimation, it is proposed to perform linear interpolation between the reference values of the age classes which are closer to the patient's age.

3.4.5 Plaque shape restriction

Atherosclerotic plaques typically have a flattened structure, *i.e.*, their length is larger than their height. This can be used to filter structures that were segmented as plaque but do not respect this length/height relation. Thus, after plaque segmentation, this criterion is used to erase narrow plaque regions which length is smaller than the maximum intima-media thickness within the plaque.

3.5 Plaque burden measurement

After being segmented, each plaque is restricted by its left and right limits along the longitudinal direction and by the LI and MA contours in the vertical direction. The area enclosed by these limits is highlighted by superimposing a red overlay in the image. For each plaque, the following measures are calculated:

$$Length\ (\text{mm}) = dx0 \times (j_R - j_L) \tag{3.23}$$

$$Area\ (\text{mm}^2) = \sum_{j=j_L}^{j_R} IMT(j) \times dx0 \tag{3.24}$$

where $dx0$ is the reference scale for pixel size normalization in mm/pixel, j_R and j_L are the image columns which correspond to the right and left plaque limits, respectively, and $IMT(j)$ is the local intima-media thickness at image column j.

The image plaque burden is calculated as total plaque area:

$$PB = \sum_{i=1}^{N} Area(i) \tag{3.25}$$

where N is the number of segmented plaques in the image.

3.6 Methodology summary

Figure 3.27 shows a block diagram of the proposed method for the automatic measurement of PB in US images of the carotid artery. The main stages of this method are:

Segmentation of the IM region: this block receives as input a 2D B-mode US image of the CCA and returns four segmented contours of the NW and FW IM region. This segmentation can be performed using two methods: 1) original method proposed by Rocha, Silva and Campilho (2012), described in sections 3.3.1 and 3.3.2, or 2) the method proposed in the present work, described in sections 3.3.3 and 3.3.4. Each method has a set of parameters that need to be optimized, referred in tables I and II, respectively.

Intima-media thickness measurements: three different measures are calculated:

- Local intima-media thickness, calculated as described in section 3.4.2.
- Surrounding intima-media thickness, calculated as described in section 3.4.3. Two methods can be used: 1) Gaussian average or 2) median of the local intima-media thickness in a neighbour region. Each method has a set of parameters that need to be optimized and are referred in sections 3.4.3.1 and 3.4.3.2, respectively.
- Normal intima-media thickness for the patient, obtained as described in section 3.4.4. Two methods can be used: 1) measurement performed by clinical experts according to standardized protocols established in a medical consensus or 2) linear interpolation using reference values that resulted from large population-based cohort studies.

Plaque delimitation: this block receives as input the segmented contours of the IM region and the three intima-media thickness measures, and returns the image columns which correspond to the left and right limits of each segmented plaque. The thickness measures are compared with reference thresholds according to three objective criteria to define plaque proposed in a medical consensus. Each criteria can be used independently (sections 3.4.2.1, 3.4.2.2 and 3.4.2.3), but they can also be combined (section 3.4.2.4).

Plaque burden measurement: Using the longitudinal and vertical limits of the segmented plaques, the plaque region is extracted and its length and area are calculated as described in section 3.5. The image plaque burden is calculated by summing the areas of all the segmented plaques.

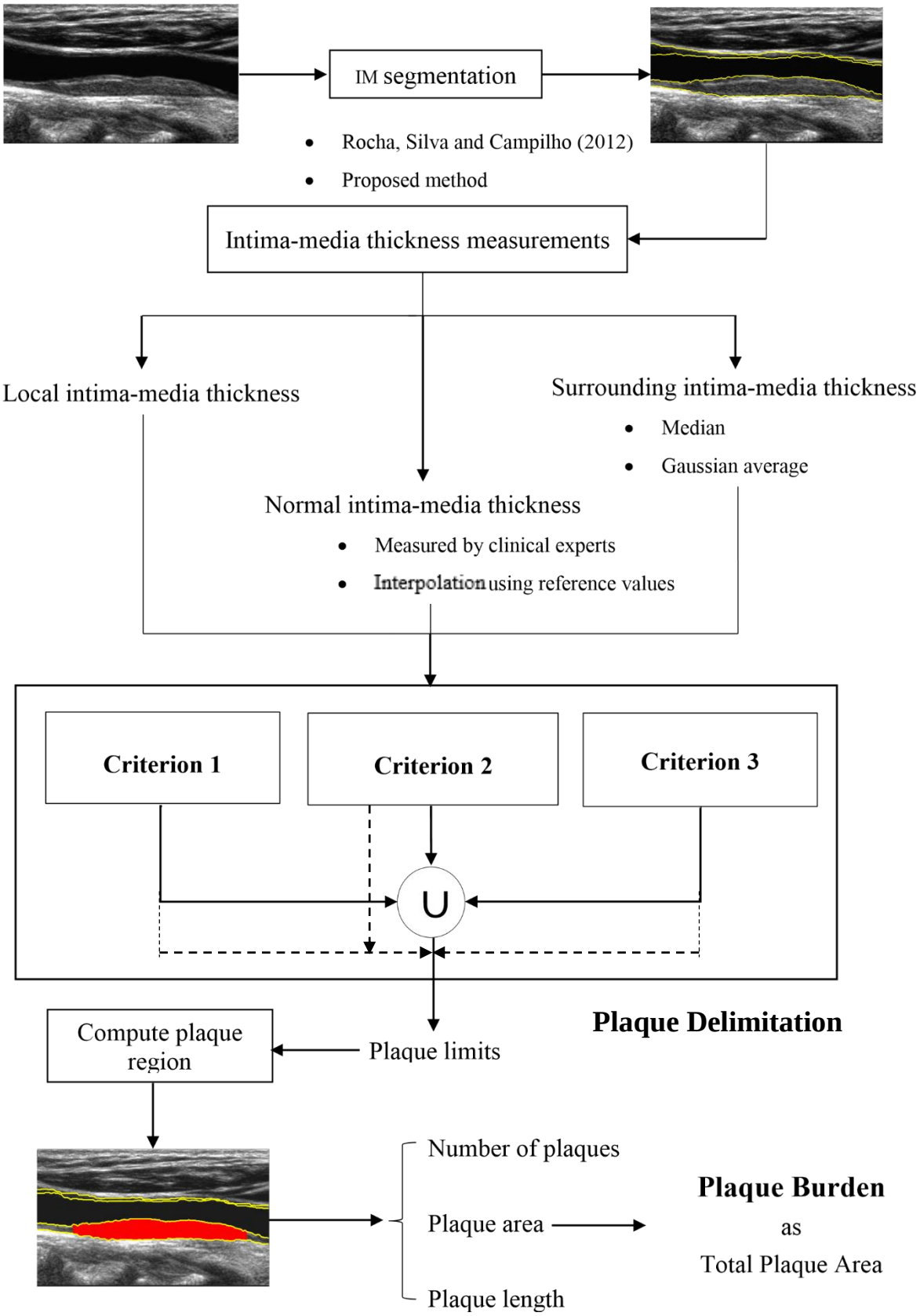

Figure 3.27 Block diagram illustrating the proposed methodology for measurement of plaque burden in ultrasound images of the carotid artery.

4 Experimental evaluation

In this chapter, the performance of the proposed method for segmentation of atherosclerotic plaques in ultrasound (US) images of the carotid artery is evaluated.

Section 4.1 describes the image database. The procedure for the acquisition of a ground truth with manual segmentations of the carotid wall and atherosclerotic plaques is provided in section 4.2.

Quantitative metrics for performance assessment are described in section 4.3.

A comparative evaluation of the two methods used for the segmentation of the intima-media (IM) region of the carotid wall is made in section 4.4.

In section 4.5, alternative methods for implementing the different blocks of the proposed algorithm for plaque delimitation using segmented IM contours are compared.

In section 4.6, a global evaluation of the proposed method for plaque segmentation is provided, along with segmentation examples and some topics that motivate future research work.

4.1 Image database

A dataset of 95 2D B-mode longitudinal US images of the common carotid artery (CCA) is used. These images come from two different sets of 35 and 60 images. Both datasets were provided by Centro Hospitalar São João (CHSJ) and were acquired following standardized protocols and with the parameters selected by specialized clinicians (Touboul *et al.*, 2012). The images were recorded with 256 levels of grey and varying pixel size, and were later processed for pixel size normalization to 0.09 mm, a common value in clinical practice (Bae *et al.*, 2006; Lee, Choi and Kim, 2010; Rocha, 2007; Rocha *et al.*, 2010, 2011; Rocha, Silva and Campilho, 2012). They show plaques with different shapes and sizes. In total, there are 120 plaques, 91 of which are located in the FW and the remaining 29 were located in the NW.

The first 35 images come from the database used by Rocha *et* al. (2010, 2011 and 2012). They were acquired using a Philips HDI 5000 US system from 25 symptomatic patients.

The second dataset of 60 images was acquired with a GE Healthcare Vivid E US system from 28 patients, 21 of which are male, with ages ranging from 48 to 79 years old.

The 95 images were randomly divided in two smaller subsets, which are the train and test sets. The train set contains 35 images and is used for algorithm development and parameter optimization. The test set contains 60 images and is used for comparing different methods for plaque segmentation and evaluating the performance of the proposed method. Regarding the test set, the age, gender and normal intima-media thickness for the patient (IMT_P) were available for 40 images (clinical set). IMT_P was measured by clinical experts in healthy and plaque-free regions of the carotid artery according to standardized protocols of a medical consensus (Touboul *et al*., 2012).

4.2 Acquisition of a ground truth

In order to evaluate the performance, a ground truth (GT) manual segmentation of the carotid wall and atherosclerotic plaques is required.

For the 35 images of the Rocha *et al.* dataset a manual segmentation of the IM region performed by a clinical expert was already available. The images were segmented using a software tool developed by Catarina Brito Carvalho (2012). This tool enables a manual segmentation of the IM region of the carotid wall in US images through a graphical user interface (GUI). This GUI is shown in figure 4.1. The user loads an image and chooses which contour to trace in the menu on the left. After this, the user superimposes points on the chosen interface through mouse clicks, which are then consecutively connected through line segments. No manual tracings were available for the rest of the images. This segmentation was performed by the author using the aforementioned software tool.

A GT segmentation of the IM region is not enough to evaluate the proposed method for plaque segmentation. A manual annotation of the left and right limits of each plaque is required to allow a comparison with the ones which are automatically produced by the proposed method. The software tool was modified to enable the user to select the right and left limits of each plaque for both carotid walls. This selection is done with mouse clicks. The IM region located between the selected limits is segmented as plaque.

Plaque delimitation is done according to the same procedure followed by clinical experts, which consists of a subjective evaluation of the criteria to define atherosclerotic plaque proposed in the medical consensus (Touboul *et al*., 2012). To have a primary indication of whether a plaque was present or not, the software tool was modified so when a lumen-intima (LI) interface was traced, an auxiliary line was simultaneously drawn 1.5 mm above (for the near-end wall (NW)) or below (for the far-end wall (FW)) the LI contour. If the manual tracing of the media-adventitia (MA) for that wall was beyond this auxiliary line, a plaque was present according to criterion 1 of the medical consensus, as explained in section 3.4.2.1.

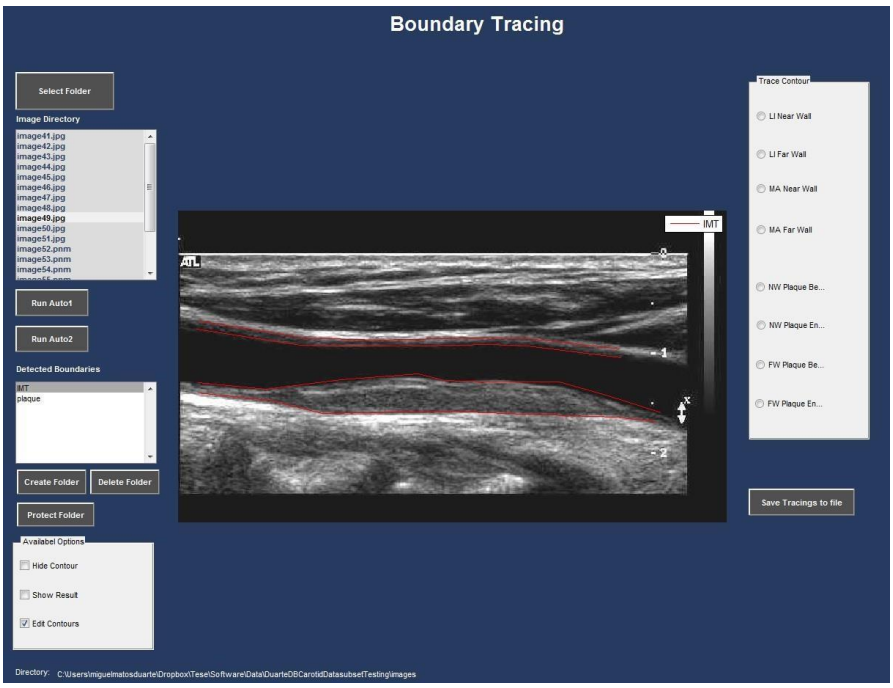

Figure 4.1 GUI for manual segmentation of the IM region of the carotid wall and atherosclerotic plaques in US images of the carotid artery.

4.3 Quantitative evaluation metrics

In order to evaluate the performance of the proposed method for automatic segmentation of atherosclerotic plaques, quantitative measures that compare the GT and automatic segmentations are required.

4.3.1 Segmentation of the intima-media region

To evaluate the quality of the segmentation of the IM region, two error measures were created. $RMSE(GT^i; A^i)$ is the root mean squared vertical distance between GT and automatic contours of the same interface for image i.

It is given by:

$$RMSE\left(GT^i; A^i\right)(\text{mm}) = \sqrt{\frac{\sum_{j=1}^{C_i}\left[\left(GT^i(j) - A^i(j)\right) \times dx0\right]^2}{C_i}} \qquad (4.1)$$

where $GT^i(j)$ and $A^i(j)$ are the rows where the GT and automatic contours are defined at column j for image i, respectively, and C_i is the number of columns in image i for which both contours are defined. GT^i and A^i represent the contour of any of the four interfaces of the carotid wall (*i.e.* the LI or the MA interfaces of both the NW and FW). A global measure for the entire database is calculated as:

$$RMSE(GT;A)(\text{mm}) = \sqrt{\frac{\sum_{i=1}^{N}\sum_{j=1}^{C^i}\left[\left(GT^i(j)-A^i(j)\right)\times dx0\right]^2}{\sum_{i=1}^{N} C^i}} \quad (4.2)$$

where N is the number of images in the database.

4.3.2 Plaque segmentation

To evaluate the quality of plaque segmentation, different error measures were created to compare the GT and automatic plaque limits.

4.3.2.1 Length measures

The relative length error between GT and manual plaque delimitations ε_L^i for a given image i is given by:

$$\varepsilon_L^i(\%) = \frac{\sum_{j=1}^{C_i} error^i(j)}{C_i} \times 100 \quad (4.3)$$

where $error^i(j)$ is an indicator function that assumes the value of 0 if column j corresponds to a plaque or plaque-free region in both delimitations and 1 if not, and C_i is the number of columns in image i of the segmented IM region.

A global measure for the entire database is calculated as:

$$\varepsilon_L = \sqrt{\frac{\sum_{i=1}^{N}\left(\sum_{j=1}^{C_i} error^i(j)\right)^2}{\sum_{i=1}^{N} C_i}} \quad (4.4)$$

where N is the number of images in the database.

4.3.2.2 Area measures

The relative area error between GT and manual plaque delimitations ε_A^i for a given image i is given by:

$$\varepsilon_A^i(\%) = \frac{\sum_{j=1}^{C_i} error^i(j)\times IMT(j)}{\sum_{j=1}^{C_i} IMT(j)} \times 100 \quad (4.5)$$

where $error^i(j)$ is an indicator function that assumes the value of 0 if column j corresponds to a plaque or plaque-free region in both delimitations and 1 if not, C_i is the number of columns in image i of the segmented IM region and $IMT(j)$ is the local intima-media thickness for column j.

A global measure for the entire database is calculated as:

$$\varepsilon_A = \sqrt{\frac{\sum_{i=1}^{N}\left(\sum_{j=1}^{C_i} error^i(j)\times IMT(j)\right)^2}{\sum_{i=1}^{N}\sum_{j=1}^{C_i} IMT(j)}} \tag{4.6}$$

where N is the number of images in the database.

4.3.3 Statistical significance

The Kruskal-Wallis statistical test (KW) is used for parameter optimization and method selection. KW is a non-parametric method for testing if the samples of a given set originate from the same distribution. It compares medians of two or more different samples. This test enables to discriminate, for one of the samples, how many samples from the initial set are significantly different. KW does not assume that the variable being analyzed is normally distributed, and is used when the data distribution is non-normal or simply unknown. This test assumes that the samples are independent (Ott and Longnecker, 2008).

KW is performed on the distributions of the different error measures: $\varepsilon_L{}^i$ and $\varepsilon_A{}^i$, for plaque segmentation, and $RMSE(GT^i; A^i)$, for contour segmentation, for the N images of a given dataset. It is used to define the left and right limits of the optimum value range for a given parameter, within which there is no statistical evidence that the results of the produced segmentation are different. Also, it provides statistical evidence that allows choosing among alternative methods to implement different blocks of the proposed segmentation method, or not. A test is considered significant if its p-value is below 0.05.

4.4 Segmentation of the carotid wall

In this section, the results of the segmentation of the IM region are discussed. This comparison is divided in two sections: algorithm for detection of the lumen axis and algorithm for segmentation of IM.

4.4.1 Lumen axis detection

The detection of the lumen axis (L) is required for the posterior selection of a region of interest. Two alternative methods for detecting L were used: the one proposed by Rocha, Silva and Campilho (2012), described in section 3.3.1, and the one proposed by Rouco and Campilho (2013), described in section 3.3.3.1.

4.4.1.1 Parameter optimization

Each one of these methods has two parameters which need to be optimized.

- Rocha, Silva and Campilho (2012): LR_{min} and CR_{max}, which are the minimum lumen vertical radius and maximum carotid vertical radius, respectively.

- Rouco and Campilho (2013): CR_{min} and CR_{max}, which are the minimum and maximum carotid vertical radius, respectively.

These parameters were initially set to:

- Rocha, Silva and Campilho (2012): $LR_{min} = 0.5$ mm; $CR_{max} = 7$ mm.

- Rouco and Campilho (2013): $CR_{min} = 2$ mm; $CR_{max} = 7$ mm.

which are the values referred by the authors in their publications.

The intervals defined by these parameters were gradually extended until the number of images in the train set ($N = 35$) where the detection of L failed remained unchanged. The optimum values for these parameters and are shown in table III.

Table III Optimum parameter values for the two methods used for lumen axis detection.

Parameter	Optimum value	Method
LR_{min}	1 mm	Rocha, Silva and Campilho (2012)
CR_{max}	7 mm	Rocha, Silva and Campilho (2012)
CR_{min}	2 mm	Rouco and Campilho (2013)
CR_{max}	12 mm	Rouco and Campilho (2013)

4.4.1.2 Method selection

For selecting the best method, the test set was used ($N = 60$). The optimum values were set for the parameters of both methods. The number of images where the detection of L failed using each method is shown in table IV.

Table IV Quantitative comparison between the two methods used for lumen axis detection.

Method	Percentage of images with a correct detection
Rocha, Silva and Campilho (2012)	56/60=93%
Rouco and Campilho (2013)	58/60=97%

Both methods show a good performance, detecting the carotid lumen axis in more than 90% of the images. The method proposed by Rouco and Campilho (2013) is marginally better, outperforming the one of Rocha, Silva and Campilho (2012) in two images highly affected by speckle noise. In this type of images, the method provides a correct detection due to the robustness of the proposed symmetry measure to echo regions with different textures, as explained in section 3.3.3.1. The algorithm proposed by Rocha, Silva and Campilho (2012) is more sensitive to noise as it uses the image intensity histogram for the threshold-based segmentation. The method proposed by Rouco and Campilho (2013) was chosen for lumen detection.

4.4.2 Intima-media segmentation

Two alternative methods for the segmentation of the IM region were used: original method proposed by Rocha, Silva and Campilho (2012), described in sections 3.3.1 and 3.3.2, and the method proposed in the present work, described in sections 3.3.3 and 3.3.4. For the comparison of both methods, the lumen axis was detected using the algorithm proposed by Rouco, and Campilho (2013), which showed the best performance.

4.4.2.1 Parameter optimization

In the proposed method, parameters k and LR_{min} were set to 1 and 0.5 mm, respectively, which were empirically observed to be appropriate values to ensure an accurate segmentation in most of the images in the train set. By setting k=1 we ensure that the lumen region for the estimation of parameter α does not include echo regions from the carotid wall, as it is defined by the minimum expected lumen vertical radius.

In both methods, the values set for λ_e are the ones referred by Rocha, Silva and Campilho (2012), and are shown in table V. This parameter was not optimized for our database as it was observed that it does not have a big influence in the segmentation results.

Table V Values set for λ_e (Rocha, Silva and Campilho (2012)).

Parameter	Wall	Contour	Value
λ_e	NW	LI	160
		MA	50
	FW	LI	80
		MA	50

Each one of the used methods has a set of parameters which need to be optimized.

- Original method: σ_{FM} andσ_{FAM}, which are scale parameters that control de fuzziness of the membership function used for the classification of LI and MA edges, respectively. Both are optimized individually for each wall.

- Proposed method: s and σ_{FAM}, which are scale parameters that control de fuzziness of the membership function used for the classification of LI and MA edges, respectively. Both are optimized individually for each wall.

For the optimization of these parameters, the train set was used ($N = 35$). Since the segmentation of the MA interface is dependent on the prior segmentation of LI, σ_{FM} and s were first optimized for each wall. These parameters were varied between 0 and 1, with increments of 0.01. $RMSE(GT; A)$ was calculated for the LI contour for each value of σ_{FM} and s. The optimum values for these parameters are the ones that minimize $RMSE(GT; A)$. KW was used to establish the optimum value range for both parameters. This is shown in table VI.

Table VI Optimum parameter values for the two methods used for segmenting the LI contour.

Parameter	Wall	Optimum value	Optimum range	Method
σ_{FM}	NW	0.13	0.10-0.39	Original
	FW	0.24	0.10-0.37	Original
s	NW	0.11	0.03-0.33	Proposed
	FW	0.17	0.03-0.33	Proposed

The exact same procedure was followed to optimize σ_{FAM} for the NW and FW in both methods. For the prior segmentation of the LI interface, the optimum values for σ_{FM} and s shown in table VI were used. The optimum values and range for σ_{FAM} are shown in table VII.

Table VII Optimum parameter values for the two methods used for segmenting the MA contour.

Parameter	Wall	Optimum value	Optimum range	Method
σ_{FAM}	NW	0.31	0.15-0.43	Original
	FW	0.60	0.34-0.60	Original
σ_{FAM}	NW	0.06	0.05-0.08	Proposed
	FW	0.56	0-28-0.57	Proposed

4.4.2.2 Method selection

The test set ($N = 60$) was used for comparing the two segmentation methods. The optimum values were set for the different parameters of each method. The two images where the detection of the lumen axis failed were excluded from the analysis.

Figure 4.2 shows cumulative distributions of $RMSE(GT^i, A^i)$ for the four segmented contours using the original (red line) and proposed (blue line) methods. The black vertical line marks the 1 mm error limit. The value of $RMSE(GT, A)$ for the whole dataset is shown in table VIII for each of the segmented contours, along with the percentage of images for which $RMSE(GT^i, A^i)$ is smaller than 1 mm.

Table VIII Quantitative comparison between the two methods for segmenting the IM region.

Method	Wall	Contour	$\boldsymbol{RMSE(GT, A)}$ **(mm)**	**% images with** $\boldsymbol{RMSE(GT^i, A^i)} < \mathbf{1\ mm}$
Original	NW	LI	3.28	40
		MA	2.12	68
	FW	LI	2.26	65
		MA	1.12	78
Proposed	NW	LI	4.52	40
		MA	3.19	55
	FW	LI	1.68	72
		MA	0.92	75

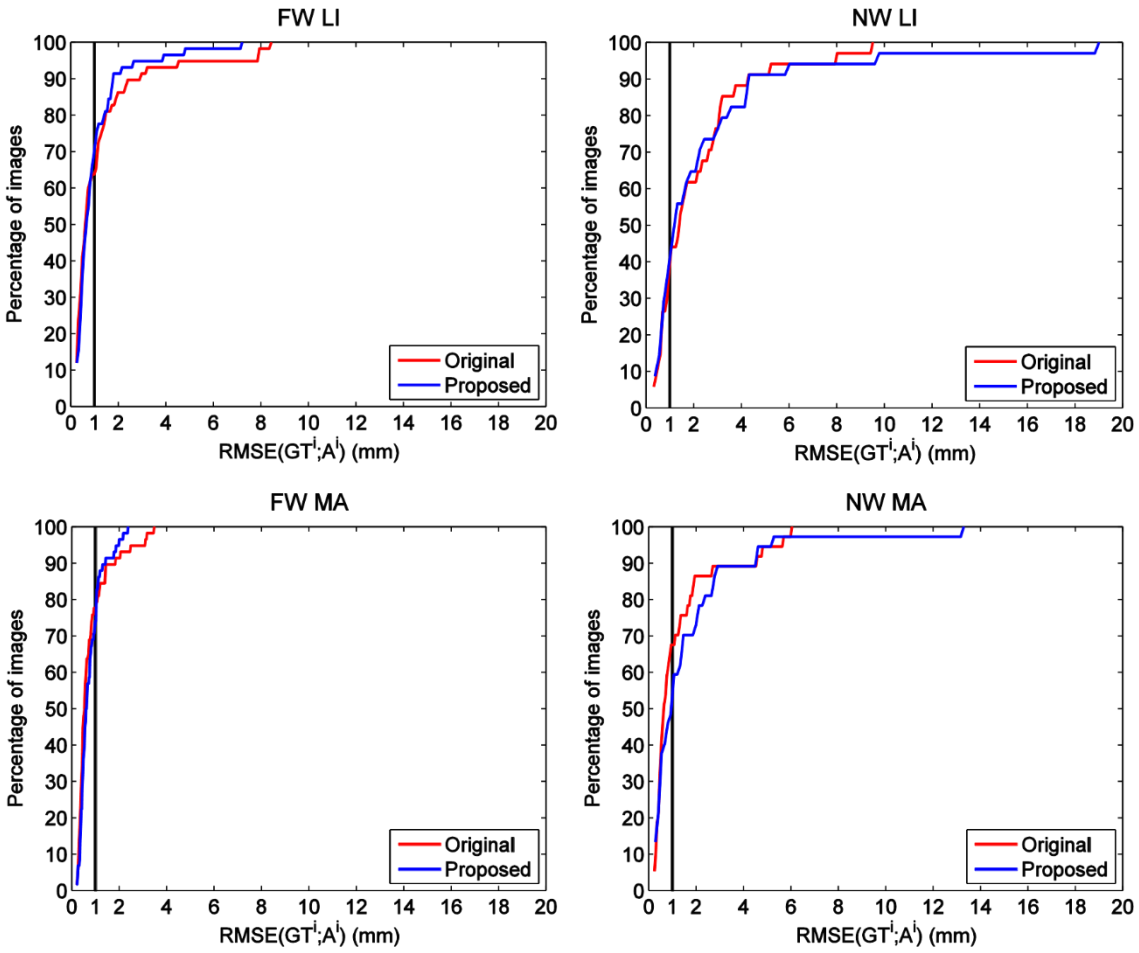

Figure 4.2 Cumulative distributions of RMSE(GTi; Ai) for the four segmented contours of the IM region using the original (red line) and proposed (blue line) methods. The black vertical line represents an RMSE(GTi; Ai) error of 1 mm.

KW showed no statistical significance for any of the contours. This may be due to the small number of samples (60 images). The p-value of the test for each contour is shown in table IX.

Table IX p-value of KW comparing the two methods for segmenting the IM region.

Contour	KW p-value
Near-wall media-adventitia	0.35
Near-wall lumen-intima	0.99
Far-wall lumen-intima	0.88
Far-wall media-adventitia	0.40

In the original and proposed methods the segmentation errors for the NW are larger than for the FW, especially in the LI contour. This observation confirms the reports from previous studies that this wall is harder to segment (Loizou *et al.*, 2007a; Faita *et* al.;

2008, Petroudi *et al*., 2012; Rocha, Silva and Campilho, 2012). This is due to echo overlap which results in poor visibility and boundary gaps in large sections of this wall. This is why the NW is not suitable for measuring the intima-media thickness, at least with the current available technology, and the FW is preferred in clinical practice (Wikstrand, 2007; Stein *et al*., 2008; Touboul *et al*., 2012).

Both methods show the best performance for the MA contour of the FW. This interface is the one which shows best visibility and contrast in the majority of the images.

For the FW, the proposed method shows a marginally better performance than the original in the segmentation of the LI contour. This is because the improvements which were made to the original method, apart from the alternative method for lumen axis detection, were all performed in the segmentation of LI and result in a better segmentation in images highly affected by speckle noise, as explained in sections 3.3.3. Regarding the MA contour, both methods show a similar performance.

For the segmentation of the NW, the original method appears to be better. It was observed that for this wall the proposed method failed to segment the LI contour in images where speckle was not uniformly distributed, which led to the calculation of a non-representative value of α for estimation of the lumen noise (section 3.3.3.4). This resulted in an incorrect segmentation of the MA contour as well. For these images, the lumen region (Ω) where this parameter is calculated was expanded by increasing the value of k (equation 3.12). When this optimization is performed, the proposed method achieved a better segmentation than the original method in these images. This shown in figure 4.3.

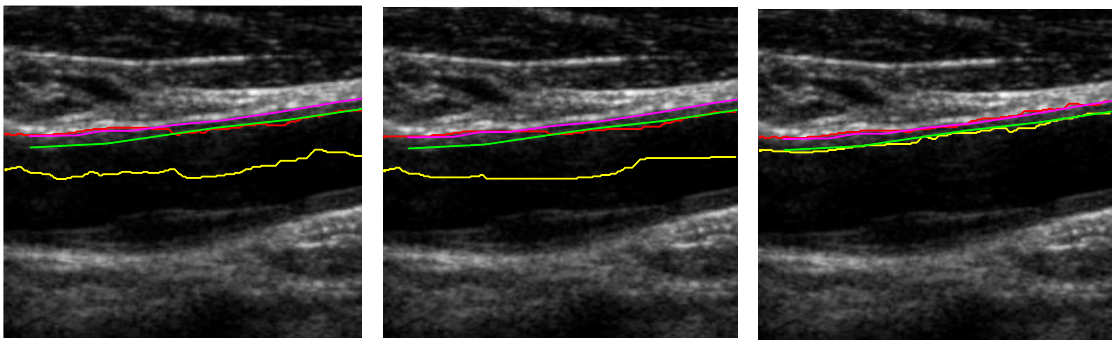

(a) (b) (c)

Figure 4.3 Segmentation of the NW improves by increasing the value of k and expanding Ω for the estimation of parameter α. (a) Original method. (b) Proposed method with $k = 1$. (c) Proposed method with $k = 8$. The red and yellow lines represent the automatic MA and LI contours, respectively. The magenta and green lines represent the manual MA and LI contours, respectively.

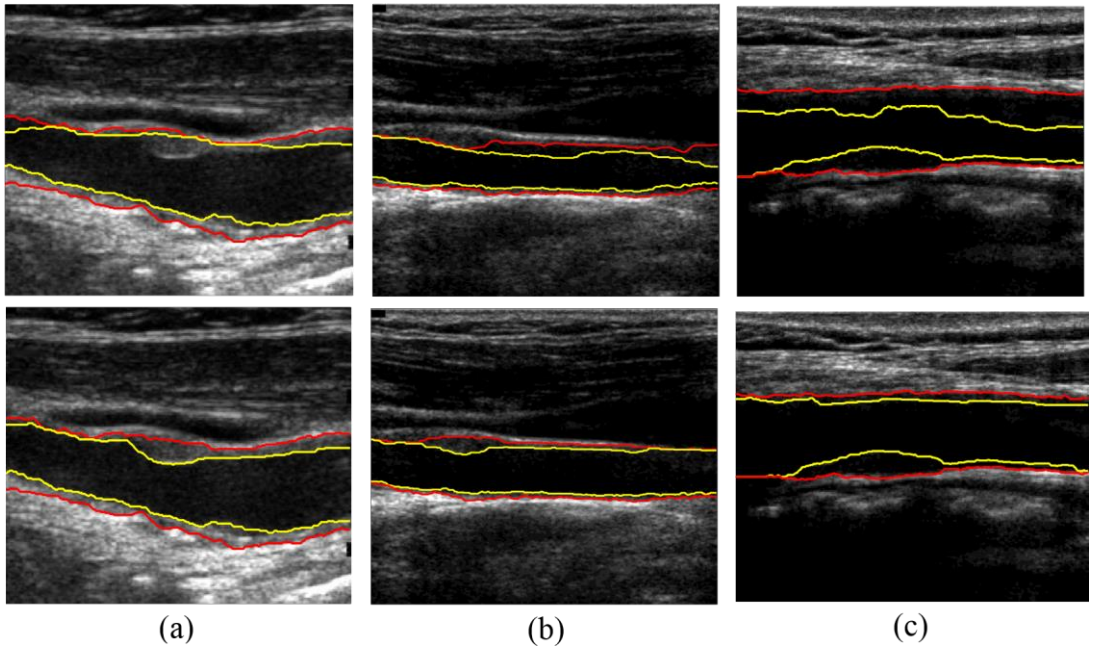

Figure 4.4 Comparison between the two methods used for the segmentation of the IM region. In the top image row the original method is used. In the bottom image row the proposed method is used. The yellow and red lines represent the LI and MA contours, respectively.

Figure 4.4 shows examples where the proposed method (top row) performs a better segmentation of the IM region than the original method (bottom row). In (a) and (b) the proposed method allows the inclusion of a plaque in the segmented IM region of the NW. In (c) it correctly segments the LI interface of the NW.

The method proposed in this work is based on the one of by Rocha, Silva and Campilho (2012) and preserves its main features, which are:

- Absence of user-interaction.
- Avoidance of methods for image normalization, such as histogram equalization, by computing specific and image-adapted thresholds.
- Avoidance of low-pass filtering for noise attenuation, which can result in loss of information, by using fuzzy classification of edges.
- Segmentation of both the NW and the FW IM region in real-time.
- Robustness to the presence of plaques with different shapes and sizes.

Additionally, the modifications introduced here improve the segmentation in images highly affected by speckle noise. These modifications apply to the segmentation of the LI contour but also improve the results for MA. The proposed method was therefore chosen to segment the contours of the IM region, required for the posterior plaque delimitation stage. Figure 4.5 shows the best and worst segmentation results of the proposed method.

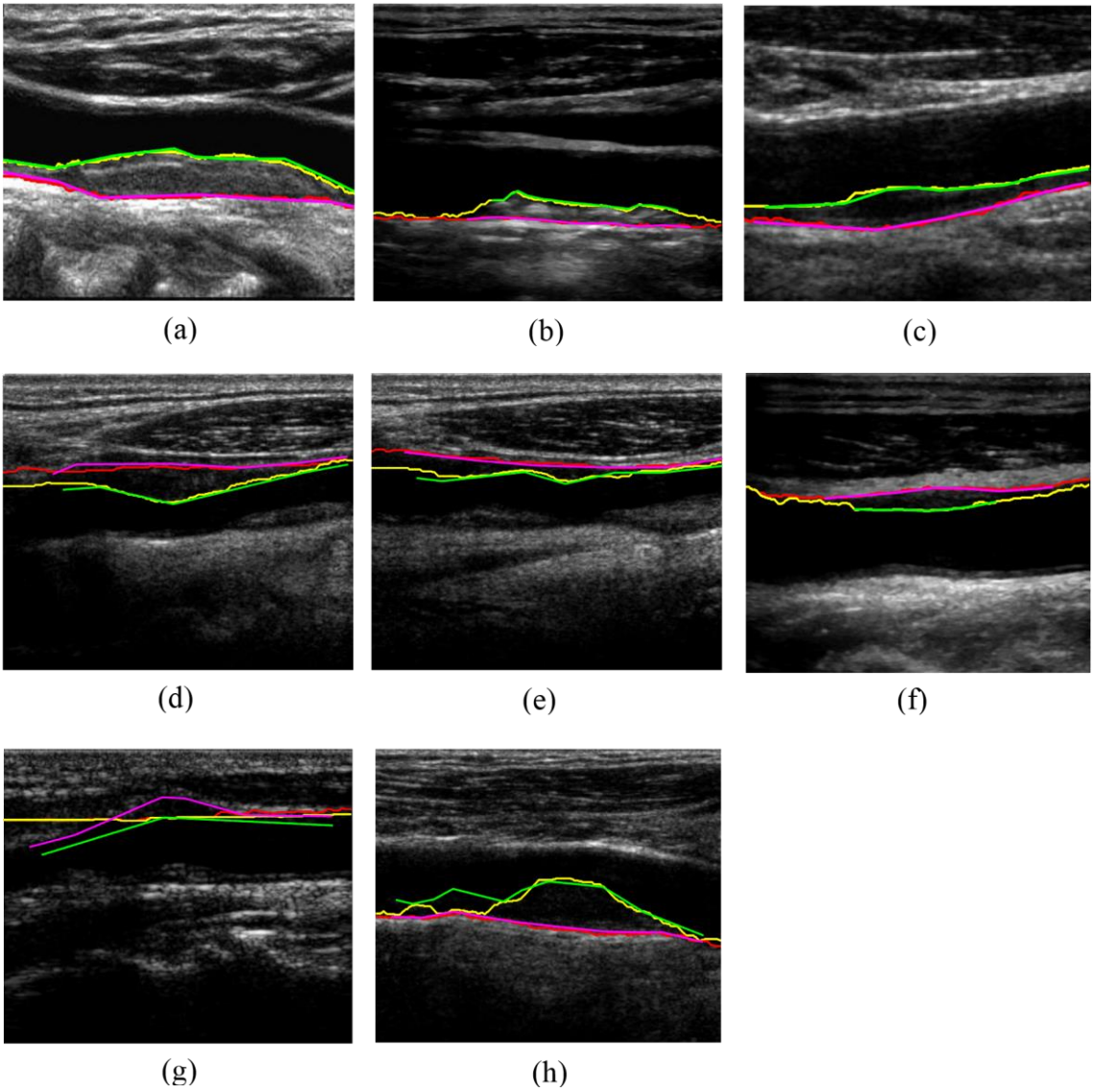

Figure 4.5 Best and worst results for the segmentation of the IM region of the carotid wall in US images as performed by the proposed method. A, B and C – FW best. D, E and F – NW best. G – FW worst. H – NW worst. The red and yellow lines represent the MA and LI automatically segmented contours, respectively. The magenta and green lines represent the MA and LI manually segmented contours, respectively.

As explained in section 3.3.3.6, one of the algorithm's main assumptions is that there are no edges in the lumen, and if there are they are caused by noise. Boundaries which show an echogenicity similar to the lumen will not be detected, as it often happens with weak echolucent edges of the LI interface in the NW. The improvement of the segmentation accuracy for this type of interfaces is a matter of research for future work.

4.5 Plaque segmentation

In this section, the results of plaque segmentation from segmented contours of the IM region are discussed. In the first section, the procedure for calculating the surrounding intima-media thickness is chosen by comparing two alternative methods of performing

this estimation. In the second section, a comparison between different ways of estimating the normal value of the intima-media thickness for the patient is made. In the third section, the results of the segmentation according to the definition of atherosclerotic plaque proposed in the medical consensus are evaluated individually for each criteria and for their combination. Finally, a global evaluation of the method's performance is provided.

4.5.1 Surrounding intima-media thickness

Two methods were used to estimate the surrounding intima-media thickness along the carotid wall: Gaussian average (G^{σ}) and median (med) of the local intima-media thickness within a neighbour region.

4.5.1.1 Parameter optimization

Each one of the used methods has a set of parameters which need to be optimized.

- Gaussian estimation: σ is the standard deviation of the Gaussian function used in the discrete convolution (equation 3.21, section 3.4.3.2) and h is the offset separating the column which surrounding intima-media thickness is being estimated from the centre column of the neighbour region.

- Median estimation: l is the length of the neighbour region (equation 3.19, section 3.4.3.1) and h is the offset separating the column which surrounding intima-media thickness is being estimated from the centre column of the neighbour region.

For the optimization of these parameters, the train set ($N = 35$) was used. The GT of the IM region were used to calculate the local intima-media thickness along the carotid wall, segmented as described in section 4.2. The two images where lumen detection failed were excluded from the analysis. Only criterion 2 was used for plaque delimitation, as it is the only one that requires the definition of the surrounding intima-media thickness.

For the Gaussian estimation, σ and h were varied between 0.05 and 380 pixels with increments of ¼ octave, derived from the fact that the length of the longest plaque found in the train set was 380 pixels. ε_L and ε_A were calculated for each combination of σ and h. Figure 4.6 shows ε_L and ε_A plotted as a function of both these parameters.

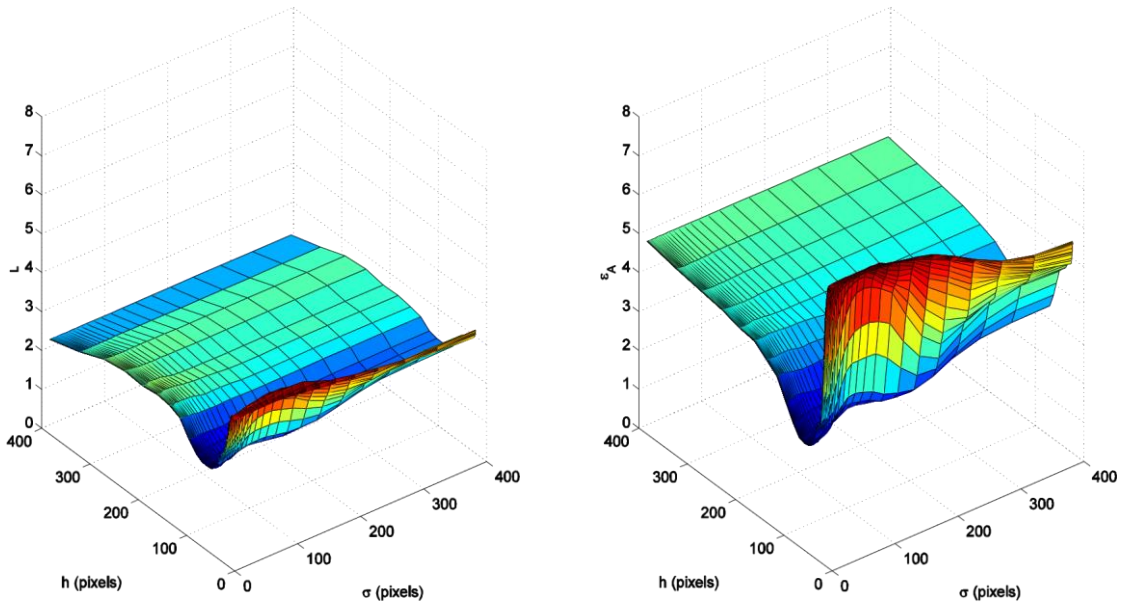

Figure 4.6 (a) – ε_L plotted as a function of h and σ for Gaussian estimation of the surrounding intima-media thickness. (b) – ε_A plotted as a function of h and σ for Gaussian estimation of the surrounding intima-media thickness.

When using Gaussian estimation, the quality of plaque segmentation is more sensitive to h than σ. This is because, when performing the Gaussian average of a 1D signal, the central data points of that signal are more influent as they are multiplied by the largest coefficients of the normal distribution. When σ changes, the central data points remain the same, being multiplied by different coefficients. When h changes, however, the neighbour region shifts, and the central data points change, causing a larger variation of the surrounding intima-media thickness and the segmented plaques.

Table X shows the optimum values for σ and h, which are the ones that minimize ε_L and ε_A. For each error measure, the optimum parameter range is defined using KW. The optimum range for these parameters is the smallest interval defined by the values shown in table X. For σ is 8-20 pixels and for h is 40-80 pixels.

Table X Optimum parameter values for Gaussian estimation of the surrounding intima-media thickness.

Parameter	$\boldsymbol{\varepsilon_L}$		$\boldsymbol{\varepsilon_A}$	
	Optimum value	**Optimum range**	**Optimum value**	**Optimum range**
σ (pixels)	14	7-24	14	8-20
h (pixels)	57	40-96	57	40-80

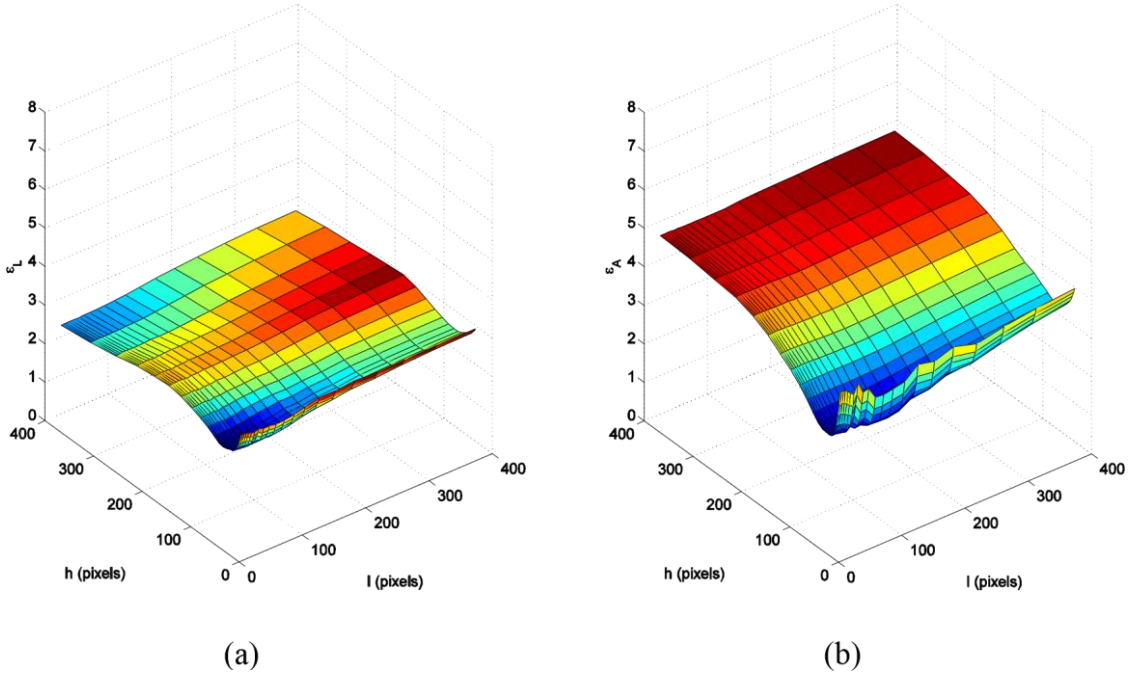

(a) (b)

Figure 4.7 (a) – ε_L plotted as a function of h and l for median estimation of the surrounding intima-media thickness. (b) $-\varepsilon_A$ plotted as a function of h and l for median estimation of the surrounding intima-media thickness.

For the median estimation, l and h were varied between 0.05 and 380 pixels with increments of ¼ octave, derived from the fact that the length of the longest plaque found in the train set was 380 pixels. ε_L and ε_A were calculated for each combination of l and h. Figure 4.7 shows ε_L and ε_A plotted as a function of both these parameters.

Table XI shows the optimum values for σ and h, which are the ones that minimize ε_L and ε_A. For each error measure, the optimum parameter range is defined using KW. The optimum range for these parameters is the smallest interval defined by the values shown in table XI. For l is 10-17 pixels and for h is 24-96 pixels. The optimum value set for h is 28 pixels because it minimizes ε_A. More focus should be given to this measure since the same error in length can give rise to very different area errors, depending on the local intima-media thickness, which result in different values for plaque burden.

Table XI Optimum parameter values for median estimation of the surrounding intima-media thickness.

Parameter	$\boldsymbol{\varepsilon_L}$		$\boldsymbol{\varepsilon_A}$	
	Optimum value	**Optimum range**	**Optimum value**	**Optimum range**
l (pixels)	14	10-17	14	8-24
h (pixels)	48	24-114	28	17-96

4.5.1.2 Method selection

For selecting one of the methods, the test set was used ($N = 60$). The automatic IM contours were used, segmented according to the proposed method selected in section 4.4.2.2. The two images where the detection of the lumen axis failed were excluded from the analysis. The optimum values were set for the different parameters of each method. Only criterion 2 was used for plaque delimitation, as it is the only one that requires the definition of the surrounding intima-media thickness.

Figure 4.8 shows cumulative distributions of ε_L^i and ε_A^i for plaque segmentation using Gaussian and median estimations of the surrounding intima-media thickness. The values of ε_L and ε_A for the whole dataset are shown in table XII. KW test showed no statistical significance when comparing both methods. The p-value of the test for each error measure is shown in table XIII.

Table XII Quantitative comparison of the two methods for the estimation of the surrounding intima-media thickness.

Method	ε_L	ε_A
Gaussian estimation	2.01	2.44
Median estimation	2.28	2.64

Table XIII p-value of KW comparing the two methods for the estimation of the surrounding intima-media thickness.

Error measure	KW test p-value
ε_L^i	0.81
ε_A^i	0.68

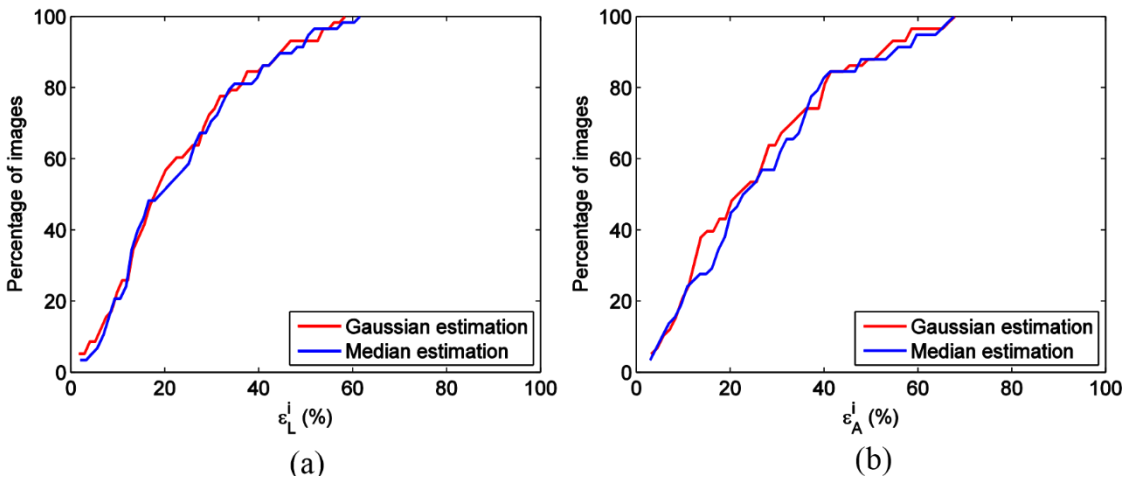

Figure 4.8 Cumulative distributions of (a) ε_L^i and (b) ε_A^i for plaque segmentation using the Gaussian (red line) and median (blue line) estimations of the surrounding intima-media thickness.

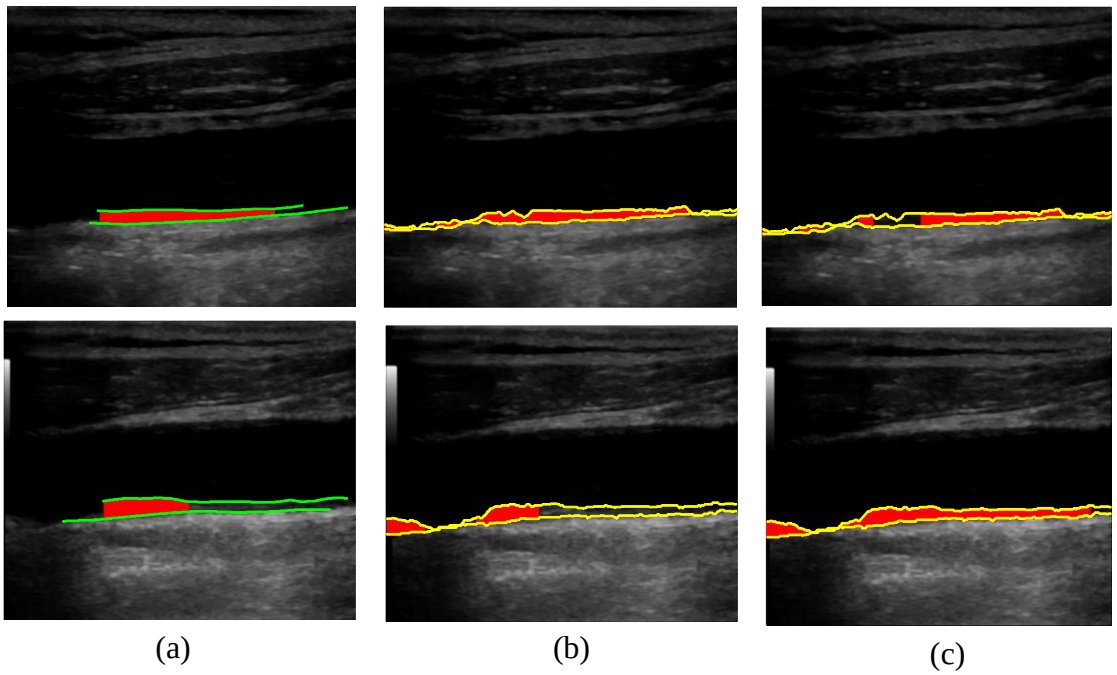

Figure 4.9 Comparison between the different methods of estimating the surrounding intima-media thickness. (a) Ground truth plaque segmentation. (b) Automatic plaque segmentation using the Gaussian estimation. (c) Automatic plaque segmentation using the median estimation. The green and yellow lines represent the manual and automatic contours of the IM region, respectively, and the segmented plaques are highlighted with a red overlay.

The Gaussian estimation is marginally better than the median. Figure 4.9 shows examples where Gaussian estimation (b) of the surrounding intima-media thickness results in better plaque segmentation when compared to the median estimation (c). In the first situation (top image row) the Gaussian estimation allows the segmentation of a continuous plaque region containing depressions. These depressions are incorrectly segmented as a plaque-free region when using the median estimation. In the second situation (bottom image row) the median estimation segments a healthy region of the artery as plaque. The Gaussian estimation was therefore chosen to calculate the surrounding intima-media thickness for plaque segmentation.

4.5.2 Normal intima-media thickness

The normal intima-media thickness for a patient is a reference measure required for plaque delimitation according to criterion 3 of the medical consensus (section 3.4.2.3). Reference measures for IMT_P were available for 40 images of the test set (clinical set), obtained by clinical experts in US images of the patient's carotid artery. However, US images do not always show suitable regions to perform the measurement. IMT_P can also be estimated using linear interpolation between reference values provided by large population-based cohort studies (Stein *et al*., 2008). Here we compare these two methods of estimating the normal intima-media thickness for the patient.

The clinical set was used ($N = 40$). Both the automatic and GT contours of the IM region were used to calculate the local-intima media thickness along the carotid wall. The automatic contours were segmented according to the proposed method selected in section 4.4.2.2, while the GT contours were manually segmented as explained in section 4.2. The two images where the detection of the lumen axis failed were excluded from the analysis. Only criterion 3 was used for plaque delimitation, as it is the only one which requires the definition of the normal intima-media thickness for the patient. This measure was obtained using two different methods:

- Expert: Measure performed by clinical experts in healthy and plaque-free regions of the carotid artery according to standardized protocols proposed in a medical consensus (Touboul *et al*., 2012).
- Linear interpolation between reference values provided by large population-based cohort studies (Stein *et al*., 2008). These values are shown in table AI in Appendix A. Three different studies were used:
  - AXA study (table AI-A).
  - Carotid Atherosclerosis Progression Study (CAPS) (table AI-B).
  - Edinburgh Artery Study (EAS) (table AI-C).

Figure 4.10 shows cumulative distributions of ε_L^i and ε_A^i for plaque segmentation using these different methods. The values of ε_L and ε_A for the whole dataset are shown in table XIV.

Table XIV Quantitative comparison of different methods to obtain the normal intima-media thickness for the patient.

Method	**Contour**	$\boldsymbol{\varepsilon_L}$	$\boldsymbol{\varepsilon_A}$
Expert	Ground truth	0.25	0.31
	Automatic	1.35	2.42
AXA	Ground truth	3.04	3.03
	Automatic	1.72	2.35
CAPS	Ground truth	2.26	2.35
	Automatic	0.86	1.32
EAS	Ground truth	2.63	2.69
	Automatic	0.86	1.32

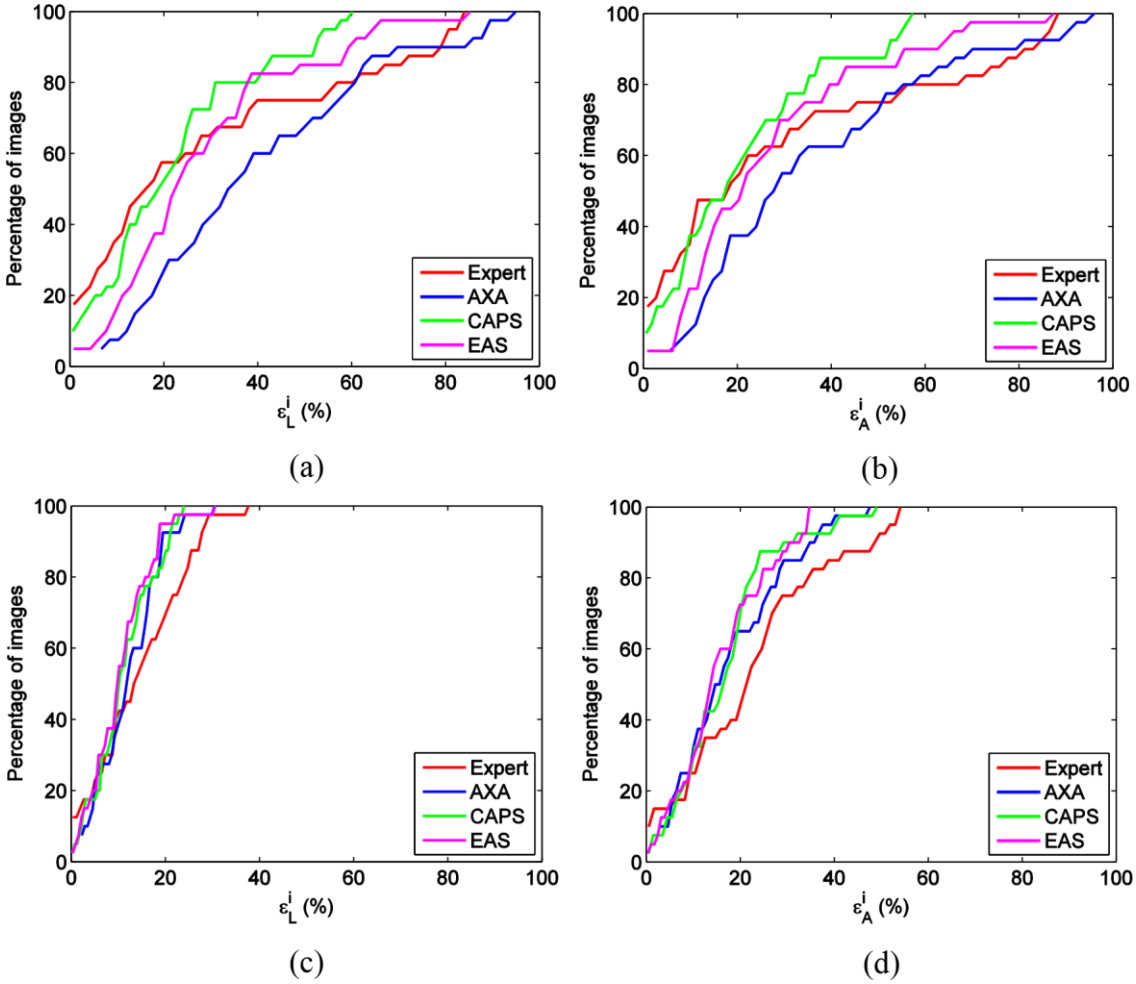

Figure 4.10 Cumulative distributions of ε_L^i and ε_A^i for plaque segmentation using different methods of obtaining IMT_P. (a) ε_L^i using the GT IM contours. (b) ε_A^i using the GT IM contours. (c) ε_L^i using the automatic IM contours. (d) ε_A^i using the automatic IM contours.

Table XIV shows that when the measure provided by clinical experts is used as normal intima-media thickness for the patient the plaque segmentation is more accurate, if the GT contours of the IM region are used. This is not the case, however, if the automatic contours are used instead. No statistical significance was obtained with KW when comparing the different methods using both types of contours. These results show that using the reference values provided by the cohort studies is a valid alternative to estimate the normal intima-media thickness for a patient in situations where this measurement cannot be performed directly by clinical experts in US images. These studies were conducted under standard protocols for US image acquisition and measurement of the intima-media thickness and are acknowledged by the international medical community (Stein *et al*., 2008). Therefore, they provide reference values that can be used as a reliable estimation of the normal intima-media thickness for the patient.

4.5.3 Plaque delimitation using different criteria to define plaque

The proposed method uses three objective criteria proposed in a medical consensus to define atherosclerotic plaque (Touboul *et al*., 2012). These definitions are based on specific measures of the intima-media thickness and reference threshold values to compare these measures with. Each criteria was implemented separately and provides an independent plaque segmentation. Here, we do a comparison between the segmentation results obtained using each criteria individually and their combination.

The clinical set was used ($N = 40$), since the use of criterion 3 requires the patient clinical data. The automatic contours of the IM region were used to calculate the local intima-media thickness along the carotid wall, segmented according to the proposed method selected in section 4.4.2.2. The two images where the detection of the lumen axis failed were excluded from the analysis. For criterion 2, the surrounding intima-media thickness was calculated using the Gaussian estimation, selected in section 5.5.1, and the correspondent optimum parameter values. For criterion 3 the value of the normal intima-media thickness for the patient was measured by clinical experts in healthy and plaque-free regions of the carotid artery according to standardized protocols of a medical consensus (Touboul *et al*., 2012).

Figure 4.11 shows cumulative distributions of ε_L^i and ε_A^i for plaque segmentation using each criteria individually and their combination. The values of ε_L and ε_A for the whole dataset are shown in table XV. The KW test showed no statistical significance when comparing the three criteria and their combination. The p-value of the test for each error measure is shown in table XVI.

Table XV Quantitative comparison of different criteria to define plaque and their combination.

Method	$\boldsymbol{\varepsilon_L}$	$\boldsymbol{\varepsilon_A}$
Criterion 1	1.35	2.42
Criterion 2	1.13	1.67
Criterion 3	1.40	2.57
Combined criteria	1.00	1.20

Table XVI p-value of KW comparing different criteria to define plaque and their combination.

Error measure	**KW test p-value**
ε_L^i	0.43
ε_A^i	0.11

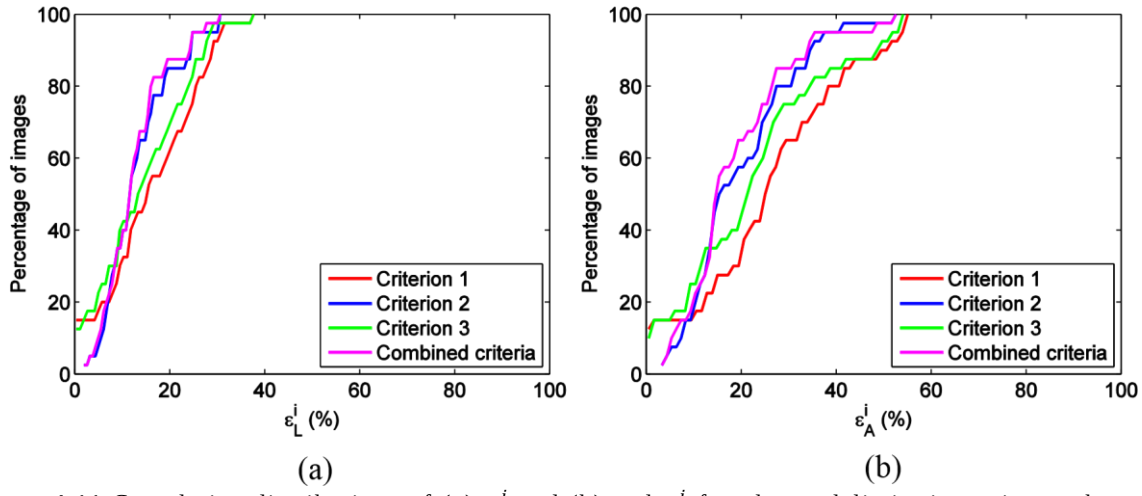

Figure 4.11 Cumulative distributions of (a) ε_L^i and (b) and ε_A^i for plaque delimitation using each criteria to define atherosclerotic plaque individually and their combination.

These results show that plaques are complex structures which objective definition is not a trivial problem. In the image database used in the present work there are plaques with different shapes and sizes and the definition given by each of the criteria is not enough to ensure a correct segmentation of all of them, if used individually. The combination of criteria provides a slightly better plaque segmentation, as shown in table XV. This observation is in accordance with the medical consensus, which states that the use of the definitions proposed by the three criteria "permit classification of the vast majority of carotid lesions observed with ultrasound." The combination of the three criteria proposed in (Touboul *et al.*, 2012) to define atherosclerotic plaque was therefore chosen for plaque segmentation.

4.6 Overall performance of the proposed method for plaque segmentation

The proposed method for plaque segmentation takes as input a 2D B-mode US image of the carotid artery. The different stages of the method are:

- First, the contours of the IM region of both carotid walls are segmented. For this, the lumen is detected using the algorithm proposed by Rouco and Campilho (2013) described in section 3.3.3.1. The optimum parameter values for this algorithm are referred in section 4.4.1.1. The LI and MA interfaces are segmented using the method proposed in the present work. This method is based on the one proposed by Rocha, Silva and Campilho (2012) and is optimized for images showing high noise contamination, as described in sections 3.3.3 and 3.3.4. The optimum parameter values for this algorithm are referred in section 4.4.2.1.

- With the segmented contours, plaque segmentation is performed using a combination of three objective criteria proposed in a medical consensus for defining atherosclerotic plaque, based on measures of the intima-media thickness and reference thresholds to compare these measures with.

    - For estimating the surrounding intima-media thickness required for plaque definition according to criterion 2, a Gaussian average of the local intima-media thickness within a neighbour region in the carotid wall is used. The process for calculating this measure is described in section 3.4.3.2. The optimum parameter values for this algorithm are referred in section 4.5.1.1.

    - The normal intima-media thickness for a given patient is measured by clinical experts in healthy and plaque-free regions of the carotid wall according to standardized protocols proposed in a medical consensus (Touboul *et al*., 2012), as described in section 3.4.4.

The overall performance of the proposed method was evaluated. For this, the clinical set ($N = 40$) was used to allow the combination of the three criteria for plaque segmentation. Figure 4.12 shows cumulative distributions of ε_L^i and ε_A^i for plaque segmentation using the proposed method. The values of ε_L and ε_A for the whole dataset are 1.00 and 1.20, respectively.

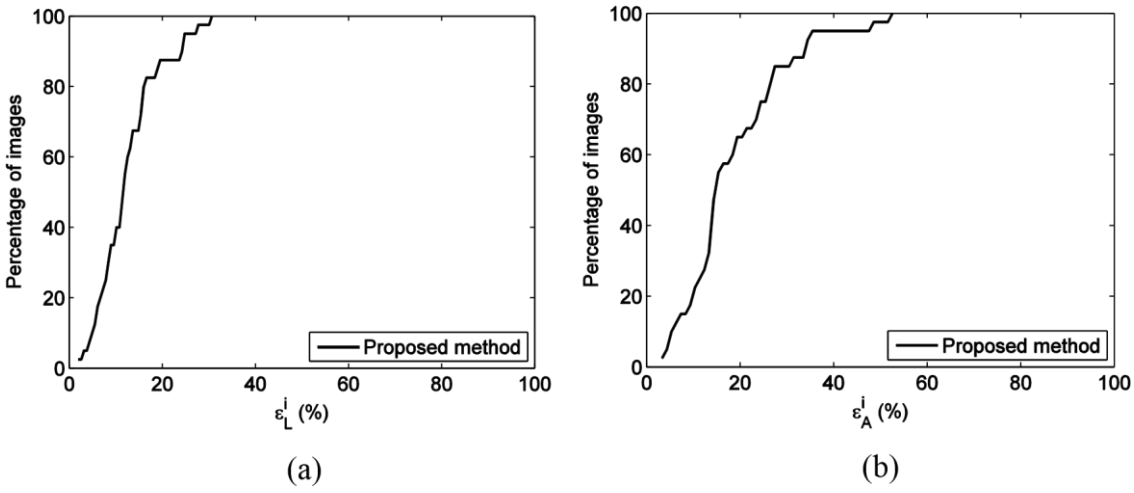

Figure 4.12 Cumulative distributions of (a) ε_L^i and (b) ε_A^i for the plaque segmentation using the proposed method.

The method for plaque segmentation proposed in this work is highly dependent on the prior segmentation of the IM region of the carotid wall. If this segmentation is performed correctly, the method shows a good performance and the produced segmentations are comparable to the manual ones. Figure 4.13 shows examples of the best plaque segmentations for both the FW and NW of the carotid artery. The segmented plaques are highlighted with a red overlay.

An incorrect segmentation of the IM region results in the worst plaque segmentations. The largest errors occur due to:

- Noisy IM contours produced by the automatic segmentation. Very irregular contours cause local depressions and peaks of the intima-media thickness which lead to the detection of false plaque flanks and to the segmentation of inexistent plaques, as shown in the top image row of figure 4.14.

- Echolucent LI boundaries: the segmentation of weak LI interfaces fails, resulting in the absence of segmented plaques, as shown in the bottom image row of figure 4.14.

For the first situation, the smoothing of the segmented contours may improve plaque segmentation by attenuating the irregularity of these boundaries, reducing abrupt variations of the local intima-media thickness and the consequent number of false plaque flanks detected by criterion 2. The second situation may only be corrected by enhancing the quality and contrast of the original US image.

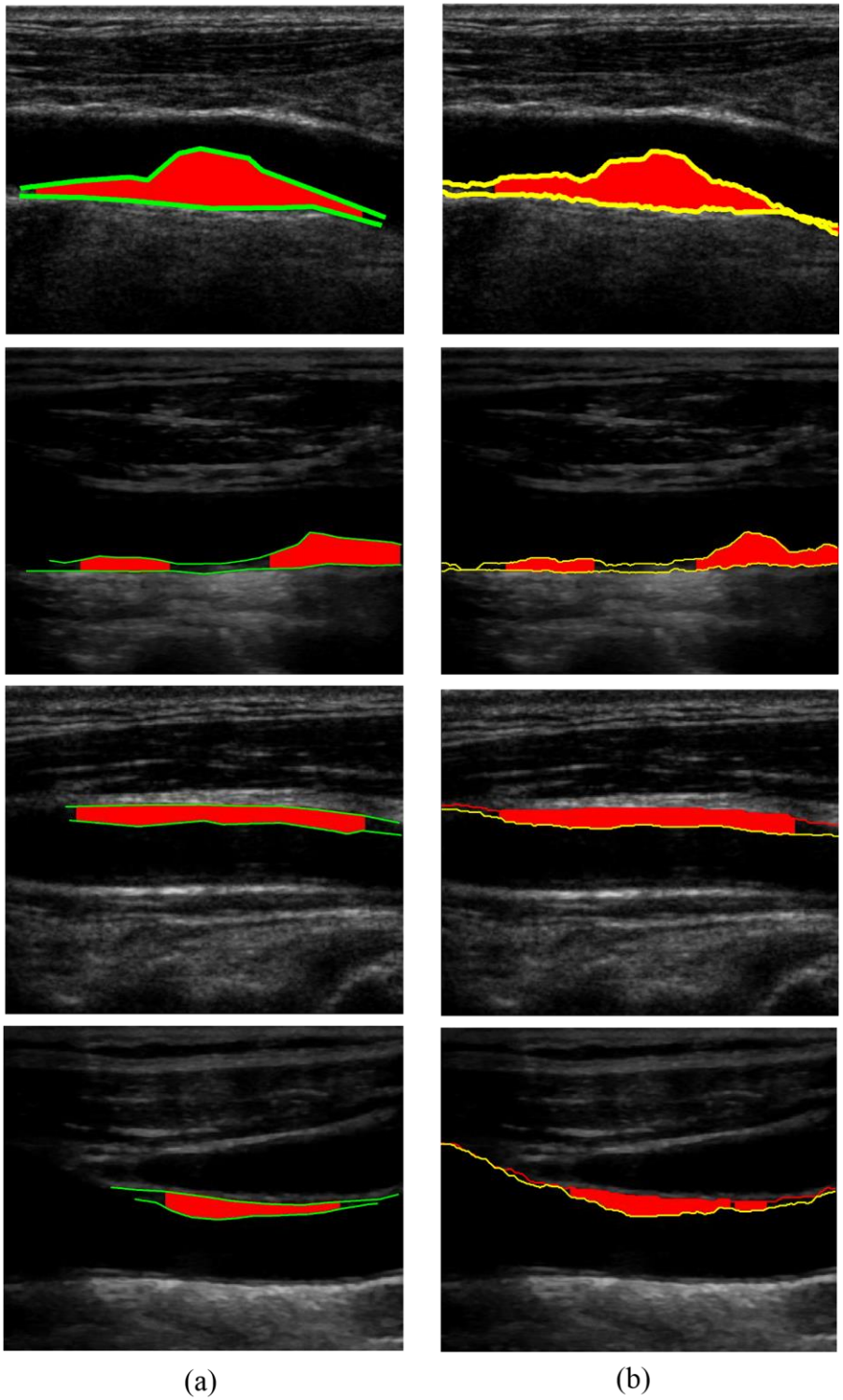

Figure 4.13 Examples of the best plaque segmentations performed by the proposed method for the FW (bottom two image rows) and NW (top two image rows) of the carotid artery. (a) GT plaque segmentation. (b) Automatic plaque segmentation. The green and yellow lines represent the manual and automatic contours of the IM region, respectively, and the segmented plaques are highlighted with a red overlay.

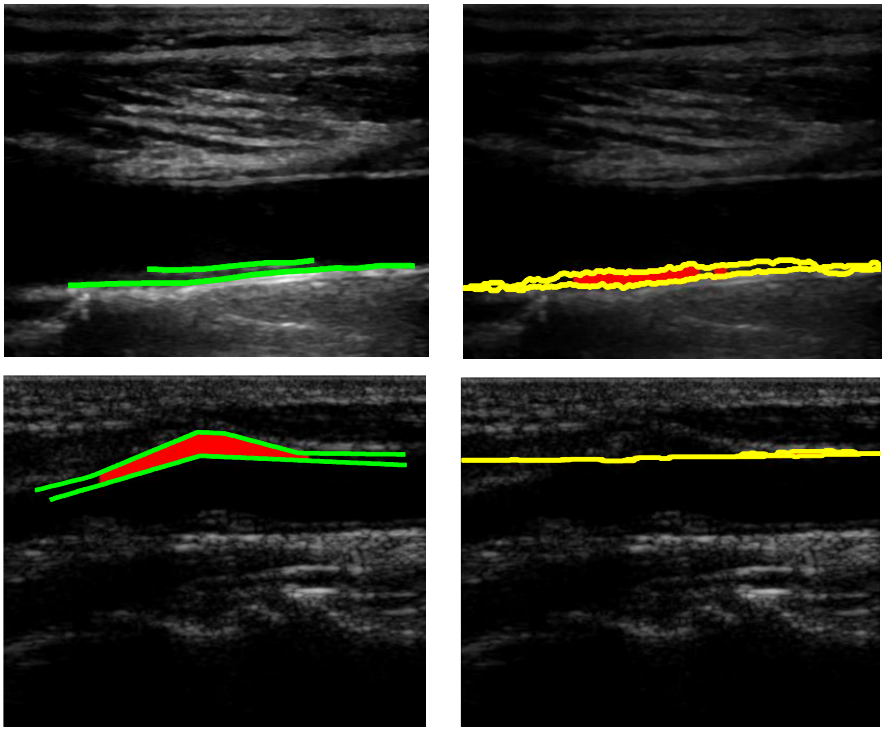

(a) (b)

Figure 4.14 Examples of the worst plaque segmentations performed by the proposed method. In the top image row noisy IM contours lead to the segmentation of an inexistent plaque in the FW. In the bottom image row the segmentation of the LI interface fails and a NW plaque is not segmented. (a) GT plaque segmentation. (b) Automatic plaque segmentation. The green and yellow lines represent the manual and automatic contours of the IM region, respectively, and the segmented plaques are highlighted with a red overlay.

After optimizing the method for plaque segmentation, we are now able to propose a CAD system for automatic measurement of plaque burden in US images of the carotid artery. A description of this system is provided in the next chapter.

5 CAD system for measuring plaque burden

Figure 5.1 shows a block diagram of the proposed CAD system for automatic measurement of plaque burden (PB) in ultrasound (US) images of the carotid artery. This system is based on a graphical user interface (GUI) that allows the user to perform the different actions that are available through mouse clicks on interactive buttons. Actions marked with the person silhouette are carried out by the user. The remaining actions are automatically performed by the system.

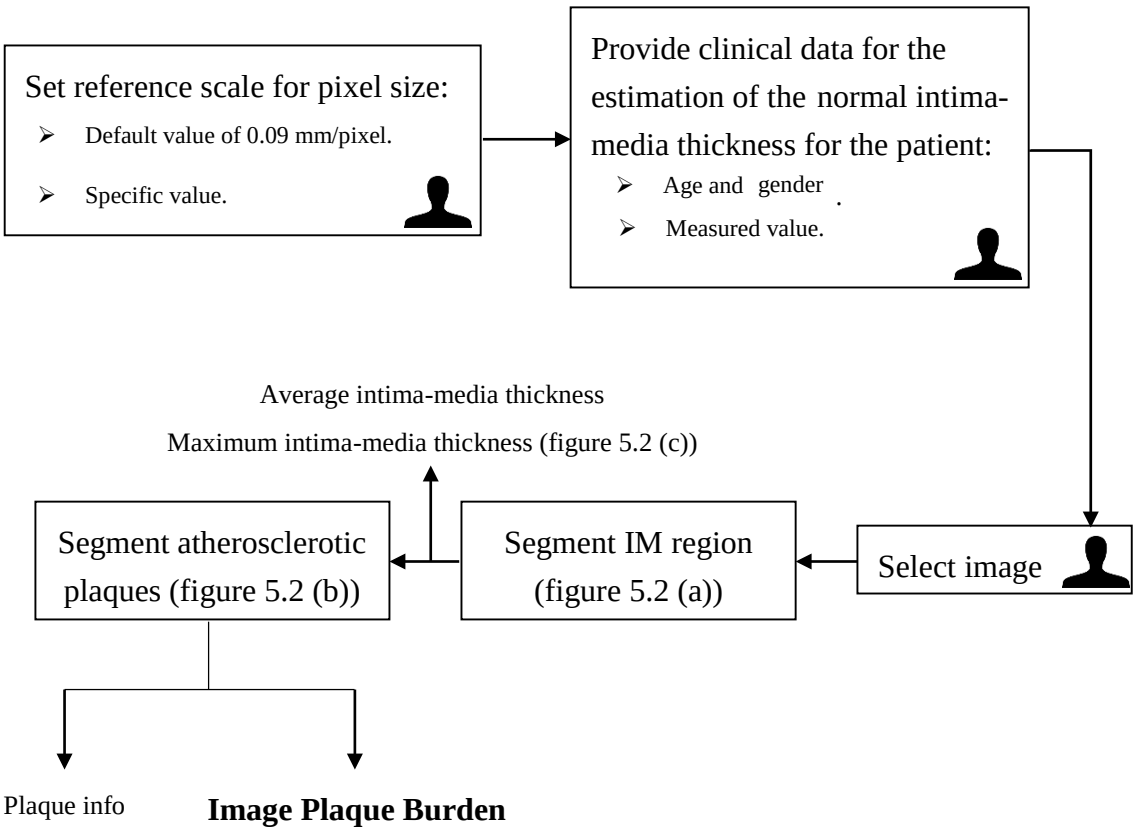

Figure 5.1 Proposed CAD system for automatic measurement of PB in US images of the carotid artery.

The user starts by defining the reference scale for pixel size normalization. For this, he can either 1) choose the default value of 0.09 mm/pixel or 2) type the desired scale into a textbox. Also, clinical data about the patient must be provided to allow calculating the normal intima-media thickness. If this measure is available, it can be directly typed into a textbox. If not, the user can introduce the patient's age and gender, and the normal intima-media thickness will be estimated as explained in section 3.4.4.

After this, the user has to upload the image. This is done by pushing the "Select Image" button, which allows the user to navigate through the different directories and reach the desired image. Supported image files are: .jpg, .png, .tiff', .pnm and .bmp. When the user selects the desired image it becomes visible on the screen.

The user must then click on the "Segment Contours" button. The automatically segmented contours are superimposed in the image with a legend for the colour code, as shown in figure 5.2 (a).

By clicking on the "Segment Plaque" button the segmented atherosclerotic plaques are superimposed in the image as a red overlay. A text box on the right side of the screen becomes visible, containing the number of plaques found in each wall, a quantitative characterization of each plaque, including its length and area, and the total image plaque burden, as shown in figure 5.2 (b). The lowest plaque number corresponds to the leftmost plaque in the NW and the highest number to the rightmost plaque in the FW. The average and maximum values for the intima-media thickness are also calculated and shown in the textbox. It is possible to visualize the region in the carotid wall which shows the maximum intima-media thickness by clicking the "Show Maximum IMT" button, as shown in figure 5.2 (c).

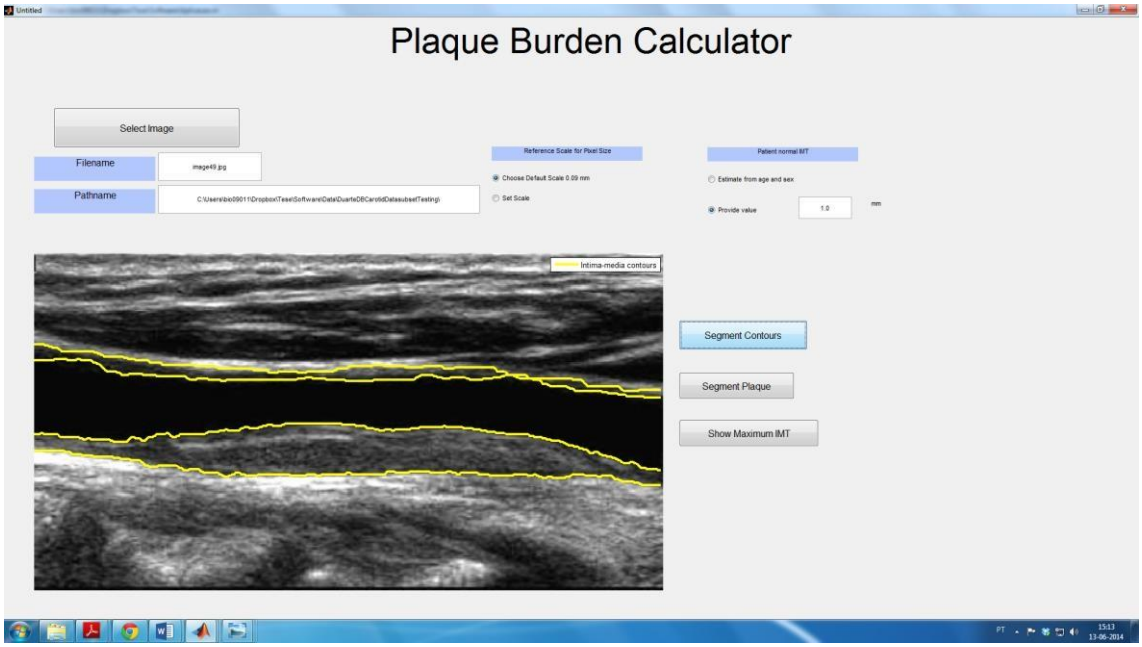

(a)

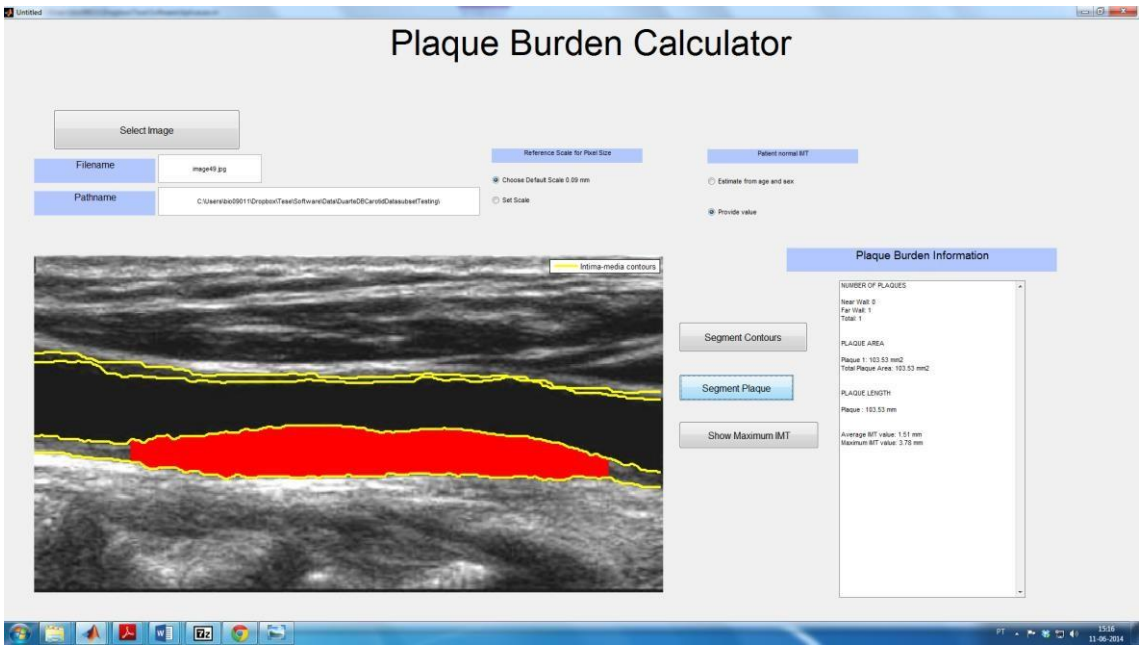

(b)

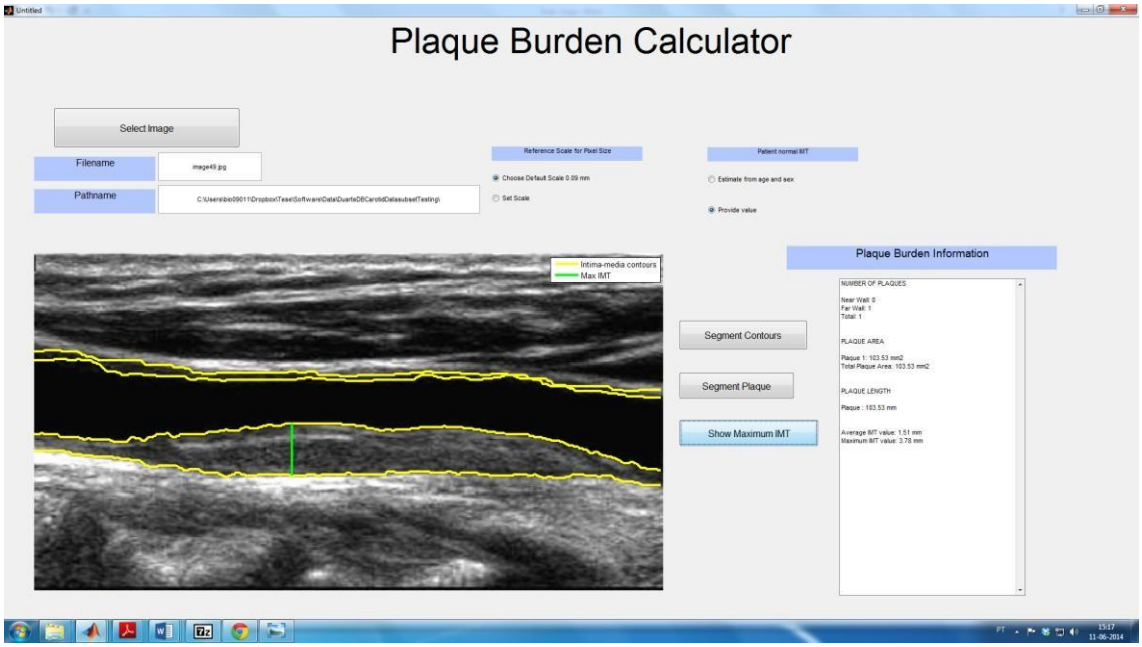

(c)

Figure 5.2 CAD system for automatic measurement of PB in US images of the carotid artery. (a) By clicking on the "Segment Contours" button the segmented contours of the carotid wall become visible in the image, represented by yellow lines. (b) By clicking on the "Segment Plaque" button the segmented atherosclerotic plaques are superimposed in the image as a red overlay. A textbox containing the quantitative characterization of each segmented plaque becomes visible, including its length and area, the image plaque burden and also the average and maximum values of the intima-media thickness. (c) By clicking on the "Show Maximum IMT" button the region of the carotid wall which shows the maximum intima-media thickness is highlighted by a green vertical line.

6 Conclusions and future work

In the research reported in this dissertation, a CAD system for the automatic measurement of atherosclerotic plaque burden (PB) in ultrasound (US) images of the carotid artery is proposed. PB is calculated as total plaque area, equal to the sum of the areas of all the plaques found in the image. To calculate this measure, a prior segmentation of the atherosclerotic plaques is performed.

A novel method is proposed for the segmentation of atherosclerotic plaques in US images of the carotid artery. This method is divided in two main steps:

- Segmentation of the intima-media (IM) region of the carotid wall.
- Delimitation of plaques from IM contours.

In order to segment the IM region, the method proposed by Rocha, Silva and Campilho (2012) is used as reference and modified to improve the segmentation in images highly affected by speckle noise. The modifications introduced in the present work are: use of an alternative method for lumen detection based on local phase symmetry patterns at appropriate scale of analysis (Rouco and Campilho, 2013); relaxation of the constraints imposed to boundary candidates during the fuzzy classification of edges; use of a new membership function for the fuzzy classification of edges that uses more image information, such as the edge strength; local estimation of the strength of false edges caused by noise in the lumen, calculated through robust statistics to help defining the penalty and gain terms of this function.

For plaque segmentation, the proposed method uses three objective criteria proposed in a European medical consensus to define the location of the left and right limits of atherosclerotic plaques in the US image. These criteria are based on the thickness of the IM layer, which is calculated locally for both walls along the entire image length using the segmented contours of this region. The local intima-media thickness is compared with reference threshold values proposed in the medical consensus to evaluate the presence of

plaques in a specific region of the carotid wall. Each of these criteria is implemented separately and provides an independent plaque segmentation.

Depending on the criterion, the reference thresholds with which the local intima-media thickness is compared can be objectively defined in the consensus or require the definition of additional measures of the carotid wall thickness, as the surrounding intima-media thickness and the normal intima-media thickness for the patient. The first is calculated as the Gaussian average of the local intima-media thickness within a neighbour region of the carotid wall. The latter can be obtained through two different and equally valid procedures: 1) directly measured by clinical experts in healthy and plaque-free regions of the patient's carotid artery, according to standardized protocols proposed in the medical consensus or 2) linear interpolation using reference values provided by large population-based cohort studies.

The plaque region is computed as the area enclosed by the right and left limits, in the longitudinal direction, and the IM contours, in the vertical direction. The area of all the segmented plaques is summed as the image PB.

Finally, a graphical-user interface (GUI) was developed to calculate the PB of an image. The GUI allows the user to upload an image, segment the contours of the carotid wall and the atherosclerotic plaques. A quantitative characterization of each segmented plaque is provided, including its length and area, along with the total image PB. The average and maximum intima-media thickness are also shown.

The method for plaque segmentation proposed in this work was evaluated in a large set of 2D B-mode US images of the common carotid artery containing manual segmentations of the IM contours and atherosclerotic plaques.

The proposed method for the segmentation of the IM region preserves the main features of the one proposed by Rocha, Silva and Campilho (2012), which are:

- Absence of user-interaction.
- Avoidance of methods for image normalization, such as histogram equalization, by computing specific and image-adapted thresholds.
- Avoidance of low-pass filtering for noise attenuation, which can result in loss of information, by using fuzzy classification of edges.
- Segmentation of both the NW and the FW IM region in real-time.
- Robustness to the presence of atherosclerotic plaques with different shapes and sizes.

Additionally, the modifications introduced here improve the segmentation in images highly affected by speckle noise. This method shows difficulties in segmenting weak echolucent lumen-intima (LI) interfaces.

The method for plaque segmentation shows the best performance when the three criteria to define atherosclerotic plaque are combined, as the definition given by each one is not enough to ensure a correct segmentation of plaques showing very different shapes and sizes, if used individually.

This method is highly dependent on the prior segmentation of the IM region. If this segmentation is performed correctly, the method shows a good performance and the produced segmentations are comparable to the manual ones. An incorrect segmentation of this layer causes the largest errors for plaque segmentation. These errors occur due to noisy and irregular IM contours that cause local depressions and peaks of the intima-media thickness. This leads to the detection of false plaque flanks and to the segmentation of inexistent plaques. For this situation, the smoothing of the segmented contours may improve plaque segmentation by attenuating the irregularity of these boundaries and reducing abrupt variations of the local intima-media thickness. Also, when very echolucent LI interfaces are present, the segmentation of these boundaries usually fails, resulting in the absence of segmented plaques. Plaque segmentation may improve in these situations only by increasing the quality and contrast of the original US image.

The adaptation of the proposed method for plaque segmentation to US images of the carotid bifurcation is an interesting topic for future research, since atherosclerotic plaques preferably form at this spot.

Regarding the developed GUI, a possible optimization of this tool would be to include the possibility of performing manual corrections to the automatically segmented contours. This would improve the accuracy of plaque segmentation by allowing the medical expert to make use of his experience to perform local corrections where the segmented contours do not overlap with the true interfaces of the carotid wall.

References

Afonso, D., Seabra, J., Suri, JS. Sanches, JM. (2012) A CAD system for atherosclerotic plaque assessment. *Annual International Conference of the IEEE Engineering in Medicine and Biology Society*, pp. 1008-1011.

Al-Shali, K., House, AA., Hanley, AJ., Khan, HM., Harris, SB., Mamakeesick, M., Zinman, B., Fenster, A., Spence, JD., Hekele, RA. (2005) Differences between carotid wall morphological phenotypes measure by ultrasound in one, two and three dimensions. *Atherosclerosis*, 178(2), pp. 319-325.

Ainsworth, CD., Blake, CC., Tamayo, A., Beletsky, V., Fenster, A., Spence, JD. (2005) 3D ultrasound measurement of change in carotid plaque volume: a tool for rapid evaluation of new therapies. *Stroke*, 36(9), pp. 1904-1909.

Amato, M., Montorsi, P., Ravani, A., Oldani, E., Galli, S., Ravagnani, PM., Tremoli, E., Baldassare, D. (2007) Carotid intima-media thickness by B-mode ultrasound as surrogate of coronary atherosclerosis: correlation with quantitative coronary angiography and coronary intravascular ultrasound findings. *European heart journal*, 28(17), pp. 2094-2101.

Aznaouridis, K., Dhawn, S., Quyyumi, A. (2010) Cardiovascular Risk Prediction by Measurement of Arterial Elastic Properties and Wall Thickness. *Advances in Vascular Medicine*. pp. 399-421.

Bae, J-H., Kim, W-S., Rihal, CS., Lerman, A. (2006) Individual Measurement and Significance of Carotid Intima, Media, and Intima–Media Thickness by B-Mode Ultrasonographic Image Processing. *Arterioesclerosis, Thrombosis and Vascular Biology*, 26, pp. 2380-2385.

Berletti, R., Casagranda, G., Bailoni, L., Giannelli, G., Barbieri, M., Caffo, O., Paganelli, F., Recla, M., Centonze, M., (2014) Grading of internal carotid artery stenosis with multidetector-row CT angiography: comparison between manual and semiautomatic measurements. *European Congress of Radiology*, C-1525.

Brown, DG. (1998) Classification and boundary vagueness in mapping presettlement forest types. *International Journal of Geographic Information Science*, 12(2), pp. 105-129.

Callahan, AS., Szarek, M., Patton, JW., Sillesen, AS., Jones, A., Churchwell, K., Holliday, HD. (2012) Maximum carotid artery wall thickness and risk factors in a young primary prevention population. *Brain and Behavior*, 2(5), pp. 590-594.

Costanzo, P., Perrone-Filardi, P., Vassallo, E., Paolillo, S., Cesarano, P., Brevetti, G., Chiariello, M. (2010) Does carotid intima-media thickness regression predict reduction of cardiovascular events? A meta-analysis of 41 randomized trials. *Journal of the American College of Cardiology*, 56(24), pp. 2006-2020.

Davis, NE. (2005) Atherosclerosis – An Inflammatory Process. *Journal of Medical Insurance*, 37, pp. 72-75.

Delsanto, S., Molinari, F., Giustetto, P., Liboni, W., Badalamenti, S. (2005) CULEX-completely user-independent layers extraction: ultrasonic carotid artery images segmentation. *Annual International Conference of the IEEE Engineering in Medicine and Biology Society*, 6, 6468-6471.

Delsanto, S., Molinari, F., Giustetto, P., Liboni, W., Badalamenti, S., Suri, JS. (2006) User-independent plaque characterization and accurate IMT measurement of carotid artery wall using ultrasound. *Annual International Conference of the IEEE Engineering in Medicine and Biology Society*, 1, 2404-2407.

Delsanto, S., Molinari, F., Giustetto, P., Liboni, W., Badalamenti, S., Suri, JS. (2007) Characterization of a Completely User-Independent Algorithm for Carotid Artery Segmentation in 2-D Ultrasound Images. *IEEE Transactions on Instrumentation and Measurement*, 56(4), pp. 1265-1274.

Eagle, M. (2006) Doppler ultrasound-basics revisited. *British journal of nursing*, 15(11), pp. S24-S30.

Elkind, MS., Luna, JM., Moon, YP., Boden-Albala, B., Liu, KM., Spitalnik, S., Rundek, T., Sacco, RL., Paik, MC. (2010) Infectious burden and carotid plaque thickness: the Northern Manhattan study. *Stroke*, 41(3), pp. 117-122.

Faita, F., Gemignani, V., Bianchini, E., Giannarelli, C., Ghiadoni, L., Demi, M. (2008) Real-time measurement system for evaluation of the carotid intima-media thickness with a robust edge operator. *Journal of ultrasound in medicine*, 27(9), pp. 1353-1361.

Falk, E., Prediman, KS., Fuster, V. (1995) Coronary Plaque Disruption. *Circulation*, 92, pp. 657-671.

Fenster, A., Downey, DB., Cardinal, HN. (2001) Three-dimensional ultrasound imaging. *Physics in Medicine and Biology*, 45(5), pp. R67-R99.

Fenster, A., Parraga, G., Bax, J. (2011) Three-dimensional ultrasound scanning. *Interface Focus*, 1(6), pp. 503-519.

Fenster, A., Parraga, G., Landry, A., Chiu, B., Egger, M., Spence, JD. (2008) 3-D US imaging of the carotid artery. In: *Advances in Diagnostic and Therapeutic in Ultrasound Imaging*. Fenster,A. *et al.* eds. 1st edition. Norwood: Artech House. Chapter 3.

Finn, AV., Kolodgie, FD., Virmani, R. (2009) Correlation between carotid intimal/medial thickness and atherosclerosis: a point of view from pathology. *Arteriosclerosis, Thrombosis and Vascular Biology*, 30(2), pp. 177-181.

Gonzalez, RC., Woods, RE. (2007) Digital Imaging Processing. 3rd edition. Prentice Hall.

Hofer, M. (2005) Ultrasound Teaching Manual: The Basics of Performing and Interpreting Ultrasound Scans. Verlag, GT. ed. 2nd edition. Stutgart, New York.

Hudson-Dixon, CM., Long, BW., Cox, LA. (1999) Power Doppler imaging: principles and applications. *Radiologic Technology*, 70(3), pp. 235-243.

Johnsen, SH., Mathiesen, EB., Joakimsen, O., Stensland, E., Wilsgaard, T., Løchen, M-L., Njølstad, I. (2007) Carotid atherosclerosis is a stronger predictor of myocardial infarction in women than in men: a 6-year follow-up study of 226 persons: The Tromsø Study. *Stroke*, 38, pp. 2873-2880.

Kuo, F., Gardener, H., Dong, C., Cabral, D., Della-Morte, D., Blanton, SH., Elkind, MS., Sacco, RL., Rundek, T. (2012) Traditional cardiovascular risk factors explain the minority of the variability in carotid plaque. *Stroke*, 43(7), pp. 1755-1760.

Lee, Y-B., Choi, Y-J., Kim, M-H. (2010) Boundary detection in carotid ultrasound images using dynamic programming and a directional Haar-like filter. *Computers in Biology and Medicine*, 40, pp. 687-697.

Lim, TK., Lim, E., Dwivedi, G., Kooner, J., Senior, R. (2008) Normal Value of Carotid Intima-Media Thickness–A Surrogate Marker of Atherosclersosis: Quantitative Assessment by B-Mode Carotid Ultrasound. *Journal of the American Society of Echocardiography*, 21(2), pp. 112-116.

Loizou, CP. (2005) Ultrasound Image Analysis of the Carotid Artery. Ph.D. thesis. School of Computing and Information Systems of Kingston University, London UK.

Loizou, CP., Pattichis, CS., Pantziaris, M., Tyllis, T., Nikolaides, A. (2007a) Snakes based segmentation of the common carotid artery intima media. *Medical & biological engineering & computing*, 45(1), pp. 35-49.

Loizou, CP., Petroudi, S., Pattichis, CS., Pantziaris, M., Kasparis, T., Nikolaides, A. (2007b) An integrated system for the segmentation of atherosclerotic carotid plaque. *IEEE Transactions on information technology in biomedicine*, 11(6), pp. 661-667.

Loizou, CP., Pattichis, CS., Pantziaris, M., Nikolaides, A. (2012) Segmentation of atherosclerotic carotid plaque in ultrasound video. *34th Annual International Conference of the IEEE Engineering in Medicine & Biology Society*, pp. 53-56.

Loizou, CP., Petroudi, S., Pantziaris, M., Nikolaides, A., Pattichis, C. (2014) An Integrated System for the Segmentation of Atherosclerotic Carotid Plaque in Ultrasound

Video. *IEEE Transactions on Ultrasonics, Ferroeletrics and Frequency Control*, 61(1), pp. 86-101.

Lorenz, MW., Markus, HS., Bots, ML., Rosvall, M., Sitzer, M. (2007) Prediction of clinical cardiovascular events with carotid intima-media thickness: a systematic review and meta-analysis. *Circulation*, 115(4), pp. 459-467.

Mallett, C., House, AA., Spence, JD., Fenster, A., Parraga, G. (2009) Longitudinal ultrasound evaluation of carotid atherosclerosis in one, two and three dimensions. *Ultrasound in medicine & biology*, 35(3), pp. 367-375.

Molinari, F., Meiburger, KM., Saba, L., Zeng, G., Acharya, UR., Ledda, M., Nikolaides, A., Suri, JS. (2012) Fully Automatic Dual-Snake Formulation for Carotid Intima-Media Thickness Measurement. *Journal of Ultrasound in Medicine*, 31(7), pp. 11231136.

Nichols, WW., Denardo, SJ., Wilkinson, IB., McEniery, CM., Cockcroft, J., O'Rourke, MF. (2008) Effects of arterial stiffness, pulse wave velocity, and wave velocity on the central aortic pressure waveform. *Journal of clinical hypertension*, 10(4), pp. 295-303.

Nikolaides, A., Beach, KW., Kyriacou, E., Pattichis, CS. (2012) Ultrasound and Carotid Bifurcation Atherosclerosis. Nikolaides, A. *et al*. eds. 17th edition. Springer.

Oppenheim, AV., Willsky, AS., Hamid S. (1996) Signals and Systems. 2nd edition. Prentice Hall.

O'Rahilly, R., Müller, F. (1983) Basic human anatomy: a regional study of human structure. Saunders.

Ott, RL., Longnecker, MT. (2008) Introduction to Statistical Methods and Data Analysis. 6th edition. Cengage Learning.

Petroudi, S., Loizou, C., Pantziaris, M., Pattichis, C. (2012) Segmentation of the common carotid intima-media complexin ultrasound images using active contours. *IEEE Transactions on Biomedical Engineering*, 59(11), pp. 3060-3069.

Pollex, RL., Spence, JD., House, AA., Fenster, A., Hanley, AJ., Zinman, B., Harris, SB., Hegele, SA. (2005) A comparison of ultrasound measurements to assess carotid atherosclerosis development in subjects with and without type 2 diabetes. *Cardiovascular Ultrasound*, 3(15), 7 pages.

Rocha, R. (2007) Image Segmentation and Reconstruction of 3D Surfaces from Carotid Ultrasound Images. Ph. D. thesis. Faculdade de Engenharia da Universidade do Porto.

Rocha, R., Campilho, A., Silva, J., Azevedo, E., Santos, R. (2010) Segmentation of the carotid intima-media region in B-mode ultrasound images. *Image and Vision Computing*, 28(4), pp. 614-625.

Rocha, R., Campilho, A., Silva, J., Azevedo, E., Santos, R. (2011) Segmentation of ultrasound images of the carotid using RANSAC and cubic splines. *Computer methods and programs in biomedicine*, 101, pp. 94-106.

Rocha, R., Silva, J., Campilho, A. (2012) Automatic segmentation of carotid B-mode images using fuzzy classification. *Medical & biological engineering & computing*, 50(5), pp. 533-545.

Rouco, J., Campilho, A. (2013) Robust common carotid artery lumen detection in Bmode ultrasound images using local phase symmetry. *International Conference on Acoustics, Speech and Signal Processing*. pp. 929-933.

Schaub, N., Reichlin T., Meune, C., Twerenbold, R., Haaf, P., Hochholzer, W., Niederhauser, N., Bosshard, P., Stelzig, C., Freese, M., Reiter, M., Gea, J., Buser, A., Mebazaa, A., Osswald, S., Mueller, C. (2012) Markers of plaque instability in the early diagnosis and risk stratification of acute myocardial infarction. *Clinical chemistry*, 58(1), pp. 246-256.

Schminke, U., Motsch, L., Hilker, L., Kessler, C. (2000) Three-Dimensional Ultrasound Observation of Carotid Artery Plaque Ulceration. *Stroke*, 31, pp. 1651-1655.

Sillesen, H., Muntendam, P., Adourian, A., Entrekin, R., Garcia, M., Falk, E., Fuster, V. (2012) Carotid plaque burden as a measure of subclinical atherosclerosis: comparison with other tests for subclinical arterial disease in the High Risk Plaque BioImage study. *JACC. Cardiovascular imaging*, 5(7), pp. 681-689.

Simon, A., Chironi, G., Levenson J. (2006) Performance of subclinical arterial disease detection as a screening test for coronary heart disease. *Hypertension*, 48(3), pp. 392-396.

Spence, JD., Eliasziw, M., DiCicco, M., Hackam, DC., Galil, R., Lohmann, T. (2002) Carotid plaque area: a tool for targeting and evaluating vascular preventive therapy. *Stroke*, 33(12), pp. 2916-2922.

Spence, JD., Matthew, RB., Hegele, RA. (2003) Lipoprotein lipase (LPL) gene variation and progression of carotid artery plaque. Stroke, 34(5), pp. 1176-1180.

Stein, JH., Korcarz, CS., Hurst, RT., Lonn, E., Kendall, CB., Mohler, ER., Najjar, SS., Rembold, CM., Post, WS. (2008) American Society of Echocardiography (ASE) Consensus Statement - Use of Carotid Ultrasound to Identify Subclinical Vascular Disease and Evaluate Cardiovascular Disease Risk: A Consensus Statement from the ASE Carotid Intima-Media Thickness Task Force. *Journal of the American Society of Echocardiography*, 21(2), pp. 93-111.

Störk, S., van den Beld, AW., von Schacky, C., Angermann, CE., Lamberts, SW., Grobbee, DE., Bots, ML. (2004) Carotid artery plaque burden, stiffness and mortality risk in elderly man: a prospective, population-based cohort study. *Circulation*, 110(3), pp. 344-348.

Suri, JS., Chirinjeev, K., Molinari, F. (2011). Atherosclerosis Disease Management. Suri, JS., Chirinjeev, K. and Molinari, F. eds. Springer.

Tauber, C. (2005) Filtrage anisotrope robuste et segmentation par b-spline snake: application aux images échographiques, Ph.D. thesis, Institut National Polytechnique de Toulouse, Toulouse.

Touboul, PJ., Vicaut, E., Labreuche, J., Belliard, JP., Cohen, S., Kownator, S., Pithois-Merli, I., (2005) Design, baseline characteristics and carotid intima-media thickness reproducibility in the PARC study. *Cerebrovascular diseases*, 19(1), pp. 57-63.

Touboul, PJ., Hennerici, MG., Meairs, S., Adams, H., Amarenco, P., Bornstein, N., Csiba, L., Desvariwux, M., Ebrahim, S., Hernandez, R., Jaff, M., Kownator, S., Naqvi, T., Prati, P., Rundek, T., Sitzer, M., Schminke, U., Tardif, JC., Taylor, A., Vicaut, E., Woo, KS. (2012) Mannheim carotid intima-media thickness and plaque consensus (2004-2006-2011). *Cerebrovascular diseases*, 34(4), pp. 290-296.

van der Meer, IM., Bots, ML., Hofman, A., del Sol, AI., van der Kuip, DA., Witteman, JC. (2004) Predictive value of non-invasive measures of atherosclerosis for incident myocardial infarction: The Rotterdam Study. *Circulation*, 109(9), pp. 1089-1094.

Vukusich, A., Kunstmann, S., Varela, C., Gainza, D., Bravo, S., Sepulveda, D., Cavada, G., Michea, L., Marusic, ET. (2010) A randomized, double-blind, placebo-controlled trial of spironolactone on carotid intima-media thickness in non-diabetic haemodialysis patients. *Clinical journal of the American Society of Nephrology*, 5(8), pp. 1380-1387.

Wannarong, T., Parraga, G., Buchanan, D., Fenster, A., House, AA., HAckam, DG., Spence, JD. (2013) Progression of carotid plaque volume predicts cardiovascular events. *Stroke*, 44(7), pp. 1859-1865.

Wikstrand, J. (2007) Methodological considerations of ultrasound measurement of carotid artery intima-media thickness and lumen diameter. *Clinical physiology and functional imaging*, 27(6), pp.341-345.

Yang, X., He, W., Li, K., Jin, J., Zhang, X., Yuchi, M., Ding, M. (2012) A review on artery wall segmentation techniques and intima-media thickness measurement for carotid ultrasound images. *Journal of Innovative Optical Health Sciences*, 5(1), 10 pages.

Yu, Y., Acton, S. (2004) Edge detection in ultrasound imagery using the instantaneous coefficient of variation. *IEEE Transactions on Image Processing*, 13(12), pp. 1640-1655.

Appendix A - Reference values for the normal intima-media thickness of the common carotid artery

Table AI Reference values for the normal intima-media thickness of the common carotid artery provided by large European cohort studies (Stein *et al. 2008*).

A. Mean far wall common carotid artery carotid intima-media thickness values from the AXA Study[79,80]

Right common carotid artery

	Male				Female			
Age, y/percentile	< 30	31-40	41-50	> 50	< 30	31-40	41-50	> 50
25th	0.39	0.42	0.46	0.46	0.39	0.42	0.44	0.50
50th	0.43	0.46	0.50	0.52	0.40	0.45	0.48	0.54
75th	0.48	0.50	0.57	0.62	0.43	0.49	0.53	0.59

Left common carotid artery

	Male				Female			
Age, y/percentile	< 30	31-40	41-50	> 50	< 30	31-40	41-50	> 50
25th	0.42	0.44	0.50	0.53	0.30	0.44	0.46	0.52
50th	0.44	0.47	0.55	0.61	0.44	0.47	0.51	0.59
75th	0.49	0.57	0.61	0.70	0.47	0.51	0.57	0.64

B. Mean far wall common carotid artery carotid intima-media thickness values from the Carotid Atherosclerosis Progression Study (Matthias W. Lorenz, MD, personal communication, December 6)[20]

	Male							Female						
Age, y/percentile	25	35	45	55	65	75	85	25	35	45	55	65	75	85
25th	0.515	0.585	0.634	0.68	0.745	0.814	0.83	0.524	0.575	0.619	0.665	0.718	0.771	0.807
50th	0.567	0.633	0.686	0.746	0.83	0.914	0.937	0.567	0.615	0.665	0.719	0.778	0.837	0.880
75th	0.633	0.682	0.756	0.837	0.921	1.028	1.208	0.612	0.66	0.713	0.776	0.852	0.921	0.935

C. Maximum* far wall common carotid artery carotid intima-media thickness values from the Edinburgh Artery Study (F. Gerald R. Fowkes, MBChB, PhD, personal communication, November 2006)[81]

	Male					Female				
Age, y/percentile	60-64	65-69	70-74	75-79	> 80	60-64	65-69	70-74	75-79	> 80
25th	0.60	0.70	0.70	0.70	0.80	0.60	0.60	0.70	0.70	0.72
50th	0.80	0.80	0.80	0.90	1.00	0.70	0.80	0.80	0.90	0.90
75th	0.90	1.00	1.00	1.20	1.20	0.80	0.90	0.90	1.00	1.40

Y, years. All values are in mm.

*Maximum of right or left common carotid artery.